

# EFFECTS OF TWO STEP ANNEALING ON DYNAMIC MAGNETIC PROPERTIES OF Co- AND Co-Fe-BASED AMORPHOUS RIBBONS

By

MD. ZAKIR HOSSAIN KHAN

Roll No. 0055503

Session: 2000- 2001



A THESIS SUBMITTED TO THE DEPARTMENT OF PHYSICS,  
KHULNA UNIVERSITY OF ENGINEERING AND  
TECHNOLOGY IN PARTIAL FULFILMENT OF THE  
REQUIRMENT FOR THE DEGREE OF  
MASTER OF PHILOSOPHY



KHULNA UNIVERSITY OF ENGINEERING AND  
TECHNOLOGY  
KHULNA-920300, BANGLADESH,  
MAY, 2005

KHULNA UNIVERSITY OF ENGINEERING & TECHNOLOGY  
DEPARTMENT OF PHYSICS  
CERTIFICATION OF THESIS WORK



A THESIS ON

*Effects of Two step annealing on dynamic magnetic properties of Co-and Co-Fe-Based amorphous ribbons*

By

**MD ZAKIR HOSSAIN KHAN**

has been accepted as satisfactory in partial fulfillment for the degree of Master of Philosophy in Physics and certify that the student demonstrated a satisfactory knowledge on the field covered by this thesis in an oral examination held on 28 June, 2005.

1. Professor Dr. Shibendra Shekher Sikder (Supervisor)  
Department of Physics  
Khulna University of Engineering and Technology

Chairman *SSikder*

2. Head  
Department of Physics  
Khulna University of Engineering and Technology

Member *SSikder*

3. Professor Dr. Md. Abu Hashan Bhuyan  
Department of Physics, BUET, Dhaka-1000

Co-Supervisor *me*

4. Professor Dr. Md. Mahbub Alam  
Department of Physics  
Khulna University of Engineering and Technology

Member *MA Alam*

5. Mr. Md Abdullah Elias Akhter  
Assistant Professor, Department of Physics  
Khulna University of Engineering and Technology

Member *Akhter*


6. Dr. Farid Uddin Ahmed  
Director, International Affairs Division  
4, Kazi Nazrul Islam Road. Ramna, Dhaka-1000

Member (External) *F. Uddin Ahmed*

## CERTIFICATE

This is to certify that this thesis which the candidate has presented for M. Phil. Degree has been done by the candidate himself and does not contain any material extracted from else where or from a work published by any body else. The work of this thesis has not been presented for another degree or diploma in any other University or Institute. No other person's work has been used without due acknowledgement.

  
.....  
Supervisor

  
.....  
candidate



**DEDICATED TO MY PARENTS**



# CONTENTS

Certificate	i
Dedication	ii
Contents	iii
List of Figures	vii
List of Tables	xii
List of Symbols and Abbreviations Used	xiii
Acknowledgements	xv
Abstract	xvii

## CHAPTER 1 INTERODUCTION

1.1 Introduction	1
1.2 Applications of Amorphous Magnetic Ribbons	7
1.3 Objectives of the Present Study	7
1.4 Thesis Layout	8

## CHAPTER 2 PREPARATION OF AMORPHOUS RIBBONS BY RAPID QUENCHING MATHOD

2.1 Introduction	10
2.2 The Structure of an Amorphous Alloy	11
2.3 Condition for Forming Amorphous Material	15
2.4 Conditions Necessary for Preparing Amorphous Materials	17
2.5 Preparation Technique of Amorphous Ribbon	17
2.5.1 The Atomic Deposition Methods	17
2.5.2 The Fast cooling of the Melt	18
2.5.3 Rapid Quenching Method	19
2.6 Experimental Details of the Preparation of Amorphous Ribbon	20
2.6.1 Important Factors to Control the Thickness of Ribbons	21
2.7 Factors Contributing to Glass Formation	21
2.8 Examining the Amorphousity	24

## CHAPTER 3 THEORETICAL ASPECTS

3.1	Stability of Amorphous Alloys	25
3.1.1	Structural Relaxation of Amorphous Alloys	27
3.1.2	Characteristics of the Glass Transition Temperature	29
3.2	Magnetization of the Amorphous Ribbons	30
3.2.1	Annealing Effects of Amorphous Alloy	32
3.3	Initial Permeability of Amorphous Ribbons	33
3.3.1	Theories of Permeability	34
3.3.2	Wall Permeability	36
3.3.3	Rotational Permeability	38
3.3.4	Losses	40

## CHAPTER 4 EXPERIMENTAL DETAILS

4.1	The Differential Thermal Analysis	42
4.1.1	Introduction	42
4.1.2	The Principle of Differential Thermal Analysis	42
4.1.3	Apparatus	44
4.2	Experimental Setup for Measurement of Magnetization	47
4.2.1	The Principle of Vibrating Sample Magnetometer	47
4.2.2	Mechanical Design of the V.S.M.	48
4.2.3	Electronic Circuits of the V.S.M.	51
4.2.3.1	Sensitivity Limits	52
4.2.3.2	Stability Tests Differential Measurements	53
4.2.3.3	Vibration Amplitude	53
4.2.3.4	Image Effects	53
4.2.3.5	Vibration Frequency	54
4.2.3.6	Vibration Problems	54
4.2.4	X-Y Recorder	54
4.2.5	Calibration of the V.S.M	55
4.2.6.1	Calibration Data	57
4.3.0	Experimental Techniques for Measuring Complex Permeability	58



4.3.1	Real and Imaginary Components of Complex Permeability	58
4.3.2	Preparation of the samples for permeability measurements	59
4.3.3	Frequency Characteristics of Amorphous Materials	59

## CHAPTER 5 RESULTS AND DISCUSSIONS

5.1	Differential Thermal Analysis	61
5.1.1	DTA Results of Amorphous Co-B-Si and Co-Fe-B-Si as Affected by Fe-Substitution	61
5.1.2	Activation energy of Co- and Co-Fe- based amorphous ribbons	65
5.1.3	Annealing Effects on the Kinetics of Structural Relaxation of Co-B-Si and Co-Fe-B-Si Amorphous Ribbons Studied by DTA	69
5.2	Effects of two- step Annealing time on Magnetization	72
5.2.1	Specific Magnetization Measurements on as cast Co- and Co-Fe- based Amorphous ribbons	73
5.2.2	Specific Magnetization Measurements on two Step time Annealed Co-and Co-Fe-Based Amorphous Ribbons	74
5.3	Dynamic Magnetic Properties of Co- and Co-Fe- based amorphous Ribbons	79
5.3.1	Initial Permeability of as cast Co-and Co-Fe-Based Amorphous Ribbons	80
5.3.2	Complex Permeability of the as cast Co- and Co-Fe- Based Amorphous Ribbons	82
5.3.3	Frequency Dependence of the real part of the complex permeability of Co- and Co-Fe- based amorphous ribbon with different annealing Temperature and two step annealing time	82
5.3.4	Frequency dependence of the Imaginary part of the complex permeability of Co- and Co-Fe-Based Amorphous Ribbon with Different Annealing Temperature and two step Annealing Time	91
5.3.5	Relative quality factor	97
5.3.6	Two-step Annealing time Effects on Frequency Spectra of Co and Co-Fe- Based Ribbons at Constant Annealing Temperature 390°C	103
5.3.7	Annealing Temperature Dependence of Initial Permeability at Constant low Field for two Step Annealing Time with Composition $\text{Co}_{80-x}\text{Fe}_x\text{B}_{10}\text{Si}_{10}$	103

## **CHAPTER 6 CONCLUSIONS**

6.1 Conclusions 109

**BIBLIOGRAPHY** 113

**PUBLICATIONS** 120





## LIST OF FIGURES

Fig- 2.1.	Short range of order as a function of radial distance	12
Fig- 2.2.	Free energy versus temperature curves	13
Fig- 2.3.	Glass formation as a function of reduced glass transition temperature	14
Fig- 2.4.	Viscosity versus Temperature curve	14
Fig- 2.5.	Compositional dependence of melting point	15
Fig- 2.6.	Experimental values of Critical velocity versus reduced glass transition temperature	16
Fig- 2.7.	Thin layer of molten alloy intimate contact with the outer surface of metallic rotor is quenched in to amorphous	19
Fig- 2.8.	Temperature dependence of enthalpy H. G and G' corresponds to glass and S corresponds to crystalline state	23
Fig- 2.9.	X-ray diffraction from the top surface of the amorphous ribbon with composition $\text{Co}_{78}\text{Fe}_2\text{B}_{10}\text{Si}_{10}$	24
Fig- 3.1.	Magnetization by wall motion and spin rotation	37
Fig- 4.1.(a)	Heating curve of sample and reference substance	43
Fig- 4.1. (b)	DTA curve	44
Fig- 4.2.	DTA Thermocouple assembly	46
Fig- 4.3.	Block diagram of a differential thermal analysis equipment, (s) sample thermocouple, (R) reference thermocouple, (M) monitor thermocouple	47
Fig- 4.4.	Mechanical construction of the vibrating sample magnetometer	50
Fig- 4.5.	Schematic diagram of the electronic system of the V.S.M.	52
Fig- 4.6.	Calibration curve of magnetic field Vs. decade transformation reading (V.S.M.)	56
Fig- 5.1.	DTA trace of the amorphous ribbon with composition $\text{Co}_{80}\text{B}_{10}\text{Si}_{10}$	62
Fig- 5.2	DAT trace of amorphous ribbons with composition $\text{Co}_{80-x}\text{Fe}_x\text{B}_{10}\text{Si}_{10}$	64
Fig- 5.3.	Vibration of $T_g$ and $T_x$ due to change in the Fe- content in $\text{Co}_{80-x}\text{Fe}_x\text{B}_{10}\text{Si}_{10}$	64
Fig- 5.4.	Effects of heating rate on DTA trace of the amorphous ribbon with composition $\text{Co}_{80}\text{B}_{10}\text{Si}_{10}$	66



Fig- 5.5.	Effects of heating rate on DTA trace of the amorphous ribbon with composition $\text{Co}_{72}\text{Fe}_8\text{B}_{10}\text{Si}_{10}$	66
Fig- 5.6	$\frac{1}{T_p} \times 10^3$ versus $\text{Ln} \left( \beta / T_p^2 \right)$ curve for $T_g$ and $T_x$ phases of the amorphous ribbon with $\text{Co}_{72}\text{Fe}_8\text{B}_{10}\text{Si}_{10}$	67
Fig- 5.7	$\frac{1}{T_p} \times 10^3$ versus $\text{Ln} \left( \beta / T_p^2 \right)$ curve for $T_g$ and $T_x$ phases of the amorphous ribbon with composition $\text{Co}_{80}\text{B}_{10}\text{Si}_{10}$	67
Fig- 5.8.	Effects on DTA trace of as cast and different annealing time at $200^\circ\text{C}$ on the amorphous ribbon with composition $\text{Co}_{80}\text{B}_{10}\text{Si}_{10}$	70
Fig- 5.9.	Effects on DTA trace of as cast and time annealed at $200^\circ\text{C}$ on the amorphous ribbon with composition $\text{Co}_{72}\text{Fe}_8\text{B}_{10}\text{Si}_{10}$	70
Fig- 5.10.	Specific magnetization versus magnetic field of as cast amorphous ribbons.	75
Fig- 5.11.	Variation of saturation specific magnetization due to change in the Fe-content	75
Fig-5.12.	Magnetization versus magnetic field for different annealing time at temperature $390^\circ\text{C}$ of amorphous ribbon	76
Fig- 5.13.	Magnetization versus magnetic field for different annealing time at temperature $390^\circ\text{C}$ of amorphous ribbon	76
Fig- 5.14.	Magnetization versus magnetic field for different annealing time at temperature $390^\circ\text{C}$ of amorphous ribbon	77
Fig- 5.15.	Magnetization versus magnetic field for different annealing time at temperature $390^\circ\text{C}$ of amorphous ribbon	77
Fig- 5.16.	Magnetization versus magnetic field for different annealing time at temperature $390^\circ\text{C}$ of amorphous ribbon	78
Fig- 5.17.	Variation of saturation specific magnetization due to change in the Fe-content of two step time annealing at annealing $390^\circ\text{C}$ of amorphous ribbon with composition $\text{Co}_{80-x}\text{Fe}_x\text{B}_{10}\text{Si}_{10}$	78
Fig- 5.18.	Permeability versus a.c. magnetic field of amorphous ribbons with composition $\text{Co}_{80-x}\text{Fe}_x\text{B}_{10}\text{Si}_{10}$	81
Fig- 5.19.	Variation of initial permeability with the change in the Fe- content in $\text{Co}_{80-x}\text{Fe}_x\text{B}_{10}\text{Si}_{10}$	81

Fig- 5.20.	Frequency dependence of the real part of initial permeability of amorphous ribbons with compositions $\text{Co}_{80-x}\text{Fe}_x\text{B}_{10}\text{Si}_{10}$	84
Fig- 5.21.	Frequency dependence of the imaginary part of initial permeability of amorphous ribbons	84
Fig- 5.22.	Frequency dependence of loss factor of amorphous ribbon	85
Fig- 5.23.	Frequency dependence of relative quality factor of amorphous ribbon	85
Fig- 5.24.	Frequency dependence of the real part of initial permeability of amorphous ribbon for different annealing temperature with composition $\text{Co}_{80}\text{B}_{10}\text{Si}_{10}$ at constant 10 minute annealing time ( $H=0.11$ A/m)	86
Fig- 5.25.	Frequency dependence of the real part of initial permeability of amorphous ribbon for different annealing temperature with composition $\text{Co}_{80}\text{B}_{10}\text{Si}_{10}$ at constant 100 minute annealing time( $H=0.11$ A/m)	86
Fig- 5.26.	Frequency dependence of the real part of initial permeability of the amorphous ribbon for different annealing temperature	87
Fig- 5.27.	Frequency dependence of the real part of initial permeability of the amorphous ribbon for different annealing temperature	87
Fig- 5.28.	Frequency dependence of the real part of initial permeability of the amorphous ribbon for different annealing temperature	88
Fig- 5.29.	Frequency dependence of the real part of initial permeability of the amorphous ribbon for different annealing temperature	88
Fig- 5.30.	Frequency dependence of the real part of initial permeability of the amorphous ribbon for different annealing temperature	89
Fig- 5.31.	Frequency dependence of the real part of initial permeability of the amorphous ribbon for different annealing temperature	89
Fig- 5.32.	Frequency dependence of the real part of initial permeability of the amorphous ribbon for different annealing temperature	90
Fig- 5.33.	Frequency dependence of the real part of initial permeability of the amorphous ribbon for different annealing temperature	90
Fig- 5.34.	Frequency dependence of the imaginary part of initial permeability of amorphous ribbons for different annealing temperature	92



Fig- 5.35.	Frequency dependence of the imaginary part of initial permeability of amorphous ribbons for different annealing temperature	92
Fig- 5.36.	Frequency dependence of the imaginary part of initial permeability of amorphous ribbons for different annealing temperature	93
Fig- 5.37.	Frequency dependence of the imaginary part of initial permeability of amorphous ribbons for different annealing temperature	93
Fig- 3.38.	Frequency dependence of the imaginary part of initial permeability of amorphous ribbons for different annealing temperature	94
Fig- 5.39.	Frequency dependence of the imaginary part of initial permeability of amorphous ribbons for different annealing temperature	94
Fig- 5.40.	Frequency dependence of the imaginary part of initial permeability of amorphous ribbons for different annealing temperature	95
Fig- 5.41.	Frequency dependence of the imaginary part of initial permeability of amorphous ribbons for different annealing temperature	95
Fig- 5.42.	Frequency dependence of the imaginary part of initial permeability of amorphous ribbons for different annealing temperature	96
Fig- 5.43.	Frequency dependence of the imaginary part of initial permeability of amorphous ribbons for different annealing temperature	96
Fig- 5.44.	Frequency dependence of the relative quality factor of amorphous ribbons for different annealing temperature	98
Fig- 5.45.	Frequency dependence of the relative quality factor of amorphous ribbons for different annealing temperature	98
Fig- 5.46.	Frequency dependence of the relative quality factor of amorphous ribbons for different annealing temperature	99
Fig- 5.47.	Frequency dependence of the relative quality factor of amorphous ribbons for different annealing temperature	99
Fig- 5.48.	Frequency dependence of the relative quality factor of amorphous ribbons for different annealing temperature	100
Fig- 5.49.	Frequency dependence of the relative quality factor of amorphous ribbons for different annealing temperature	100
Fig- 5.50.	Frequency dependence of the relative quality factor of amorphous ribbons for different annealing temperature	101
Fig- 5.51.	Frequency dependence of the relative quality factor of amorphous ribbons for different annealing temperature	101

Fig- 5.52.	Frequency dependence of the relative quality factor of amorphous ribbons for different annealing temperature	102
Fig- 5.53.	Frequency dependence of the relative quality factor of amorphous ribbons for different annealing temperature	102
Fig- 5.54.	Frequency dependence of the real part of initial permeability of amorphous ribbons	104
Fig- 5.55.	Frequency dependence of the real part of initial permeability of amorphous ribbons	104
Fig- 5.56.	Frequency dependence of the real part of initial permeability of amorphous ribbons	105
Fig- 5.57.	Frequency dependence of the real part of initial permeability of amorphous ribbons	105
Fig- 5.58.	Frequency dependence of the real part of initial permeability of amorphous ribbons	106
Fig- 5.59.	Initial permeability versus annealing temperature of amorphous ribbons	108
Fig- 5.60.	Initial permeability versus annealing temperature of amorphous ribbons	108

## LIST OF TABLES

Table 2.1: Thickness of Co and Co-Fe-based samples	23
Table 5.1: $T_g$ and $T_x$ of amorphous ribbons with compositions $Co_{80-x}Fe_xB_{10}Si_{10}$ at constant heating rate $20^\circ C/min$	63
Table 5.2: Energy products for $T_g$ and $T_x$ of amorphous ribbons with compositions $Co_{80-x}Fe_xB_{10}Si_{10}$ at constant heating rate $20^\circ C/min$	65
Table 5.3: Activation energies for $T_g$ and $T_x$ of amorphous ribbons with compositions $Co_{80-x}Fe_xB_{10}Si_{10}$	68
Table 5. 4: Two steps annealing time effects on Energy products of the amorphous ribbon with compositions $Co_{80}B_{10}Si_{10}$ at constant heating rate $20^\circ C/min$	69
Table 5.5: Annealing time effects on Energy products of the amorphous ribbon with compositions $Co_{72}Fe_8B_{10}Si_{10}$ at constant heating rate $20^\circ C/min$	69
Table 5.6: Two step annealing time effects on saturation magnetization of amorphous ribbons with composition $Co_{80-x}Fe_xB_{10}Si_{10}$ at constant annealing temperature $390^\circ C$	79
Table 5.7: The initial permeability in the vanishing field region of the amorphous ribbon with composition $Co_{80-x}Fe_xB_{10}Si_{10}$ at constant annealing	80
Table 5.8: The initial permeability of the amorphous magnetic ribbon $Co_{80-x}Fe_xB_{10}Si_{10}$ at different annealing temperature at a constant low field of $H= 0.11 A/m$ and constant 10 minutes time annealing	106
Table 5.9: The initial permeability of the amorphous magnetic ribbon $Co_{80-x}Fe_xB_{10}Si_{10}$ at different annealing temperature at a constant low field of $H= 0.11 A/m$ and constant 100 minutes time annealing	107



## LIST OF SYMBOLS AND ABBREVIATIONS USED

TM	Transition Metal
TM-M	Transition Metal- Metalloid
RE-TM	Rear- Earth transion Metal
DTA	Differential Thermal Analysis
f	Frequency
$\tau$	Reduced glass transaction temperature
$T_m$	Melting temperature
$T_g$	Glass transition temperature
$T_x$	Crystallization temperature
$T_x'$	Secondary crystallization temperature
$T_c$	Curie temperature
$T_p$	Crystallization peak temperature
$H_c$	Coercive force
B	Magnetic induction
$B_m$	Maximum magnetic induction
$B_s$	Saturation magnetic induction
$\mu$	Permeability
$\mu_m$	Maximum permeability
$\mu_i$	Initial permeability
$\mu'$	Real part of the complex permeability
$\mu''$	Imaginary part of the complex permeability
$L_s$	Self- inductance of the sample core
$L_o$	Inductance of the winding coil without sample



$\tan \delta$	Loss factor
$\mu_r/\tan \delta$	Relative quality factor
V.S.M.	Vibrating Sample Magnetometer
H	Magnetic Field
M	Magnetization
$M_s(0)$	Saturation magnetization at 0 K
$M_s(T)$	Saturation Magnetization at T K
C	Curie constant
k	Boltzmann constant
$\sigma_s$	Saturation specific magnetization
$\sigma_s(0)$	Saturation specific magnetization at 0 K
$\sigma_s(T)$	Saturation specific magnetization at T K
m	Reduced magnetization
$E_a$	Total anisotropy energy
$K_u$	Stress induced anisotropy
$K_u(T)$	Stress induced anisotropy at T K
$K_u(0)$	Stress induced anisotropy at 0 K
$K_0$	Zero order anisotropy constant
FWFM	Full Width Half Maximum

## ACKNOWLEDGEMENTS

I express my deep sense of sincere gratitude to my supervisor Professor Dr. Shibendra Shekher Sikder, Head, of the department, Department of Physics, Khulna University of Engineering and Technology (KUET), for his continuous guidance, fruitful discussions, and encouragement to perform this research work successfully.

I am very much indebted to my Co-Supervisor Professor Dr. Md. Abu Hashan Bhuiyan, Department of physics, Bangladesh University of Engineering and Technology (BUET), Dhaka 1000, Bangladesh, for his interest, guidance and valuable assistance during this experimental work.

I am deeply grateful to Professor Dr. Md. Mahbub Alam, Department of Physics, (KUET), for his interest and encouragement in my thesis.

I would like to express my gratitude to Dr. A.K.M. Abdul Hakim, Chief Engineer, Magnetic Materials Division, Atomic Energy Center, Dhaka for their generous help and for allowing me to use their facilities.

I would like to express their thanks to Prof. Nguyen Chau National University of Hanoi and Prof. Neguyen Houng Nghi vice Director, Chief of the Laboratory of Amorphous Magnetic Materials, Hanoi University of Technology, Vietnam for the preparation of the amorphous ribbons. We are also grateful to IPPS, Uppsala University, for supporting the visit to S.S. Sikder to Prof. Negyen Houng Nghi at the Amorphous Laboratory of Hanoi, Vietnam.

I am grateful to Dr. Md. Abdul Gafur, S.O., Bangladesh Council for Scientific and Industrial Research (BCSIR) Laboratory, Dhaka, for their generous help in doing the Differential Thermal Analysis.

I am grateful to Professor, Dr. Mominul Huq, Head of the Department of Physics, BUET, Dhaka for providing me with the necessary experimental facilities, kind co-operation and inspiration.

I am thankful to Md. Shafiur Rahaman, Head, Department of Chemistry KUET, Khulna, for allowing to use Chemistry laboratory of KUET.

My thanks are due to Mr. Monoz Datta, Lecturer, Department of Electrical and Electronic Engineering, KUET for his co- operation and help in Computation.

I gratefully acknowledge Mr. Md. Abdullah Elias Akhter and Jolly Sultana, Assistant Professor, Department of Physics, and Munshi Tauhiduzzaman, Assistant

Professor and Head Department of Humanities in KUET, for their co- operation and inspiration during this work.

I would like to extend my special thanks to Mr. Abul Kalam Azad, Principal, Phultala M. M. College for his tireless co-operation in my thesis work.

I would like to thank Khan Alal Uddin, Pritish Kumar Ray, Saroaut Noor, Shaheena Parvin, Firoza Akhter Banu for their fruitful co- operation and assistance.

I am greatly indebted to my parents, brother and sisters for their consistent encouragement and inspiration.

I wish to express my thanks to my wife Marzia Zakir for keeping me free from family affairs during my work and also for her sustained inspiration, encouragement and continuous co- operation. Finally my thanks are due to my only son Arian Nafis Khan.

My thanks are due to my dearest Ashikur Rahaman for his tireless co- operation in writing my thesis.

Finally I record my sincerest gratitude to Khulna University of Engineering and technology, Khulna for providing me with the financial assistance during the period of the work.



## ABSTRACT

Co-and Co-Fe-based amorphous ribbons with general composition  $\text{Co}_{80-x}\text{Fe}_x\text{B}_{10}\text{Si}_{10}$  have been prepared by the melt- spinning technique where Co has been substituted by Fe from 0 to 8 At%. The amorphousity of the samples has been confirmed by X-ray diffraction technique. The kinetics of crystallization of different crystalline phases of the samples has been studied by DTA. Two exothermic peaks in the curve indicate two distinct crystallization temperatures, the exothermic reaction caused by the first crystallization process, may responsible for a absence of a clear glass transition Temperature ( $T_g$ ) and the second stage of crystallization ( $T_x$ ) corresponds to the another sharp exothermic peak. It is observed that, with increasing amount of Fe, the  $T_g$  increases monotonically. The values of  $T_x$ , which are higher than those of  $T_g$  remain practically constant for all the compositions. DTA traces of amorphous ribbons taken in argon atmosphere with continuous heating rate of 10 to  $50^\circ\text{C}/\text{min}$  at a step of  $10^\circ\text{C}$ . The peak temperature shifts to higher values with increasing heating rate. The crystallization activation energy determined from the Kissinger plot using DTA thermograms for two crystallization phases are found. The thermal activation energies for  $T_g$  phases only slightly increase with increasing Fe-content in the amorphous ribbon.

A vibrating sample magnetometer (VSM) has been used for measuring magnetization of Co-Fe-based ribbons of different composition at room temperature to look for the composition dependence of magnetization. The study of magnetization process as affected by two step annealing time at constant annealing temperature  $390^\circ\text{C}$  and is interpreted interms of domain reorganization by heat treatment. The effect of annealing time on magnetization has also been measured using VSM and is slightly increased in saturation state. The complex permeability of amorphous ribbon with composition  $\text{Co}_{80-x}\text{Fe}_x\text{B}_{10}\text{Si}_{10}$  [ $x= 0, 2, 4, 6 \& 8$ ] are measured as a function of frequency in the range 1KHz to 13 MHz using impedance analyzer. Two step annealing time effect on initial permeability ( $\mu_i$ ), loss factor and relative quality factor have been measured for different annealing temperature in the range 25 to  $450^\circ\text{C}$ . The real part of the permeability ( $\mu'$ ) of all the samples as affected by annealing at different temperature with two step annealing time in each case, is measured at low frequency (1 KHz) and at very low field ( $H= 0.11 \text{ A/m}$ ). The  $\mu'$  decreases



monotonously with increasing annealing temperature and with increasing annealing time. These effects of annealing lead to the ordering of magnetic atomic pairs, which increases anisotropy and decreases permeability. Our results of annealing on Co-Fe based samples, which show a decrease of  $\mu'$  with step annealing time, are explained as due to the growth of the nucleation centers of the crystallites from atom during preparation. These effects contribute to an increase of the  $\mu'$  but at the same time the imaginary component is also influenced, particularly due to eddy current effects. It is evident from the results that annealing temperature and annealing time are both important parameters in controlling the frequency response of permeability of the samples. The best choice of these parameters depends on the desired characteristics of the material in respect of permeability value and its annealing time effects.

## **CHAPTER 1: INTRODUCTION**

- 1.1 Introduction
- 1.2 Applications of amorphous magnetic ribbons
- 1.3 Objectives of the present study
- 1.4 Thesis layout



## 1.1 Introduction

It was believed for many years that because of the lack of atomic ordering ferromagnetism could not exist in amorphous solids. The term's amorphous solid and glass have no precise meaning. These terms are generally accepted to mean "non crystalline on any significant scale" <sup>(1.1-1.2)</sup>. Simple amorphous solids have random structures but with differing degrees of short range order depending on the nature of their atomic bonding. The principal order present is imposed by roughly constant separation of nearest neighbors. Other types of order may also be present for example directional ordering due to magnetic or stress annealing. However, not all disordered materials are amorphous since there are disordered crystalline alloys where different atoms regularly occupy sites of a regular crystal lattice <sup>(1.3-1.4)</sup>. Thus amorphous metal in which nearest neighbor central forces dominate, form structures similar to the random packing of hard spheres. Amorphous alloys, some times called metallic glasses or glassy metals, have received much attention in the last two decades due to their interesting properties and their applicability in new devices.

However, in 1960 Gobanov A.I. <sup>(1.5)</sup> predicted the possible existence of ferromagnetic ordering in non- crystalline solids on the basis of theoretical analysis. The first report of an amorphous metallic alloy appears to have been made by Brenner A. <sup>(1.6)</sup>. The present interest in amorphous metals research stems from reports by Duwez P.R. <sup>(1.7)</sup> on the preparation technique of amorphous metallic alloys. Simpson and Brambley D.R. <sup>(1.8)</sup> appear to have been the first to point out that the amorphous alloys are expected to have no magnetocrystalline anisotropy and should have very low coercivity. Amorphous alloys of Fe-Ni-P-B prepared by the melt spinning technique in the form of ribbons by solidification of the melt on the surface of rapidly rotating drum exhibit even lower coercivities of the order of 8 A/m. Luborsky F.E. *et al.* <sup>(1.9)</sup> first demonstrated the reduction of coercivity in these alloys, down to less than 0.8 A/m by suitable annealing and showed that the changes in their properties are correlated with the relief of internal strains. At about the same time Egami T. *et al.* <sup>(1.10)</sup> showed that annealing under tensile stress reduced the coercivity of an Fe-Ni-P-B-Si alloy at 0.3 A/m.

Precisely this is why the current interest in metallic ribbon is born. The subject is of interest to physicists, material scientists, and electrical or electronic engineers. To



physicists the attraction lies to look at how the absence of crystal structure modifies collective magnetic phenomena, which are mainly governed by short-range interactions. Material scientists are interested in the spectrum of new materials produced by this method capable of yielding microscopically homogeneous alloys of compositions unattainable in crystals, and the new possibilities of tailoring the magnetic properties as desired. Electronic and electrical engineers are interested to find possible uses they can make of metallic ribbon in electronic or power applications. Amorphous states for pure metals like Fe, Co, Ni etc. are obtained only at extremely low temperature, whereas this disorder in the amorphous state is more complex than that in the crystalline alloys. The disorder can be classified into two types- one is structural disorder which is lack of periodicity in the atomic arrangements and the other is chemical disorder in which the chemical compositions loses its periodicity. The macroscopic quantities which are the average of properties in the atomic scale are more perturbed by structural disorders that interfere with each other. There is no theory developed to explain the thermal irreversible behavior of magnetization in amorphous magnetic alloys.

In the present work attempts are made to describe the unusual character of the thermodynamic parameters in amorphous ribbons using a theoretical model developed by Cong B.T. <sup>(1.11)</sup> for disordered localized Ising spin lattice. Recently soft magnetic amorphous alloys have been developed by Miyakazki T. *et al.* <sup>(1.12)</sup> and Komoto O. *et al.* <sup>(1.13)</sup> and they are used for the magnetic cores of switched mode power supplies, magnetic recording heads and other devices. Most of the amorphous materials useful for these applications manufactured from Co-based amorphous ribbons are reported by Fujimori H. *et al.* <sup>(1.14)</sup> with nearly zero magnetostriction. Studies on Fe-based amorphous ribbons were reported by Warliment H. *et al.* <sup>(1.15)</sup> and Sikder S.S. *et al.* <sup>(1.16)</sup>. Fe-based amorphous ribbons are excellent in the higher saturation flux density, but they are inferior in the soft magnetic properties in comparison with Co- based amorphous ribbons.

Increased attention is being put to the production of wide ribbons and the preparation of amorphous ribbons for particular applications and for understanding the origin of their intrinsic and extrinsic properties. In a qualitative sense, the *intrinsic* properties are magnetization( $\sigma_s$ ), Curie temperature ( $T_c$ ), glass transition temperature ( $T_g$ ), induced magnetic anisotropy, magnetostriction ( $\lambda$ ) and hyperfine field (H) and the

*extrinsic* properties are coercive force ( $H_c$ ), remanence to saturation ratio, permeability ( $\mu_i$ ), relative quality factor ( $\mu_i/\tan\delta$ ) and the loss factor ( $\tan\delta$ ) as a function of frequency. These are important for practical applications of magnetic materials and for evaluating and understanding the step annealing time effect of different temperature on magnetic properties and long- term stability of these amorphous ribbons.

Present research involves the preparation of Co-and Co-Fe-based amorphous ribbons. In based amorphous ribbons Co have been slightly replaced by Fe, keeping the glass forming materials Si and B fixed; the general composition being  $\text{Co}_{80-x}\text{Fe}_x\text{B}_{10}\text{Si}_{10}$  [ $x = 0, 2, 4, 6 \text{ \& } 8$ ]. The melt spinning technique has been used for the preparation of the ribbons. The amorphousity of the samples has been confirmed by X-ray diffraction technique. The preparation procedure, conditions for forming amorphous materials and factors controlling the thickness of the ribbons are discussed in chapter- 2. Short accounts of other methods of preparing amorphous ribbon are also given in this chapter along with a short review of works.

Important thermodynamic parameters of amorphous ribbons like  $T_g$  and crystallization temperature ( $T_x$ ) have been studied by Differential Thermal Analysis (DTA). There is no direct relation between the cause of formation and the resultant stability of amorphous ribbons. Cohen M.H. and Turnbull D.,<sup>(1.19)</sup> noted that the composition which is most favourable for glass formation is near the eutectic; the deeper the eutectic the better is the glass forming ability. Various empirical criteria have been proposed to reflect the good glass forming ability of alloys in previous studies <sup>(1.20-1.24)</sup>. Turnbull proposed that the reduced glass transition temperature ( $T_{rg}$ ), defined as  $T_g$  divided by the liquidus temperature ( $T_l$ ), could be regarded as a measure to evaluate the glass forming ability of an alloy<sup>(1.20)</sup>. This correlation has been confirmed in many experiments <sup>(1.25)</sup>. Inouc A. and Masumoto T. adopted the temperature difference  $\Delta T_x$  between  $T_g$  and the first crystallization ( $T_x$ ) upon heating at a constant rate as a measure for the stability of the super cooled liquid above  $T_g$ <sup>(1.23)</sup>. Zhu F. *et al.*<sup>(1.26)</sup> and Bigot J. *et al.*<sup>(1.27)</sup> found that the first DTA peak corresponds to the precipitation of an ordered bcc  $\alpha$ -Fe(Si) solid solution embedded in an amorphous phase and the second to the crystallization of Fe-B-Si compounds. DTA trace of Fe-B ribbons with composition



$\text{Fe}_{82}\text{B}_{18}$  and  $\text{Fe}_{80}\text{B}_{20}$  showed two exothermic peaks in temperature versus time curve. The first peak corresponds to  $T_g$  and second peak to the  $T_x$  by Sikder S.S. *et al.*<sup>(1.28)</sup>.

By DTA we looked for  $T_g$  and crystallization phase transition. The thermal stability of the Co-based and Co-Fe-based amorphous alloy is important for the following reasons and the crystallization activation energies phases are determined.

The resultant amorphous solid generally has higher energy than the corresponding crystalline phase. The energy barriers to nucleation and growth of crystalline phase are so high compared with the thermal energy that the metastable state can be retained for a time annealing which are very long compared with the period during which experiments are done. The energy barriers originate from the difference between the structure of a liquid and a crystal and a considerable rearrangement is needed to pass from one to the other. In this work the thermal stability of  $\text{Co}_{80-x}\text{Fe}_x\text{B}_{10}\text{Si}_{10}$  has been studied systematically by means of DTA. The theoretical basis of the stability of the amorphous ribbons has been discussed in chapter- 3 and experimental arrangements for DTA is described in chapter-4. The results of DTA for different compositions are presented in chapter- 5.

Magnetization is the most common parameter of a magnetic material. Measurements are usually expressed as average moment in unit emu/gm. A brief discussion of this approach, applied to amorphous alloys, may be obtained from Alben, R.<sup>(1.29)</sup>, which followed from ideas of local chemical bonding. In atomic states of high spin the magnetic systems have low electron-electron coulomb repulsion energies. Apparently a small amount of impurity was necessary to stabilize the strong ferromagnetism in the amorphous Fe-Si reported by Felsch, W.<sup>(1.30)</sup>. The behavior of the amorphous Fe-based ribbon is very different from Co-based ribbons. Wright, J.<sup>(1.31)</sup> has recently reviewed the status of the information available on "pure" amorphous elements. In all cases it appears that the saturation moment is the same or less than its value in the crystalline state, which shows that no effective electron transfer occurs from the magnetic atoms to the matrix. The room temperature saturation magnetization has more practical importance.

The detailed quantitative analysis of the situation is, therefore, very complex and the present understanding of the problem of magnetization process as affected by these defects is very incomplete. The present work therefore aims at experimental determination of the effect of annealing on relaxation of strains and corresponding change in the field dependence of the magnetization and effects on step time annealing. We can distinguish reversible and irreversible types of relaxation due to annealing. Irreversible types of relaxation are those which are connected with thermally initiated microscopic jumps of defects or ordering atomic pairs which correspond to irreversible domain wall movements under external fields <sup>(1.32-1.34)</sup>. The measurement of specific magnetization at room temperature and the study of its variation with magnetic field and two step time annealing with different annealing temperature are important for the understanding and characterization of amorphous Co-based and Co-Fe-based ribbons. Magnetization is measured by using a highly sensitive vibration sample magnetometer (VSM). The theories of magnetization in amorphous system as distinct from crystalline materials are discussed in chapter-3 and the experimental technique used is described in chapter- 4. The results and discussions for Co-based and Co-Fe-based samples are discussed in chapter- 5.

The low-field behavior corresponds to the reversible initial permeability of domain walls, which are pinned due to inhomogeneities of the sample as reported by Amano E. *et al.* <sup>(1.35)</sup> and Irvin J. T. S. <sup>(1.36)</sup>. The measurement of complex permeability gives us valuable information about the domain wall movements. Earlier complex permeability measurements by Ban G. *et al.* <sup>(1.37)</sup> performed on polycrystalline permalloy and permivar materials could be fitted as developed by Polivanov K.M. *et al.* <sup>(1.38)</sup>. The real and imaginary components of the complex permeability in ac condition have been measured as a function of the instantaneous value of a sine wave to those of Co-based amorphous ribbons.

The initial permeability of the amorphous magnetic ribbons may be strongly affected by the presence of an electric current due to its heating effect, particularly in ac conditions. Thus the magnetic characteristics are rather different in annealed specimens with time annealing effect from those of as cast ribbons. The dynamic measurements on the amorphous  $\text{Co}_{80-x}\text{Fe}_x\text{B}_{10}\text{Si}_{10}$  [ $x = 0, 2, 4, 6, \& 8$ ] magnetic alloy have been carried out



to determine the frequency dependence of the complex permeability, loss factor and relative quality factor. The soft magnetic properties of the amorphous ribbons can be tailored by annealing. The measurement of magnetic response of the ribbon as a function of frequency and its analysis by means of the complex permeability formalism has recently led to the resolution of the core current density by means of an adapted ac bridge method as described by Battino G. *et al.* <sup>(1.39)</sup>. The amorphous ribbon specimens of ring shaped cores with outside/inside diameter = 34/30 were made from the as- cast ribbons.

At room temperature the frequency and field dependence of the complex permeability  $\mu = \mu' - i\mu''$  and the core loss of the tape wound core were measured by impedance bridge up to the MHz range. Amorphous Co- based and Co-Fe- based ribbons are of great interest as soft magnetic material for their static as well as dynamic application. Measurement has been carried out to determine the frequency dependence of complex permeability, loss factor and relative quality factor. Many workers <sup>(1.40-1.41)</sup> have studied amorphous magnetic ribbons for various applications. Fe- based magnetic ribbons that have large magnetic flux density are usually used in the low frequency region compared magnetization mechanism <sup>(1.42-1.44)</sup>. The initial permeability which gradually decreases with time after demagnetization undergoes a sudden drop with a certain time period which depends on the applied field amplitude and frequency as well as pre annealed temperature as measured by Jagielinski T. <sup>(1.45)</sup>.

Our measurements involve the determination of  $\mu_i$ ,  $\mu'$ ,  $\mu''$ ,  $\tan \delta$  &  $\mu_i/\tan \delta$  and their two step annealing time effects with different annealing temperature on our samples. Theoretical aspect of initial permeability is described in chapter-3 and the experimental set-up in chapter-4. The results of  $\text{Co}_{80-x}\text{Fe}_x\text{B}_{10}\text{Si}_{10}$  [ $x = 0, 2, 4, 6, \& 8$ ] amorphous ribbon discussed in chapter- 5.

In the conclusions we would like to emphasis the fact that large gaps between theoretical and experimental results themselves exist, which demand more careful experiments in this fields specially with more varied composition, step annealing time and annealing temperature variation.



## 1.2 Applications of Amorphous Magnetic Ribbons

The class of amorphous transition metal metalloid (TM-M) alloys with TM= Fe, Co or Ni and M= B, P, C, Al or Si have received much attention for their magnetic properties favorable for various technical devices such as power generators, transformer, magnetic head, and magnetic shield etc. The suitability of amorphous ribbons as magnetic materials are determined both by its static and dynamic properties. Amorphous ferromagnetism have interesting magneto elastic coupling and magnetic softness due to absence of crystalline anisotropy Glassy metals are unusually corrosion free because of the absence of crystalline and grain boundaries. The magnetic properties such as initial permeability, saturation magnetization, Curie temperature, crystallizations kinetics, magnetostriction and induced anisotropy can be controlled by the alloy composition and a subsequent annealed effect. The Fe- based amorphous ribbon exhibit the highest saturation flux density and the Co- based amorphous ribbons are characterized by low magnetostriction, very high permeabilities and low magnetic losses.

Amorphous ribbons are practically suited to devices such as switch cores, high gain magnetic amplifiers and frequency inverters and transformers, where hystereses and eddy current losses need to be minimized. The high electrical resistivity and the small thickness of the melt-quenched ribbons lead to low eddy current losses. Co-based amorphous ribbons are also suitable soft magnetic materials for magnetic shielding due to their high permeability.  $\text{Co}_{80-x}\text{Fe}_x\text{B}_{10}\text{Si}_{10}$  [ $x = 0, 2, 4, 6, \& 8$ ] amorphous ribbons have many refined applications like development of magnetic bubbles for computer memory, amorphous super conductors etc.

Research in the development and application of amorphous ribbon can thus be profitable, specially at its present new phase of local electrochemical potential difference. Thus by a recently developed technique called laser glazing, surfaces of extensive metallic equipment are made amorphous to avoid corrosion.

## 1.3 Objectives of the Present Study

Amorphous Co-and Co-Fe-based alloys are of great interest as soft magnetic materials and the magnetic properties of amorphous alloys are currently the focus of considerable attention. The dynamic measurements on the amorphous Co-and Co-Fe-

based ribbons will be carried out to determine the frequency dependence of complex permeability, loss factor, relative quality factor and initial permeability and its two step annealing time effect and field effect. The dynamic measurement of the eddy current losses which occurs due to irreversible domain wall movements that are frequency dependent is very important. The measurement of complex permeability gives us valuable information about the domain walls. Theoretical models have been suggested for describing the motion of  $180^\circ$  Bloch walls. As known controlled annealing of amorphous ribbon leads to the new materials with a polycrystalline structure, which have excellent soft magnetic properties, for example an enhanced permeability and very low power losses. There are only a few papers dealing with the frequency dependent behavior of this quantity for amorphous ribbons <sup>(1.44-1.45)</sup>. The aim of this work is to compare the frequency and magnetic field dependence of permeability of amorphous Co-and Co-Fe-based ribbons in this as cast and two steps annealing time condition. Moreover amorphous ribbons are made by melt-spinning technique, which is very efficient and give the final product in the form thin ribbons. These materials can be tailored by choosing different composition, cooling rates during the preparation and by controlling the annealing process to be used for high frequency transformation, magnetically soft ribbons can also be used for magnetic shielding and in delay lines. Research in the development and application of amorphous ribbon can thus be profitable, especially at its present new phase.

#### **1.4 Thesis Layout**

Organization of this thesis is divided into six chapters.

Chapter- 1 gives general introduction followed by a review of earlier research work, applications of amorphous magnetic ribbons, the objectives of the study and the thesis layout.

The preparation procedures are described in chapter- 2. The theoretical aspects of the stability of amorphous alloys, theories of permeability and magnetization are discussed in chapter- 3.

Chapter- 4 contains the experimental details including Differential Thermal Analysis (DTA), Vibrating Sample Magnetometer (VSM) and Impedance Analyzer. The

details of step annealing time effects on results regarding DTA, activation energy corresponding crystallization temperature, field dependence of specific magnetization, two step annealing time effects on saturation specific magnetization, field dependence of permeability, frequency dependence of real and imaginary parts of permeability are discussed in chapter- 5. It also contain on the suitability of the specimen studied, in respect of relative quality factor, loss factor and two step time annealing effects on frequency spectrum in which these materials can be used.

Chapter- 6 contains conclusion, achievement of works and further suggestion of this work.



## **CHAPTER 2: PREPARATION OF AMORPHOUS RIBBONS BY RAPID QUENCHING METHOD**

- 2.1. Introduction
- 2.2. The structure of an amorphous alloy
- 2.3. Condition for forming amorphous material
- 2.4. Conditions necessary for preparing amorphous materials
- 2.5. Preparation technique of amorphous ribbon
  - 2.5.1. The atomic deposition methods
  - 2.5.2. The fast cooling of the melt
  - 2.5.3. Rapid quenching method
- 2.6. Experimental details of the preparation of amorphous ribbon
  - 2.6.1. Important factors to control the thickness of ribbons
- 2.7. Factors contributing to glass formation
- 2.8. Examining the amorphousity

## 2 PREPARATION OF AMORPHOUS RIBBONS BY RAPID QUENCHING METHOD

### 2.1 Introduction

Amorphous alloys sometimes called metallic glasses, have received much attention in the last decade due to their interesting properties and their applicability for new devices. Since the discovery of metallic glass by Duwez P. *et al*<sup>(2.1)</sup>, in the same year Gobonov A.I.<sup>(2.2)</sup> predicted the possible existence of ferromagnetic ordering in non-crystalline solids on the basis of theoretical analysis. The present great interest in amorphous metals research stems from by Duwez P. *et al*<sup>(2.1)</sup> on the preparation and properties of amorphous metallic alloys. They introduced two new methods of achieving very rapid quenching from the molten state. Methods propelled a liquid alloy drop onto a cold surface where it would be spread into a thin film and then rapidly solidify. The interest in amorphous materials is increasing steadily for technological application and scientific understanding. A real technological interest developed after Pond R. Jr. and Maddin R. in 1969<sup>(2.3)</sup> reported on the preparation of continuous ribbons of amorphous alloys.

Amorphous alloys are all in a metastable state. Their preparation, and stability at room temperature, thus depends on various kinetic barriers to growth of crystal nuclei, if nuclei are present or to nucleation barriers which hinder formation of stable. Amorphous state of pure metals like Fe, Co, Ni etc can be obtained only at a very low temperature. Alloys of these metals with glass forming materials can be obtained in the amorphous state by cooling the melt at a relatively lower rate of million degrees per second which can remain in the metastable state over an extended range of temperature. Two important classes of amorphous magnetic materials are being studied intensively in recent time. They are the TM-M glass and the rare-earth transition metal glass (RE-TM) reported by Mizoguchi T.<sup>(2.4)</sup>, Alben R. *et al.*<sup>(2.5)</sup>, Gyorgy E. M.<sup>(2.6)</sup> and Cargill G. S.<sup>(2.9)</sup>. TM-M glasses are stable for composition around 75-80% of TM (Fe, Co, Ni, etc or in their combinations) and 25-30% of metalloid (B, C, Si, P, Al or in their combinations). Typical composition for RE-TM glass is RE<sub>33</sub> TM<sub>67</sub>, where RE is one of the heavier rare earth metals like Gd, Tb, Dy, Y etc and TM is one of the 3d transition metals like Fe, Co, or Ni. Recently the metalloids in TM-M glass are replaced by non-magnetic metals like Zr,

Hf. etc by Masumoto T. *et al.* <sup>(2.8)</sup>. The new amorphous ribbons were prepared by such techniques used, in the early works to explore the many possibilities opened up by new rapid quenching technique.

## 2.2 The Structure of an Amorphous Alloy

The structure of amorphous ribbons have been given by Cargill G.S. <sup>(2.9)</sup> and also a detail discussion is given by Asgar M.A. <sup>(2.10)</sup>. An amorphous ribbon material has no long range order and the co-relations that exist must be of short range order in the sense that certain values of the interatomic distance  $r$  are more common than others. Structure can be discussed on many levels. For example, in terms of the external size and shape of the solid; in terms of cracks, voids, inclusions, composition gradients and other heterogeneities resolvable by optical microscopy or other technique. Most work on the structure of amorphous metallic ribbons has, of course been concerned with this short-range atomic order. The stability increases with the number of components in an amorphous ribbon. The disorder can be classified into two types following Alben R. *et al.* <sup>(2.11)</sup>.

- (1) Structural disorder –lack of periodicity in atomic arrangement and
- (2) Chemical disorder –lack of periodicity in chemical environment.

Since the most important magnetic interactions are dependent on what happens at quite short-range, then atomic scale properties, such as magnetic moments, are controlled by chemical disorder. The structural arrangement of the atoms in amorphous solids can be given interms of a radial distribution function. The radial distribution function (RDF)  $F(r)$  is defined as the number of atoms lying between  $r$  and  $r + dr$  of the centre of any given atom

$$F(r) = 4\pi r^2 \rho(r) \quad (2.1)$$

Where  $\rho(r)$  is the atomic pair correlation function:

$$\rho(r) = 0 \text{ for } r < \text{nearest neighbor separation}$$

$$\rho(r) = \rho_0, \text{ average density at larger.}$$

Radial distribution functions are defined for systems of different atoms as weighted average. The distribution functions are sometimes presented in slightly different forms as

$$G(r) = 4\pi r [\rho(r) - \rho_0] \quad (2.2)$$



If we consider the density  $\rho_0$  as constant, then  $F(r) = 4\pi\rho_0 r^2$ . Since the density is constant so  $F(r)$  follows the parabolic distribution

$$w(r) = \frac{R(r)}{4\pi r^2 \rho_0} = \frac{4\pi r^2 \rho(r)}{4\pi r^2 \rho_0}$$

$$w(r) = \frac{\rho(r)}{\rho_0} \quad (2.3)$$

often called the 'reduced radial distribution function' and the "pair correlation function" respectively, where  $\rho_0$  is the average atomic density. Theoretical curve of the radial distribution function as a function  $r$  is shown in Fig -2.1

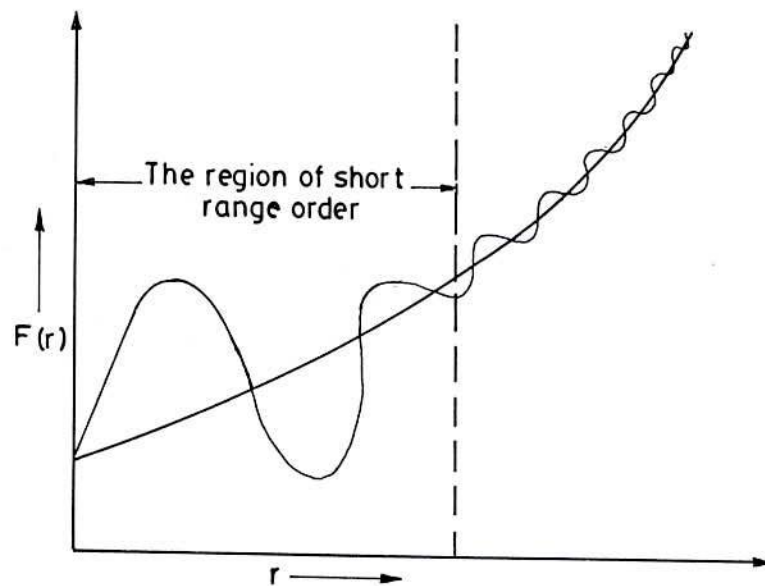


Fig-2.1 Short range order as a function of radial distance.

Amorphous solids can be considered as a super cooled liquid. A metallic glass is distinct from a liquid or a solid, because of its deviation from thermodynamic equilibrium, while both a melt and its corresponding crystalline phase have minimum free energy, an amorphous materials because of its non equilibrium state is at a higher values of free energy. Free energy as a function of temperature for a crystalline solid, an amorphous solid and a liquid is shown in Fig-2.2

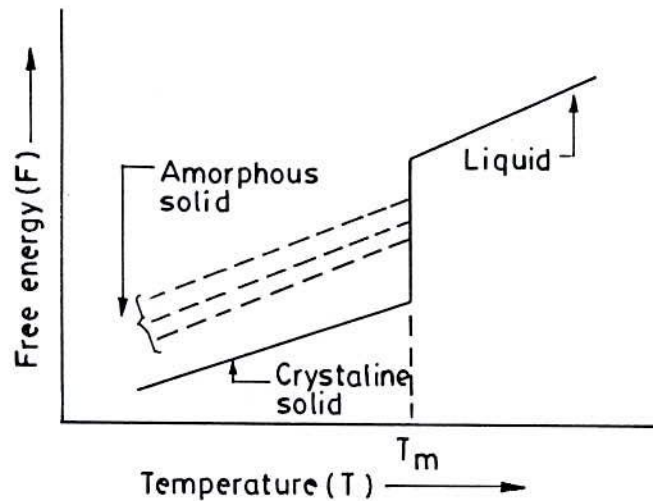


Fig-2.2 Free energy versus temperature curves.

Fig-2.3 shows the reduced glass transition temperature  $\tau = \frac{T_g}{T_m}$  for amorphous solids compared to crystalline solids. It is to be noted that for higher values of  $\tau$  only glass formation is possible.

When a melt is cooled too rapidly, its viscosity and relaxation time increase to the point where the internal equilibrium can no longer be maintained and the equilibrium configuration become inaccessible.

Two ways of solidification

- (i) Crystallization process and
- (ii) By increasing viscosity

Mechanical hardness of the condensed mater is dependent on the viscosity such that although amorphous structurally resemble a liquid state, their viscosity become comparable to that of a solid and this determines the stability of amorphous materials. Fig-2.4 represents the variation of viscosity of amorphous materials with temperature.

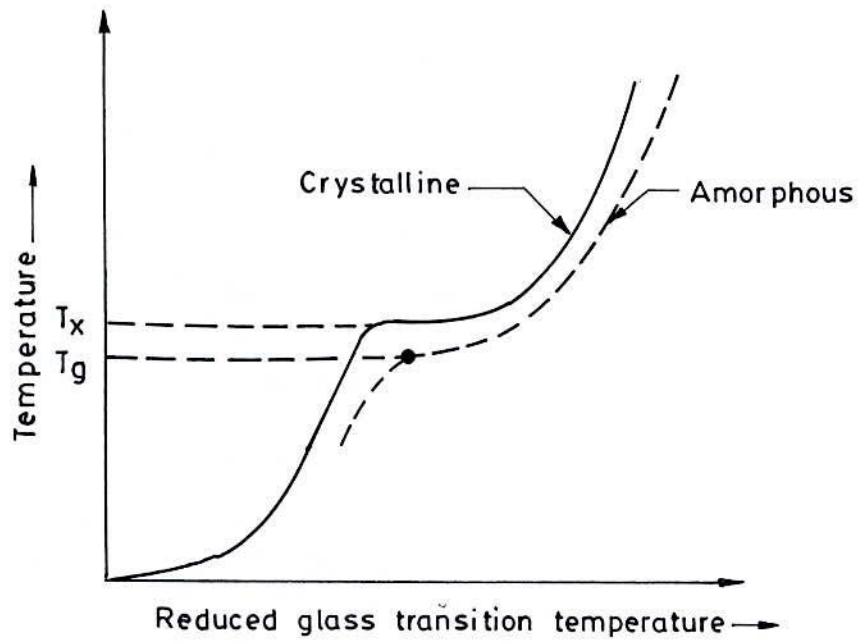


Fig-2.3 Glass formation as a function of reduced glass transition temperature.

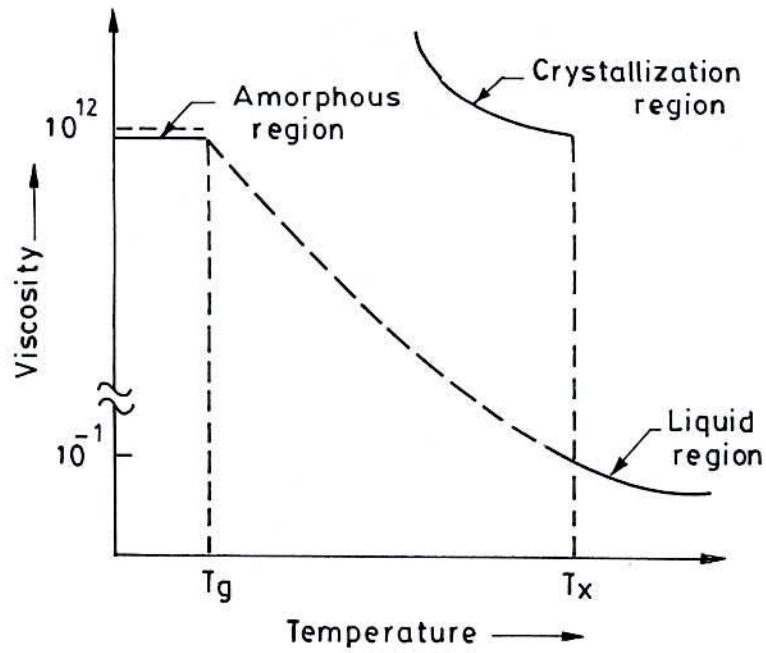


Fig-2.4. Viscosity versus Temperature curve.



### 2.3 Conditions for Forming Amorphous Material

It is very difficult to get pure metals in the amorphous state. It is necessary to add glass-forming materials to pure metals or alloys to get the amorphous state and to bring to the cooling rate within a reasonable rate. Usually around 20% of glass forming materials like B, Si, P, C etc, which have atomic radii relatively small compare to these of metallic atoms and the glass forming atoms occupy the voids left between the bigger atoms of metals when they are closely packed. It can be showed that when there is random close packing of hard spheres there is about 20% voids created between these atoms. The glass forming materials also reduces the melting point of the alloys and there by the separation between the glass forming temperature and the crystallization temperature is reduced. In fact  $T_g / T_m$  which is called the reduced glass transition temperature is an important parameter determining the glass forming tendency of an alloy.

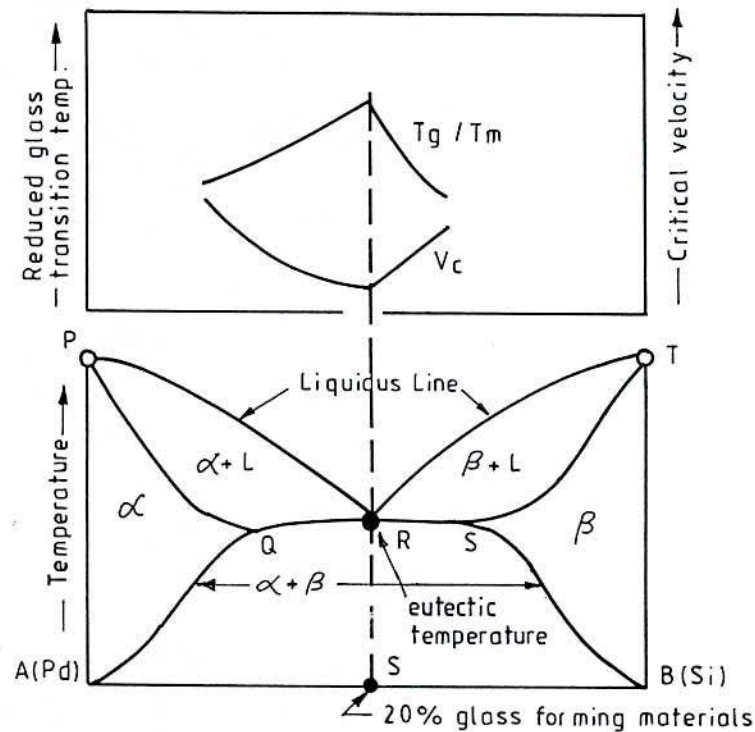


Fig-2.5 Compositional dependence of melting point.

The more complex an alloy is greater is the possibility of forming the amorphous state. This is because the arrangement of the atoms in the crystalline form of complex system takes more time, which means a greater relaxation time. The presence of glass forming materials contributes to this complexity and thereby increase the relaxation time. The stability of a metallic glass is also increased due to the presence of the glass forming material. Since as metallic glass is in a metastable state the stability with respect to temperature is determine by the local potential barrier produced by the disordered state of the amorphous material. When  $T_g/T_m$  is large the cooling rate needed for glass formation may be reduced, this mean that critical velocity of the copper disk can be reduced. The dependence of reduced glass transition temperature and the phase diagram indicating the dependence of melting point on composition of the melt is shown in Fig-2.5.

To increase the stability it is necessary to introduce some atoms of B, Si, or P (i. e. atoms with smaller radius) in the matrix. From statistics we know that the amorphous material has a porosity of 20% on the average therefore  $TM_{80}M_{20}$  [M =B, P, Si, C etc=20% at atomic) is generally introduced to form a good amorphous marital. From Fig-2.6 it is observed that the minimum linear

Velocity of the drum is around 10m/min for preparation of an amorphous ribbon by melt spinning technique.

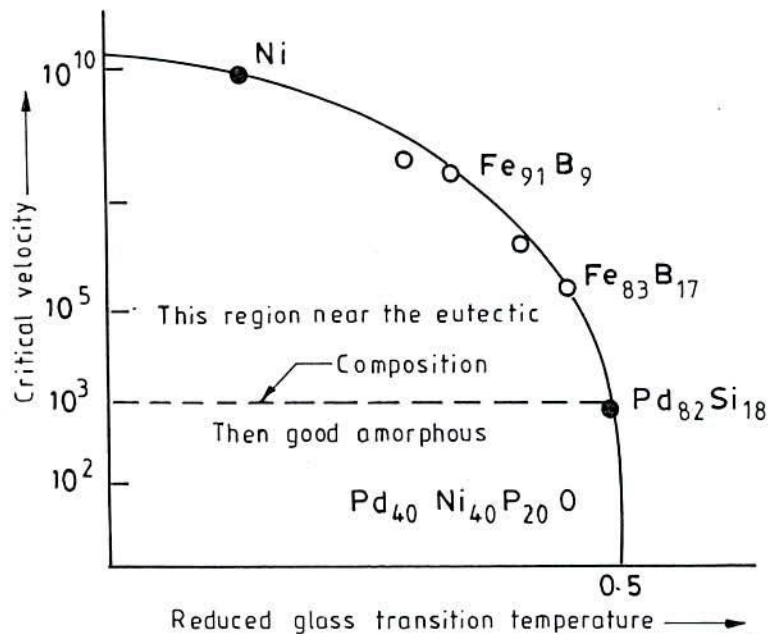


Fig2.6 Experimental values of critical velocity versus reduced glass transition temperature.

## 2.4 Conditions Necessary for Preparing Amorphous Materials

In terms of viscosity and diffusion Co-efficient we can find the condition for formation of glass.

- i) For metals atomic bonding is metallic and the viscosity is lower than the diffusion co-efficient and mobility high.
- ii) In the case of amorphous materials viscosity is very high and the mobility and the diffusion co-efficient is low. Atomic bonds tends to be covalent-as in the case of silicate ( $\text{SiO}_2$ ).

## 2.5 Preparation Technique of Amorphous Ribbons

There are various techniques in use to determine whether a particular metallic alloy in amorphous, i.e. consisting of an atomic arrangement which has no long range periodicity. Amorphous materials such as common glasses and plastics are familiar articles of use to everyone. These are usually prepared by the direct solidification from the melt since they require easily attainable cooling rates to inhibit crystallization. All of the techniques to be described result in effective cooling rates orders of magnitude faster than used for conventional silicate glasses or for casting of ingots into models. These higher cooling rates are a necessary condition for achieving the amorphous state in metallic alloys. The different experimental techniques developed to produce amorphous metallic glass can be classified into two groups.

- i) The atomic deposition methods and
- ii) The fast cooling of the melt

### 2.5.1 The Atomic Deposition Methods

Deposition can be described in terms of whether the added atom is prevented from diffusing more than an atomic distance before it is fixed in position due to cooling and increased viscosity. The atomic deposition methods include condensation of a vapor on a cooled substrate by



- a) Vacuum deposition
- b) Sputter deposition
- c) Electro deposition
- d) Chemical deposition

### 2.5.2 The fast cooling of the Melt

For producing an amorphous state by any of the liquid quenching devices, the alloy must cool through the temperature range from the melting temperature ( $T_m$ ) to the glass transition temperature ( $T_g$ ) very fast allowing no time for crystallization. The factors controlling  $T_g$  and crystallization are both structural and kinetic. The structural factors are concerned with atomic arrangement, bonding and atomic size effects. These factors tend to have limited predictive value, and kinetic factors tend to be dominant. The kinetic factors as discussed by Turnbull D. <sup>(2.12)</sup> are the nucleation, crystal growth rate and diffusion rate compared to the cooling rate. The interest in this method stems from the wide variety of alloys that can be made as well as from the potential low cost of preparation. The pioneering work of Duwez P. *et al.* <sup>(2.13)</sup>, a number of devices have been reported for obtaining the necessary high quenching rates and for producing continuous filaments. The methods using the principle of fast cooling of melt techniques are:-

- i. The gun techniques
- ii. Single roller rapid quenching techniques
- iii. Double roller rapid quenching techniques
- iv. Centrifuge and rotary splat quencher techniques
- v. Torsion catapult techniques
- vi. Plasmat-jet spray techniques
- vii. Filamentary casting techniques
- viii. Melt extraction techniques
- ix. Free jet spinning techniques
- x. The melt spinning techniques

Although the different methods used in preparing amorphous metallic ribbons are mentioned here, only the single roller rapid quenching technique, which was used to prepare the specimens for the present work, will be discussed.

### 2.5.3 Rapid Quenching Method

As shown in a schematic diagram in Fig.2.7, the rapid quenching technique apparatus consists mainly of a copper roller, an induction heater and a nozzle. The roller was driven by a variable speed motor via a tooth belt. The angular velocity was 2000 rev/min. Use of log wheel rotation enable us to vary the surface velocity in the range 20 to 30 m/sec. The diameter of the copper roller was 10cm. The use of copper for the roller material was chosen for its good conductivity and mechanical softness, which allowed cleaning and polishing to be carried out easily. For room temperature work, it showed no contamination of the ribbon from the roller material and the careful preparation of the surface was more important than the material of the roller.

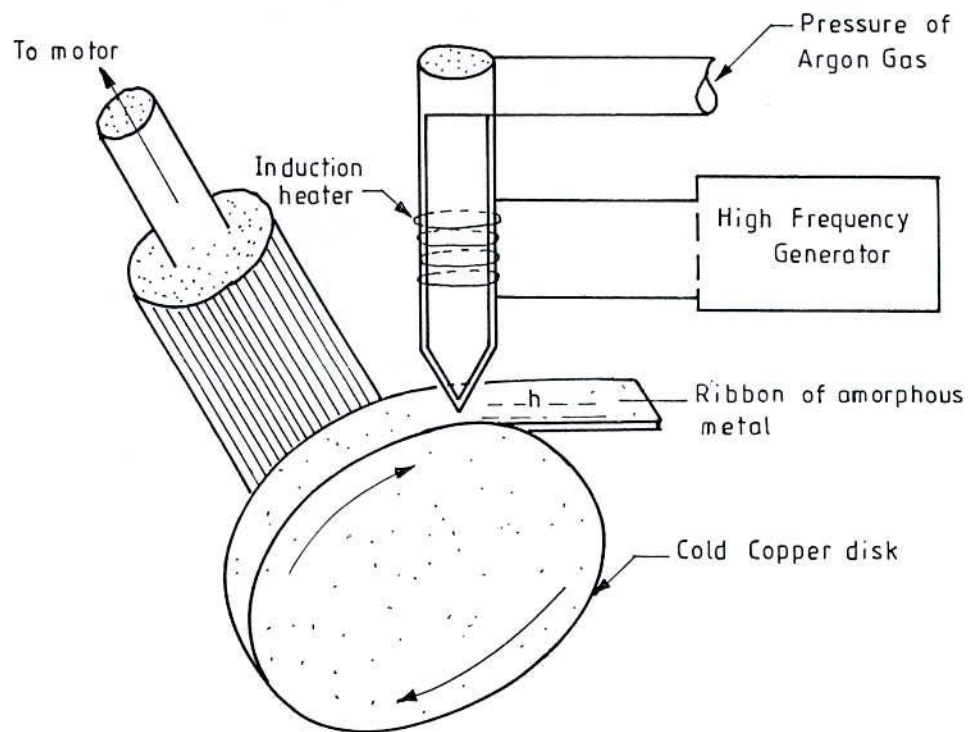


Fig: 2.7. Thin layer of molten alloy intimate contact with the outer surface of metallic rotor is quenched in to amorphous.

In this process one has to consider that vibration of the roller should be well below the high frequency vibration of the melt puddle to avoid any influence of it on the geometry and uniformity of the ribbon. One has to be careful and see that the ribbon does not remain in contact with the surface of the roller for a whole revolution and be hit, from the back. A bigger diameter is thus preferred for the roller. The induction heater coil is made of hollow copper tubing, which is cooled simultaneously by circulating water through its inner hole. The shape and diameter of the induction heater as also its winding is to be adjusted to produce proper temperature gradient. This is to avoid, sudden cooling of the melt in its way out of the crucible and blocking the nozzle, the quartz tubing having outer diameter 20mm which is narrowed down conically to 1mm with a hole for the nozzle 0.1 to 0.2mm.

The nozzle geometry is selected to minimize the contraction in the cross-sectional area of the molten metal as it leaves the nozzle orifice. Quartz tube is suitable for repeated use in several successful runs and should be transparent to make the melting process visible. It should withstand the sudden fast changes in temperature.

## **2.6 Experimental details of the preparation of Amorphous ribbon**

The amorphous ribbons are prepared in a furnace in an argon atmosphere (0.2 to 0.3 atms). The buttons prepared are about 50 grams each. Care is taken to ensure thorough mixing and homogeneity of the alloy composition, by turning over and remelting each button few times. The mother alloys, which are formed in the form of buttons in a furnace by sudden cooling and is then cut in to small pieces and is introduced in the quartz tube. The quartz tube is connected from the top by rubber "O" ring and metal rings to the argon cylinder through a valve and pressure gauge.

After proper cleaning of the roller surface and adjusting its speed to the desired value, as measured by stroboscope, the induction furnace is powered using high frequency generator. When the melting temperature is reached as observed through a protective spectacle, the injection pressure is applied by opening the pressure valve. To avoid the turbulence of the wind, arising from the high speed of the roller in disturbing the melt puddle, cotton pad and metallic shield are usually used just beneath the roller. To



avoid oxidation of the ribbon during its formation an inert atmosphere can be created around the roller by a slow stream of helium gas.

The speed of the roller, the volumetric flow rate, the orifice diameter, the substrate orifice distance, the injection angle etc, are adjusted by trial and error to get the best result in respect of the quality and the geometry of the ribbons.

### 2.6.1 Important factors to control the thickness of ribbons are

- i) Rotating speed
  - a) Angular velocity = 2000rev/min. and
  - b) Surface velocity = 20m/s.
- ii) Gap between nozzle and rotating copper drum (h) = 100 to 150  $\mu\text{m}$
- iii) Oscillation of the rotating copper drum both static and dynamic have maximum displacement 1.5 to 5  $\mu\text{m}$
- iv) Pressure = 0.2 to 0.3 argon atmosphere
- v) Temperature of metals  $T_m \sim 1500^\circ\text{C}$

The temperature did not exceed  $1800^\circ\text{C}$  otherwise quartz tube would be melt.

- vi) Stability was ensured for the drop in the surface of drum.

### 2.7 Factors Contributing to Glass Formation

There are three interrelated factors that determine glass-forming tendency. These are thermodynamic conditions that favour the liquid phase relative to the crystalline phase, the kinetic conditions that inhibit crystallization and the process factors that arise due to experiential conditions.

The thermodynamic factors for glass formation are liquidus temperature  $T_m$  at which the alloy melts, the heat of vaporization and the free energy of all the phase that arise or could potentially arise during solidification process. Viscosity of the melt, the glass transition temperature  $T_g$  and the homogeneous nucleation rate belongs to kinetic parameters. The glass transition temperature is defined as the temperature at which the super cooled liquid takes on the rigidity of a solid or more specifically at which the viscosity approaches 15 poise.

Processing parameters are the cooling rate, the heterogeneous nucleation rate and the super cooling temperature interval. The temperature of the glass transition is slightly dependent on the cooling rate. At each cooling rate the glass will freeze in a different state of internal energy. This shown in Fig-2.8.

At the melting point  $T_m$ , the enthalpy  $H$  of a crystal includes latent heat of fusion due to long range order. In the case of rapid cooling the melt the free energy decreases since long range order do not take place, thus leaving the system at a higher energy state. Heat treatment, relaxation and stability are thus important considerations in metallic glass. The glass-forming tendency also arises from as size difference between the constituent elements. It appears that appreciable size difference between the components in the glassy alloy is a necessary condition for ready glass formation.

A single parameter that expresses glass-forming tendency is the ratio of the glass transition temperature to the melting temperature defined as reduced glass transition temperature

$$\tau = \frac{T_g}{T_m} \quad (2.4)$$

Higher values of  $\tau$  obviously favour glass formation. For metallic glass to be formed by rapid cooling,  $\tau$  should be greater than 0.45 by Chen H.S. <sup>(2.14)</sup>. Based on alloy composition here are two major groups that rapidly form glasses. In one of these groups the metal is from Fe, Co, Ni, Pd or Pt and the metalloid is B, C, Si, Ge or P. These metallic glasses constitute soft amorphous magnetic materials. Our working sample prepared shown by table-1

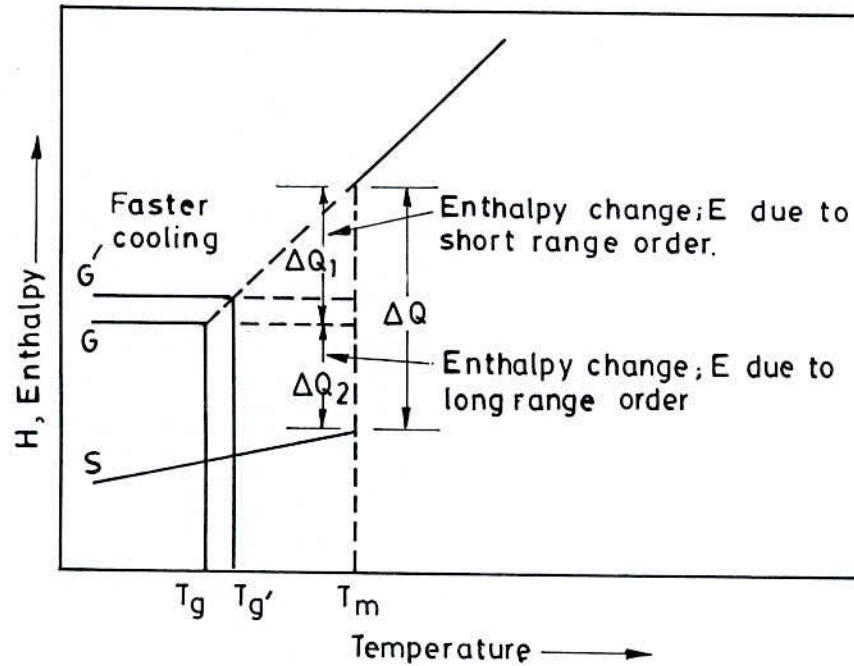


Fig: 2.8. Temperature dependence of enthalpy  $H$ ,  $G$  and  $G'$  corresponds to glass and  $S$  corresponds to crystalline state.

Table 2.1: Thickness of Co-and Co-Fe-based samples

Co-based ribbons	Thickness ( $\mu\text{m}$ )
$\text{Co}_{72}\text{Fe}_8\text{Si}_{10}\text{B}_{10}$	$24 \mu\text{m}$
$\text{Co}_{74}\text{Fe}_6\text{Si}_{10}\text{B}_{10}$	$26 \mu\text{m}$
$\text{Co}_{76}\text{Fe}_4\text{Si}_{10}\text{B}_{10}$	$26 \mu\text{m}$
$\text{Co}_{78}\text{Fe}_2\text{Si}_{10}\text{B}_{10}$	$28 \mu\text{m}$
$\text{Co}_{80}\text{Si}_{10}\text{B}_{10}$	$21 \mu\text{m}$



## 2.8 Examining the Amorphousity

The amorphousity of all the ribbons have been confirmed by X-ray diffraction using  $Cu - K_{\alpha}$  radiation. Representative ribbons were found to be amorphous as shown in Fig-2.9.

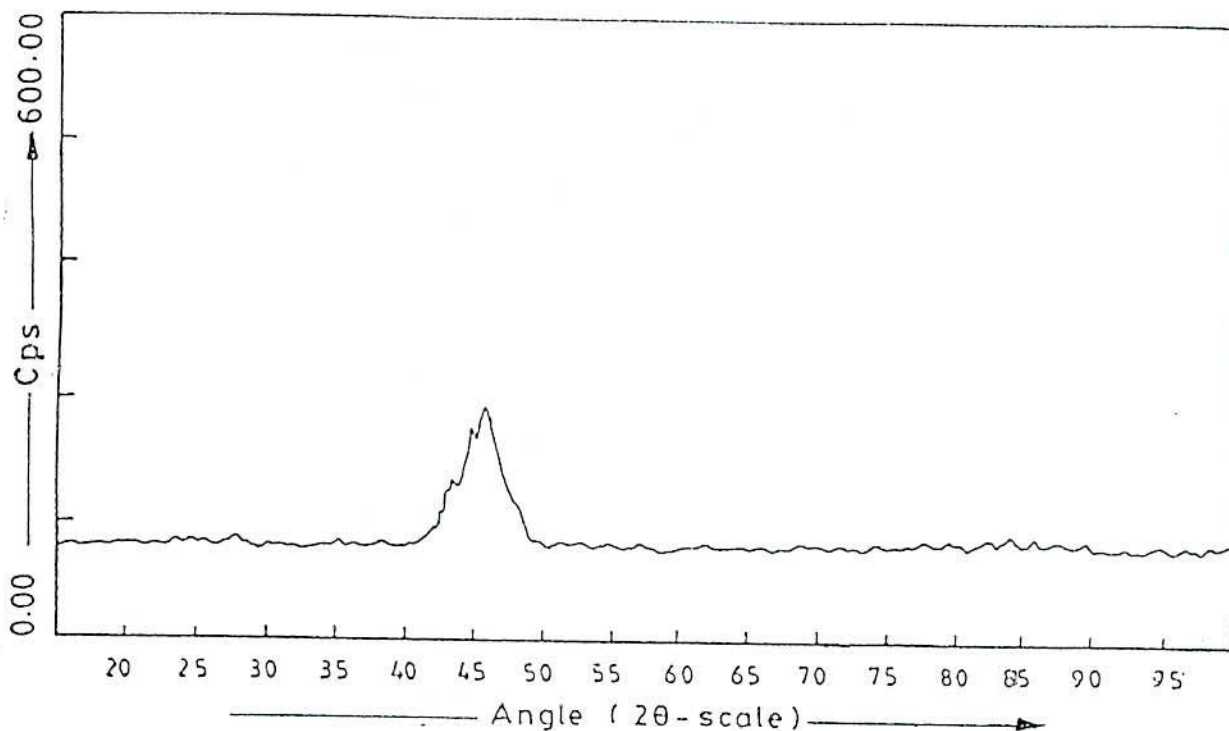


Fig-2.9. X-ray diffraction pattern from the top surface of the amorphous ribbon with composition  $Co_{78}Fe_2Si_{10}B_{10}$ .

The ribbons showed broad diffraction on maximum and no low angle scattering. These ribbons were also ductile and those cases for which low angle scattering appear and the broad diffraction peak are subdued there is some presence of micro crystalline phase. These could be removed if the speed of the roller was increased. The thickness of an amorphous is controlled by the liner speed of roller, the gap between the nozzle and the rotating drum which was about 1.5 to 5  $\mu m$ , oscillation of the drum, both static and dynamic, pressure and temperature of the melt and the stability of the drop on the surface of the drum. The nature of the broad diffraction peak as observed is shown in Fig-2.9.

## **CHAPTER- 3**

## **THEORETICAL ASPECTS**

- 3.1. Stability of Amorphous Alloys
  - 3.1.1. Structural relaxation of amorphous alloys
  - 3.1.2. Characteristics of the glass transition temperature
- 3.2. Magnetization of the Amorphous ribbons
  - 3.2.1. Annealing effects of amorphous alloy
- 3.3. Initial Permeability of Amorphous Ribbons
  - 3.3.1. Theories of Permeability
  - 3.3.2. Wall Permeability
  - 3.3.3. Rotational Permeability
  - 3.3.4. Losses

### 3 THEORETICAL ASPECTS

#### 3.1 Stability of Amorphous Alloys

Amorphous alloys are in a metastable state and tend to transform into stable crystalline phases. There are three kinds of stability of significance for amorphous magnetic ribbons:

- i) Their resistance to the initiation of crystallization.
- ii) Structural relaxation effects and
- iii) The relaxation or reorientation of directional order.

At temperatures below the crystallization temperature, structural relaxation effects take place and are caused by atomic rearrangements. The formation and resultant stability of amorphous alloys are important topics both theoretically and technologically. Which has been treated by turnbull D.<sup>(3.1)</sup> and Takayama S.<sup>(3.2)</sup> from thermodynamic view point. The ability of an alloy to be quenched into the glassy state is generally measured by the magnitude of the quantity

$$\Delta T_g = T_m - T_g \quad (3.1)$$

where  $T_m$  and  $T_g$  are the melting and glass Temperature respectively. In a similar manner the stability of the glass after formation is generally measured by the magnitude of the quantity.

$$\Delta T_x = T_x - T_g \quad (3.2)$$

where  $T_x$  is the temperature for the onset of crystallization. As the temperature decreases from  $T_m$  the rate of crystallization will increase rapidly but then fall rapidly as the temperature decreases below  $T_g$ . Thus if one quenched a molten alloy rapidly enough to a temperature below  $T_g$  a quasi – equilibrium amorphous phase is obtained. There is no direct relation between the cause of formation and the resultant stability of an amorphous



alloy. The amorphous alloy composition most favorable for glass formation is near the eutectic, the deeper the eutectic the better is the glass forming ability as noted by Cohen M. H. and Turnbull D.<sup>(3.3)</sup>. At eutectic point the liquid is particularly stable against crystallization. The crystallization is associated with nucleation and growth processes<sup>(3.3-3.6)</sup>. Since the formation of an amorphous alloy depends on the absence of long range order, change of composition is expected to affect  $T_g$  and  $T_x$ . This is because, the long range ordering of atoms depends on the free energy difference between the crystalline state and the amorphous state. The transition to the crystalline state is accompanied by an exothermic heat effect-giving rise to a sharp peak in the temperature dependence of the exothermic heat. The change of composition affects the growth kinetics in a complicated way, which can only be determined experimentally. Therefore, differential thermal analysis (DTA) is a widely used technique to study thermally induced transformations in amorphous alloys and to determine  $T_g$  and  $T_x$ . The magnitude of  $T_g$  and  $T_x$  are very different for amorphous materials and depend strongly on composition. The amorphous alloys exhibit a pronounced dependence on composition, the overall  $T_x$  values remain high. This applies to most of the alloys containing glass formers, leading to a high stability of these alloys in the room temperature range, which is of importance for technical applications.

The dependence of  $T_x$  on the heating rate  $S = \frac{dT}{dt}$  can be used to determine the activation energy of crystallization<sup>(3.7)</sup>. Considering the fraction  $x$  of amorphous material transformed into the crystalline state in time  $t$  and at temperature  $T$ , one obtains for the first-order rate process<sup>(3.8-3.9)</sup>.

$$\left( \frac{\delta x}{\delta t} \right)_T = K(1-x) \quad (3.3)$$

For thermally activated process, the rate constant  $K$  obeys an Arrhenius type of equations

$$K = K_0 e^{-\left( \frac{\Delta E}{RT} \right)} \quad (3.4)$$

Where  $K_o$  is a constant and  $\Delta E$  is the activation energy. Combining eq<sup>n</sup>(3.3) and eq<sup>n</sup>(3.4) and using  $dx = \left(\frac{\delta x}{\delta t}\right)_T dt + \left(\frac{\delta x}{\delta T}\right)_t dT$  with  $\left(\frac{\delta x}{\delta T}\right)_t dt \cong 0$ , one obtains

$$\frac{dx}{dt} = K_o(1-x)e^{-\left(\frac{\Delta E}{RT}\right)} \quad (3.5)$$

At the peak of the exothermic heat, the change of the reaction rate  $\frac{d^2x}{dt^2} = 0$ , yielding with  $T=T_x$ ,

$$K_o e^{-\left(\frac{\Delta E}{RT_x}\right)} = \left(\frac{\Delta E}{RT_x^2}\right) S \quad (3.6)$$

$\Delta T_x$  for the stability of amorphous alloys as given by eq<sup>n</sup>(3.2) and is obtained from DTA. The values of  $\Delta E$  also appear to correlate well with the number of atomic species in the alloy; the more complex the alloy the greater is  $\Delta E$ . Similar correlation between thermal stability as measured by  $\Delta T_x$  and  $\Delta E$  appears to small.

From the measured data of the heating rate ( $S$ ) and the respective crystallization temperature ( $T_x$ ), the activation energy can be deduced from the slope of a plot of  $\ln\left(\frac{T_x^2}{S}\right)$  versus  $\frac{1}{T_x}$ . Eq<sup>n</sup> (3.6) can be derived from transformation theory, where  $\Delta E$  is the activation energy for viscous flow, and other terms have been omitted because they have an insignificant temperature dependence in this region of temperature. The values of  $\Delta E$  also appear to correlate well with the number of atomic species in the alloy; the more complex the alloy the greater is  $\Delta E$ .

### 3.1.1 Structural Relaxation of Amorphous Alloys

The structure of amorphous alloys is temperature dependent due to its metastable state. Therefore, temperature treatments tend to change the atomic arrangement. Annealing at temperatures below the glass or crystallization temperature is thus

associated with a change of various properties which depends on that particular annealing time and temperature<sup>(3.10-3.11)</sup>. Two ways of structural relaxation

- i) Reversible relaxation phenomena are associated with different effects and properties such as the field induced anisotropy, isothermal changes in the Curie temperature, electrical resistivity, elastic constant etc.
- ii) The reversible relaxations effects occur even at very low temperature while the irreversible processes take place at higher temperatures as compared to the glass or crystallization temperature. Generally three typical effects are observed: (a) reversibility (b) 'Crossover' effects involving a crossover of the changes of a property versus annealing time,  $t_a$ , for two different annealing temperatures and (c) The presence of 'ln  $t_a$ ' kinetics: First approaches to account for these effects utilize an activation energy being linearly related to the instantaneous magnitude of the measured property<sup>(3.12)</sup> on an discrete spectrum of activation energies<sup>(3.13)</sup>. Another new approach based on a continuous spectrum of relaxation process<sup>(3.14 - 3.15)</sup>. Then, the total measured change of a property can be expressed by Gibbs M. R. *et al*<sup>(3.14)</sup> and Fish G. E.<sup>(3.15)</sup>

$$\Delta P(t) = \int_E C(E)q(E, T_a, t_a) dE \quad (3.7)$$

where  $q(E, T_a, t_a)$  in the case of first order kinetics is of the form

$$q(E, T_a, t_a) = q_o(E, T_a) \left\{ 1 - \exp \left[ -\nu t_a e^{-\left(\frac{E}{kT_a}\right)} \right] \right\} \quad (3.8)$$

provided each process is thermally activated.  $C(E)$  is the measured property change if only one such process having an activation energy  $E$  is thermally activated per unit volume of the material.  $q(E, T_a, t_a)$  is the number density of processes of the activation energy  $E$  which have contributed to the relaxation after annealing time  $t_a$ .  $C(E) q(E, T_a, t_a)$  thus is the property change related to relaxation process having activation energies in the range  $E$  to  $E + dE$ . The parameter  $\nu$  appearing in eq<sup>n</sup> (3.8) is the frequency factor. In



the case of one isothermal annealing experiment and where  $q(E, T_a, t_a)$  is approximated by a step function <sup>(3.16)</sup> with  $q(E, T_a, t_a) = 0$  for  $E < E_o$ , the property change is given by

$$\Delta P = C_o(E)q_o(E_o, T_a)KT_a \ln(\nu t_a) \quad (3.9)$$

$$\text{Where } E_o = KT_a \ln(\nu t_a) \quad (3.10)$$

representing the typical  $\ln t_a$  kinetics.

Irreversible changes are associated with a reduction in volume <sup>(3.17)</sup>, where the kinetics of the variation in linear dimensions. These changes in volume involve changes in the radial distribution function and, thus, can be studied by diffraction methods. Also diffusivity and viscosity changes with annealing temperature <sup>(3.18)</sup>. Any structural relaxation affects the local electron density and thus gives rise to changes in the magnetic properties.

### 3.1.2 Characteristics of the Glass Transition Temperature

Glass transition temperature ( $T_g$ ) occurs when the timescale of molecular rearrangements are too long for equilibrium to be maintained.

- i)  $T_g$  means the timescale of the experiment matters.
- ii) A high frequency/short timescale experiment allows less long for equilibrium to be established – even for an identical cooling rate.
- iii) So NMR (high frequency technique  $10^{15}$ Hz) always measures a higher  $T_g$  than DTA (Differential thermal analysis, 1Hz).
- iv) In the glass itself, entropy is similar to the crystal, and originals in vibrational modes which are still present.
- v) Long range translational motions are frozen out. By the temperature  $T_g$  Configurational relaxation (including translational motion) are frozen out, but vibrational relaxations are still in equilibrium.
- vi)  $T_g$  decreases as melt cooled more and more slowly.
- vii) When the timescale of the experiment and the configurational relaxation time coincide, begin to see departure from equilibrium.

- viii) The timescale for configurational relaxation will be related to rotational or translational diffusion co-efficients.
- ix) Operational definition of  $T_g$  is when the viscosity of the super cooled liquid exceeds  $10^{13}$  NSm<sup>-2</sup>. Where as in the liquid there is an Arrenhivs type with a Boltzmann factor containing an activation energy.

### 3.2 Magnetization of the Amorphous Ribbons

The theoretical treatment of spin ordering in amorphous solids is quite complex. The topological disorder on the amorphous alloys affect the magnetic moment of the transition metal atoms, because of the change of environment of each magnetic atom. The exchange integral also varies at each point because of the varying interatomic distance and the overlap of the electronic wave functions. The third factor determining the magnetization processes is the single ion magnetocrystalline anisotropy, which also changes because of the changing crystalline field. However, the magnetization of amorphous alloy is computed by introducing some drustic simplifying assumptions which are applicable in regular crystalline lattices.

The saturation magnetization of a material at a temperature of 0 K is one of its basic properties. Measurements are usually expressed as average moment per magnetic atom in units of the Bohr magneton,  $\mu_B$ , or as specific saturation magnetization for the amorphous alloy,  $\sigma_s$ , in units for Am<sup>2</sup>/kg. The moments of most amorphous alloys are lower than those of the pure crystalline transition metal which they contain. However, the direct effect of the structural disorder on the moments is very small. The moments are lower because of the change in the local chemical environment provided by the presence of the metalloids. The reduction is least in B- based glass and highest in P- based glass. The observed moments on TM-M glasses can approximately fitted to a formula<sup>(3.19)</sup>

$$\mu = \frac{(\mu_{TM} C_{TM} - C_B - 2C_{Sic} - 3C_p)}{C_{TM}}, \quad (3,11)$$

where  $\mu_{TM}$  is the magnetic moment of TM-M atoms, taken as 2.6, 1.6 and 0.6 respectively in Bohr magneton for Fe, Co and Ni. C's are respective concentrations. This

clearly demonstrates the charge transfer from metalloid to d-band of transition metal and seems to suggest that 1, 2 or 3 electrons are transferred from each of B, Si (C, Ge) or P atom. The relative number of electrons donated can be listed as -  $P_{13}C_7$  -  $S_{15}B_{10}$  -  $P_{16}B_6Al_3$  -  $P_{14}B_6$  -  $Si_9B_{13}$  -  $B_{20}$  based on the relative magnitudes of  $M_s$ .

The theoretical treatment of spin ordering in amorphous solids is a much more difficult problem than in regular crystalline lattices and has not been satisfactorily solved. If the molecular field approximation is used, even though its use is doubtful, the paramagnetic Curie temperature can be expressed as

$$T_c = \left[ \frac{2S(S+1)}{3K} \right] \sum_{ij} J_{ij}, \quad (3.12)$$

where  $S$  is the spin number,  $K$  is Boltzmann's constant and  $J_{ij}$  is the exchange interaction between atoms at the positions  $r_i$  and  $r_j$  and can be expressed in terms of the radial distribution function. The Curie temperature of amorphous transition metal-metalloid alloys are always found to be significantly lower than those of the pure crystalline transition metals. Reduction of  $T_c$  in the amorphous alloys appears to be largely the result of chemical composition and or chemical disorder. First approach to a unique constant exchange interaction between the magnetic atoms is assumed and the amorphous nature of the alloy is taken into account by calculating a random distribution of the local anisotropy field<sup>(3.20)</sup>. Another approach to treating this problem, a distribution of exchange integrals is assumed in order to reflect the structural fluctuations of exchange integrals is assumed in order to reflect the structural fluctuations in the amorphous alloy<sup>(3.21)</sup>. Both approaches predict that the  $M$  versus  $T$  curve will fall below that for the crystalline counterpart. Amorphous alloys should exhibit a structureless Mössbauer spectrum, contrary to the observed spectra. Thus the second approach is preferred of the various theories the molecular field approach (MFA) and mean field theories.



### 3.2.1 Annealing Effects of Amorphous Alloy

The amorphous structure represents a metastable state and thus any thermal treatment causes a continuous change of the atomic arrangement. Different processes can be distinguished:

- i) Corrosion and oxidation
- ii) Structural relaxation and
- iii) Crystallization

The latter describes the transition to the crystalline state and this process requires an activation energy of the order of 2.5 eV. The first two processes affect the structural, magnetic and electrical properties in a specific way <sup>(3.22)</sup>. The structurally sensitive properties like the compensation temperature, the uniaxial anisotropy, the coercivity or the conductivity thus are suitable parameters to investigate the time and temperature dependence of these processes. The oxidation and structural relaxation of magnetic glasses is less important because they exhibit an even higher corrosion resistance than the corresponding crystalline alloys <sup>(3.23)</sup>. However, annealing in a magnetic field leads to strong changes in the magnetic properties <sup>(3.24)</sup>.

The structural relaxation process can be described by a spectrum of activation energies according to the various atomic rearrangement possible in an amorphous material. However, the structural degradation causes only small changes in the magnetic and electronic properties as compared to the oxidation process that is associated with a very low activation energy. The structural disorder of magnetic amorphous ribbon gives rise to significant changes of the mechanical, electrical, magnetic and magneto-optical properties as compared to the crystalline counterparts. Therefore, amorphous Co-based ribbons are predominantly strong ferromagnets, although significant differences in the magnetic properties are observed for Co-based ribbons containing constant metalloids and other element like Fe. Two step annealing of magnetic moment variation was interpreted in terms of the magnetic valence model or the environment model. In both cases the experimental data were well described for certain classes of Co-based and Co-Fe-based amorphous ribbons.

### 3.3 Initial Permeability of Amorphous Ribbons

Amorphous Co-B-Si and Co-Fe-B-Si alloys are of great interest as soft magnetic materials for their static as well as dynamic applications. For application in small electronic device, the amorphous alloy have some what poorer losses and permeabilities than the conventional Fe-Ni alloys, but have better performance than the Fe-Co-B-Si and Fe-Si alloys in other respects many workers <sup>(3.25-3.26)</sup> have studied amorphous magnetic alloys for various applications. Fe-based magnetic alloys that have large magnetic flux density are usually used in the low frequency range, because of their inferior soft magnetic properties in the high frequency region compared to those of Co- based amorphous ribbons. The measurement of magnetic properties as a function of frequency and its analysis by means of the complex permeability formalism has recently led to the resolution of several aspects of the magnetization process <sup>(3.27-3.28)</sup>. The measurement of complex permeability gives us valuable information about the nature of the domain wall and their movements.

The  $\mu_i$  of the amorphous magnetic ribbons may be strongly affected by the presence of an electric current due to its heating effect, particularly in ac conditions. In dynamic measurements the eddy current loss is very important which occurs due to irreversible domain wall movements that are frequency dependent. A large number of possible mechanisms can contribute to the magnetic loss such as local variation of exchange energy, surface defects, compositional in homogeneities, anisotropy and magnetostriction<sup>(3.29-3.30)</sup>, whose relative values are determined by grain size, grain orientation and thickness of the sample. Thus the magnetic characteristic are rather different in step annealed specimens from those of as quenched amorphous ribbons. The present goal of most of the recent amorphous ribbons researches is to fulfill this requirement. But in this research, we apply these techniques to investigate the two step time annealing effects of various thermal treatments on Co and Co- Fe based amorphous ribbons. Before going into the complexity of initial permeability measurement, we discuss in short the theories and mechanism involved in frequency spectrum of initial permeability.

### 3.3.1 Theories of Permeability

The primary requirement is the highest possible permeability, together with low losses in the frequency range of interest. The initial permeability  $\mu_i$  is defined as the derivative of induction B with respect to the internal field H in the demagnetization state

$$\mu_i = \frac{dB}{dH}, H \rightarrow 0, B \rightarrow 0 \quad (3.13)$$

At microwave frequencies, and also in low anisotropic amorphous materials, dB and dH may be in different directions, the permeability then has a tensor character. In the case of amorphous materials containing a large number of randomly oriented magnetic atoms the permeability will be scalar, at low frequencies with

$$B = \mu_0(H + M) \quad (3.14)$$

and the susceptibility  $\chi = \frac{dM}{dH} = \frac{d}{dH} \left( \frac{1}{\mu_0} B - H \right)$

$$= \left( \frac{\mu_i}{\mu_0} - 1 \right) \quad (3.15)$$

The magnetic energy density

$$E = \frac{1}{\mu_0} \int H \cdot dB \quad (3.16)$$

For time harmonic fields  $H = H_0 \sin \omega t$ , the dissipation can be described by a phase difference  $\delta$  between H and B. In the case of permeability is namely define as the proportional its constant between the magnetic field induction B and applied intensity H;



$$B = \mu_i H \quad (3.17)$$

This naïve definition needs further sophistication's. If a magnetic material is subjected to an ac magnetic field as given below

$$B = B_0 e^{i\omega t}, \quad (3.18)$$

then it is observed that the magnetic flux density B experiences a delay. The delay is caused due to the presence of various losses and is thus expressed as

$$B = B_0 e^{i(\omega t - \delta)}, \quad (3.19)$$

where  $\delta$  is the phase angle and marks the delay of B with respect to H. The permeability is then given by

$$\begin{aligned} \mu_i &= \frac{B}{H} = \frac{B_0 e^{i(\omega t - \delta)}}{H_0 e^{i\omega t}} \\ &= \frac{B_0 e^{-i\delta}}{H_0} = \frac{B_0}{H_0} \cos \delta - i \frac{B_0}{H_0} \sin \delta \\ &= \mu' - i\mu'', \end{aligned} \quad (3.20)$$

$$\text{where } \mu' = \frac{B_0}{H_0} \cos \delta \text{ and } \mu'' = \frac{B_0}{H_0} \sin \delta \quad (3.21)$$

The real part  $\mu'$  of complex permeability  $\mu_i$  as expressed in eq<sup>n</sup> (3.20) represents the components of B which is in phase with H, so it corresponds to the normal

permeability. If there are no losses, we should have  $\mu_i = \mu'$  at very low frequency. The imaginary part  $\mu''$  corresponds to that part of B, which is delayed by phase angle  $90^\circ$  from H. The presence of such a component requires a supply of energy to maintain the alternating magnetization, regardless of the origin of delay.

It is useful to introduce the loss factor or loss tangent ( $\tan \delta$ ). The ratio of  $\mu''$  to  $\mu'$  as is evident from eq<sup>n</sup> (3.21), gives

$$\frac{\mu''}{\mu'} = \frac{\left(\frac{B_0}{H_0}\right) \sin \delta}{\left(\frac{B_0}{H_0}\right) \cos \delta} = \tan \delta \quad (3.22)$$

This  $\tan \delta$  is called the loss factor. The Q-factor or quality factor is defined as the reciprocal of this loss factor, i.e.

$$Q = \frac{1}{\tan \delta} \quad (3.23)$$

and the relative quality factor =  $\frac{\mu_i}{\tan \delta}$  (3.24)

The behavior of  $\mu'$  and  $\mu''$  versus frequency is called the permeability spectrum. The initial permeability of a ferromagnetic or ferromagnetic substance is the combined effect of the wall permeability and rotational permeability mechanisms.

### 3.3.2 Wall Permeability

The mechanism of wall permeability arises from the displacement of the domain walls in small fields. Let us consider a piece of material in the demagnetized state, divided into Weiss domains with equal thickness L by means of  $180^\circ$  Bloch walls shown

in fig-3.1. The walls are parallel to the Y, Z plane. The magnetization  $M_s$  in the domains is oriented alternately in the +Z or -Z direction. When field H with a component in the +Z direction is applied, the magnetization in this direction will be favoured. A displacement  $dx$  of the wall in the direction shown by the dotted lines will decrease the

energy density by an amount:  $\frac{2M_s H_z dx}{L}$

This can be described as a pressure  $2M_s H_z$  exerted on each wall. The pressure will be counteracted by restoring forces, which for small deviations may be assumed to be  $Kdx$  per unit wall surface. The new equilibrium position is then given by

$$d = \frac{M_s H_z dx}{L} \quad (3.25)$$

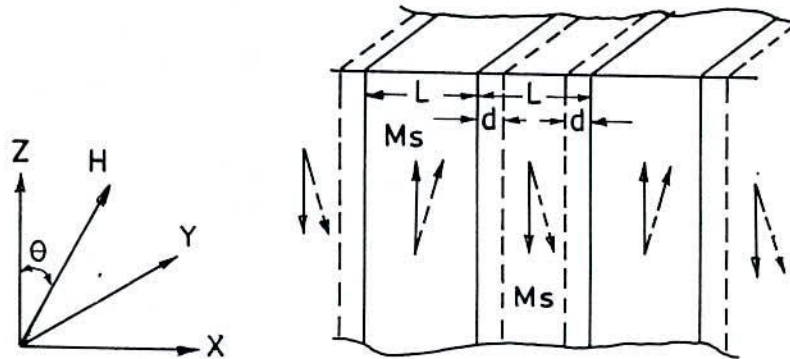


Fig.-3.1. Magnetization by wall motion and spin rotation.

From the change in the magnetization

$$\Delta M = \frac{2M_s d}{L} \quad (3.26)$$



The wall susceptibility  $\chi_w$  may be calculated. Let H make the angle  $\theta$  with Z direction.

The magnetization in the direction becomes

$$(\Delta M)_0 = \frac{2M_s d}{L} \cos \theta, \quad (3.27)$$

and with  $H_z = H \cos \theta$  and  $d = \frac{2M_s H_z}{K}$

We obtain

$$\chi_w = \frac{(\Delta M)_0}{H} = \frac{4M_s^2 \cos^2 \theta}{KL} \quad (3.28)$$

### 3.3.3 Rotational permeability

The rotational permeability mechanism arises from rotation of the magnetization in each domain. The direction of M can be found by minimizing the magnetic energy E as a function of the orientation. Major contribution to E comes from the crystal anisotropy energy. Other contributions may be due to the stress and shape anisotropy. The stress may influence the magnetic energy via the magnetostriction. The shape anisotropy is caused by the boundaries of the sample as well as pores, nonmagnetic inclusions and inhomogeneities. For small angular deviations  $\alpha_x$  and  $\alpha_y$  of M, where

$$\alpha_x = \frac{M_x}{M_s} \text{ and } \alpha_y = \frac{M_y}{M_s}, \quad (3.29)$$

from the equilibrium Z-direction may be expressed as

$$E = E_o + \frac{1}{2} \alpha_x^2 E_{xx} + \frac{1}{2} \alpha_y^2 E_{yy}, \quad (3.30)$$

where it is assumed that x and y are the principal axes of the energy minimum. Instead of  $E_{xx}$  and  $E_{yy}$ , the anisotropy field  $H_x^A$  and  $H_y^A$  are often introduced. Their magnitude is given by

$$H_x^A = \frac{E_{xx}}{2M_s} \quad \text{and} \quad H_y^A = \frac{E_{yy}}{2M_s}, \quad (3.31)$$

where  $H_x^A$  and  $H_y^A$  represent the stiffness with which the magnetization is bound to the equilibrium direction for deviations in the x and y directions, respectively. The rotational susceptibilities  $\chi_{r,x}$  and  $\chi_{r,y}$  for fields applied along x and y directions, respectively are

$$\chi_{r,x} = \frac{M_s}{H_x^A} \quad \text{and} \quad \chi_{r,y} = \frac{M_s}{H_y^A} \quad (3.32)$$

For cubic materials it is often found that  $H_x^A$  and  $H_y^A$  are equal. For  $H_x^A = H_y^A = H^A$  and a field H which makes an angle  $\theta$  with the Z direction as shown in fig-3.1. The rotational susceptibility,  $\chi_{r,c}$  in one crystallite becomes

$$\chi_{r,c} = \frac{M_s}{H^A} \sin^2 \theta \quad (3.33)$$

A polycrystalline material consisting of a large number of randomly oriented grains of different shapes, with each grain divided into domains in a certain way, the rotational susceptibility  $\chi_r$  of the material has to be obtained as a weighted average of  $\chi_{r,c}$  of each crystallite, where the mutual influence of neighboring crystallites has to be taken into account. If the crystal anisotropy dominates other anisotropies, then  $H^A$  will be

constant throughout the material, so only the factor  $\sin^2 \theta$  from eq<sup>n</sup>(3.25) has to be averaged. Snoek (3.34) assuming a linear averaging of  $\chi_{r,c}$  and found

$$\chi_r = \frac{M_s}{3H^A} \quad (3.34)$$

the total internal susceptibility

$$\chi = \chi_w + \chi_r = \frac{4M_s^2 \cos^2 \theta}{KL} + \frac{2M_s}{3H^A} \quad (3.35)$$

If the shape and stress anisotropies can not be neglected,  $H^A$  will be larger. Any estimate of  $\chi_r$  will then be rather uncertain as long as the domain structure, and the pore distribution in the material are not known. A similar estimate of  $\chi_w$  would require knowledge of the stiffness parameter  $K$  and the domain width  $L$ . These parameters are influenced by such factors as imperfection, porosity and crystallite shape and distribution which are essentially unknown.

### 3.3.4 Losses

The most important loss in ferromagnetic substance is the hysteresis loss. In the Rayleigh region where the amplitude of magnetization is very small, the loss factor due to the hysteresis loss depends on the amplitude of magnetic field. The physical origin of the hysteresis loss is eddy current or other damping phenomena associated with irreversible wall displacement or irreversible rotation magnetization.

The hysteresis loss becomes less important in the high frequency range, because of the wall displacement which is the main origin of hysteresis, is most damped in this range and is replaced by the rotation magnetization. The next important loss for ferromagnetic metal and alloys is the eddy current loss. Since a power loss of this type increases in proportion to the square of the frequency in the high frequency range. Magnetic after effect also given rise to a magnetic loss for which frequency



magnetization. This happens because of the insertion of a boron atom between iron atoms has a remarkable effect in changing the intensity of pseudo dipolar interaction between the iron atoms<sup>(3.32)</sup>.

At intermediate and high inductions, when Core losses are significant in applications, the total power losses are often expressed as the sum of a hysteresis loss and eddy current loss as

$$W = \eta B^{1.6} + eB^2 f^2, \quad (3.36)$$

when  $f$  is small, e.g  $<100$  Hz. At low induction,  $B$ , the hysteresis loss term is more nearly proportional to  $B^3 f$ . At high frequency, the losses are controlled predominately by eddy currents and are given by

$$W_e = \frac{\Pi t B^2 f^r}{(\mu \Omega)^{\frac{1}{2}}}, \quad (3.37)$$

where  $f$  varies from  $f^2$  at lower frequencies to  $f^{\frac{3}{2}}$  at higher frequencies,  $t$  is the thickness,  $\mu_i$  is the permeability and  $\Omega$  is resistivity. Loss results for both the amorphous and crystalline alloys show dependence given by

$$W \propto B^\beta f^\gamma \quad (3.38)$$

The values of the exponents  $\beta$  and  $\gamma$  vary in a given alloy after stress release, depending of the magnitude and direction of the induce anisotropy as described by Luborsky F.E. *et al.*<sup>(3.33)</sup>. The considerable improvement in losses as the result of annealing as a function of frequency.

## **CHAPTER 4:                   EXPERIMENTAL DETAILS**

- 4.1.     The Differential Thermal Analysis
  - 4.1.1.   Introduction
  - 4.1.2.   The Principle of Differential Thermal Analysis
  - 4.1.3.   Apparatus.
- 4.2.     Experimental setup for Measurement of Magnetization
  - 4.2.1.   The Principle of Vibrating Sample Magnetometer
  - 4.2.2.   Mechanical Design of the V.S.M.
  - 4.2.3.   Electronic Circuits of the V.S.M.
    - 4.2.3.1. Sensitivity limits
    - 4.2.3.2. Stability Tests Differential Measurements
    - 4.2.3.3. Vibration Amplitude.
    - 4.2.3.4. Image Effects
    - 4.2.3.5. Vibration Frequency
    - 4.2.3.6. Vibration Problems
  - 4.2.4.   High Temperature Magnetization Measurements
  - 4.2.5.   X-Y Recorder
  - 4.2.6.   Calibration of the V.S.M
    - 4.2.6.1 Calibration Data
- 4.3.0.   Experimental Techniques for Measuring Complex Permeability
  - 4.3.1.   Real and Imaginary Components of Complex Permeability
  - 4.3.2.   Preparation of the samples for permeability measurements
  - 4.3.3.   Frequency Characteristics of Amorphous Materials

## 4 EXPERIMENTAL DETAILS

### 4.1 The differential Thermal Analysis

#### 4.1.1 Introduction

The differential thermal analysis (DTA) is an important technique for studying the structural change occurring both in solid and liquid materials under heat treatment. These changes may be due to dehydration, transition, from one crystalline variety to another destruction of crystalline lattice, oxidation, decomposition etc. The principle of DTA consists of measuring the heat changes associated with the physical or chemical substance is gradually heated. This technique can also be used to identify magnetic ordering of amorphous ribbons. In order to discuss the possible applications of DTA in amorphous materials, let us briefly define the various temperature, that are useful in characterizing and amorphous alloys.

The glass transition temperature  $T_g$  is defined as the temperature at which the alloy passes from the “solid” to the “liquid” state. For our purposes, it is sufficient to describe  $T_g$  as the temperature at which atomic mobility is great enough to allow diffusive atomic rearrangement to occur in a matter of minutes. The crystallization temperature  $T_x$  defined as the temperature at which crystallization occurs with long range ordering and is usually determined by DTA technique by a heating rate of  $\approx 20^\circ\text{C}/\text{min}$ . Metallic glass ribbons usually are ductile in the ‘as- quenched’ condition, but may often be embrittled by exposure to elevated temperature. DTA measurements on as- cast ribbons where performed with increasing rates of  $10^\circ\text{C}/\text{min}$  to  $50^\circ\text{C}/\text{min}$  in argon atmosphere. Based on the Kissinger plots, we have evaluated the crystallization activation energy of  $T_g$  and  $T_x$  Phases. The DTA technique has been used in determining  $T_g$  and  $T_x$  of our amorphous ribbon with composition  $\text{Co}_{80-x}\text{Fe}_x\text{B}_{10}\text{Si}_{10}$  [ $x=0,2,4, 6 \& 8$ ].

#### 4.1.2 The Principle of Differential Thermal Analysis

The DTA technique was first suggested by chatelier H. Le <sup>(4.1)</sup> in 1887 and was applied to the study of clays and ceramics. DTA is the process of accurately measuring



the difference in the temperature between a thermocouple embedded in a sample and a thermocouple in a standard inert material such as aluminium oxide, while both are being heated at the uniform rate. The difference of temperature that arise due to the phase transition or chemical reactions in the sample involving the evolution of heat or absorption of due to exothermic reaction or endothermic reaction measured. The exothermic and endothermic reactions are generally shown in the DTA trace as positive and negative deviations respectively from the base line. DTA curves indicate a continuous thermal record of reactions occurring in a sample.

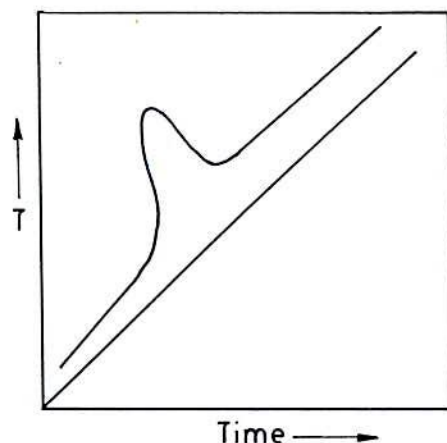


Fig- 4.1 (a) Heating curve of sample and reference substance.

When a sample and reference substance are heated or cooled at a constant rate under identical environment, their temperature difference are measured as a function of time and temperature as shown in Fig- 4.1 (a). The temperature of the reference substance, which is thermally inactive rises uniformly when heated while the temperature of the sample under study changes anomalously when there is a physical or a chemical change in it at a particular temperature. For an exothermic reaction there is a peak in the temperature versus time curve due to the additional heat supplied by the specimen accompanied by the reaction. When the reaction is over the sample temperature gradually catch up the temperature of the inactive specimen. The temperature difference  $\Delta T$  is detected, amplified and recorded by a peak is shown in Fig- 4.1 (b).

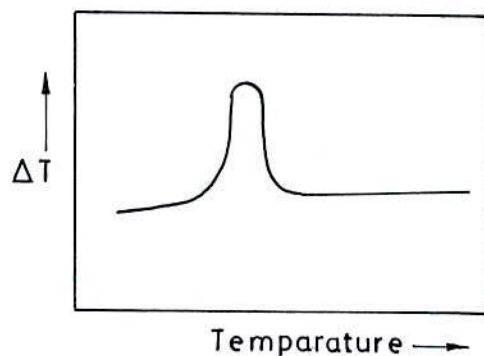


Fig- 4.1 (b) DTA curve.

For any endothermic reaction or change the active specimen absorbs heat which is reflected in the corresponding the trough in temperature versus time curve. The temperature in the sample holder is measured by a thermocouple, the signal of which is compensated for the ambient temperature and fed to the temperature controller. This signal is compared with the program signal and the voltage impressed to the furnace is adjusted. Thus the sample and reference substance are heated or cooled at a desired rate. The temperature in the sample holder is digitally displayed on the DTA measurements model TG/DTA 6300 and is also recorded on the recorder.

### 4.1.3 Apparatus

The apparatus for the differential thermal analysis consists of a thin walled refractory specimen holder made of sintered alumina with two adjacent cubical compartments of exactly the same size, 1 cm in length shown in Fig- 4.2. Of these one is for the reference inert material and the other for the test material, the compartments being separated by a 1 mm wall. The specimen holder is placed in the cavity of the heating block which is operated in the centre of the cylindrical refractory tube of an electrical furnace. This supplies a uniform heating rate. The furnace (9" × 6" × 9" deep) is packed with calcined china clay. The input of current into the furnace is secured through the secondary of a variac transformer, which controls the current. Fine chromelalumel wires (28 gauge) are used for thermocouple.

A cold junction is used for thermocouple leads and the emf is recorded almost continuously, while the temperature of the inert material is measured at 3 minute intervals. It is essential to use perfectly dry materials, as otherwise errors will be introduced in the analysis. Approximately 0.1 gm anhydrous alumina is used in the reference cup and the sample weights varies over a range 0.05 to 0.125 gm; depending on their peaked density. A heating rate of 10°C per minute of the furnace is conveniently kept, and this gives satisfactory results in most cases. A block diagram of DTA is shown in Fig- 4.3.

The thermal analysis runs generally for 1 to 1.5 hrs. Thermal analysis curves are obtained by plotting heating temperature and the difference between the temperature of the test and reference substances. From these plots the reaction temperature could be determined. Under standard conditions of the experiment; characteristic curves for different compositions of Co-based and Co-Fe-based amorphous ribbons.  $T_g$  and  $T_x$  points are indicated, by sharp exothermic peaks.



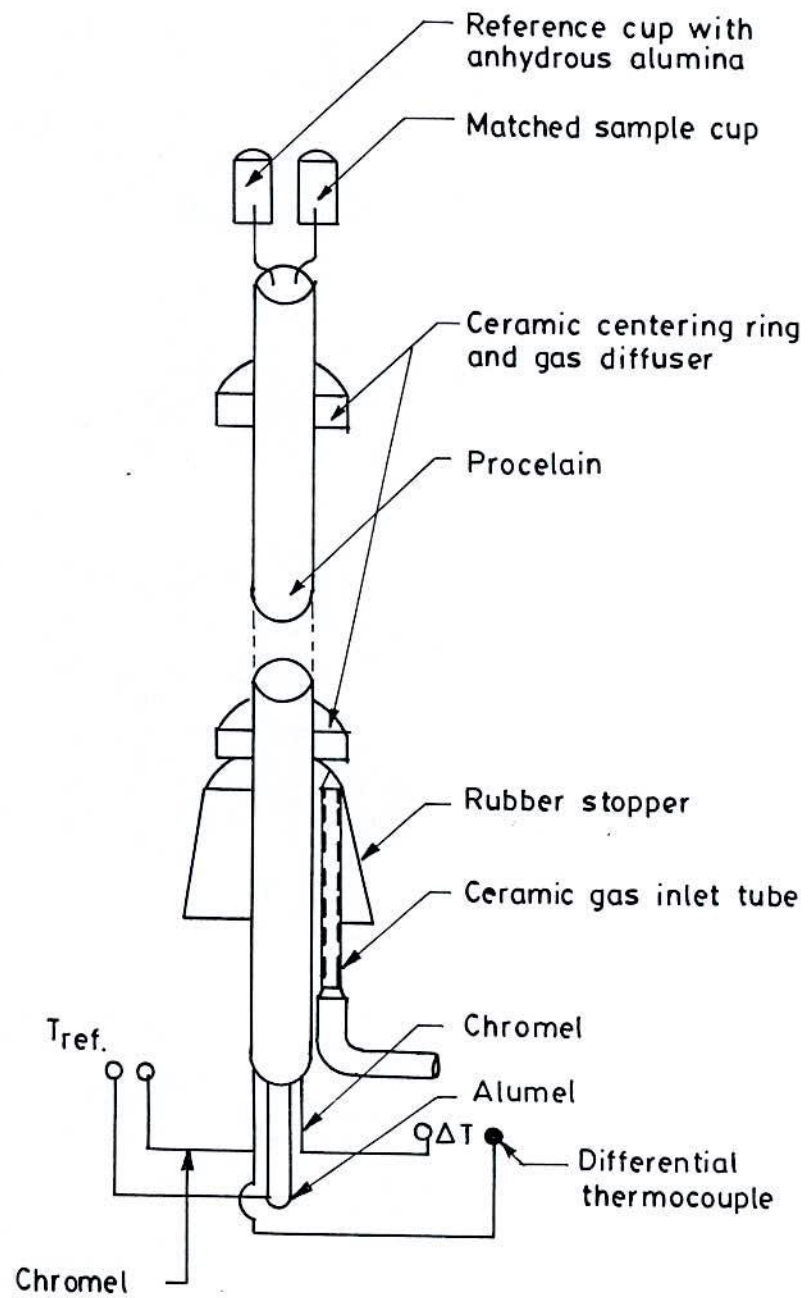


Fig- 4.2 DTA Thermocouple assembly.

All experiments are run at atmospheric pressure in continuous flow of a purified inert gas argon. Gases are normally purged into the furnace chamber at the lower end through a purification train in which oxygen and water are removed by heated copper wool and exhausted from the top into a condensate trap for collecting the condensable volatile products.

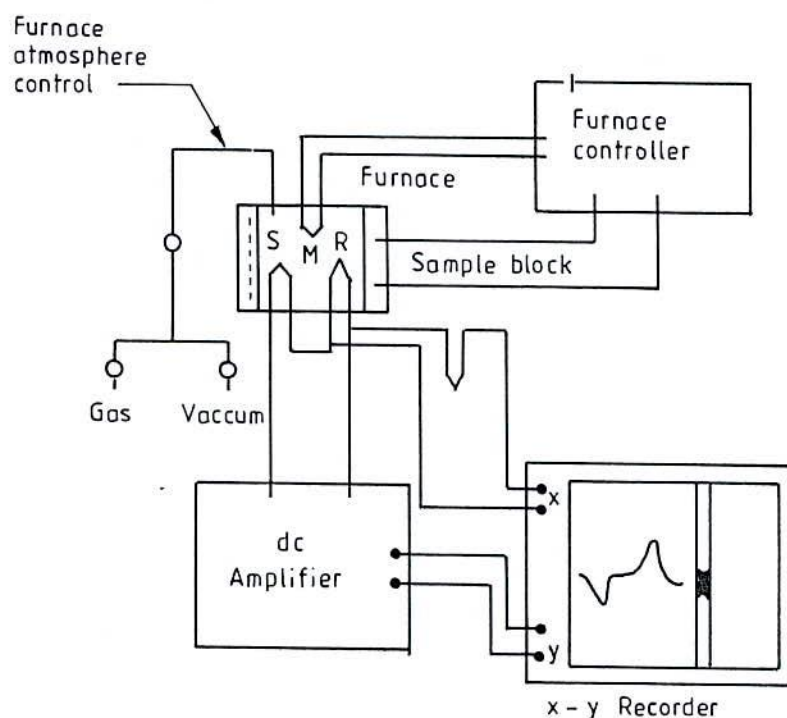


Fig-4.3. Block diagram of a differential thermal analysis equipment, (s) sample thermocouple, (R) reference thermocouple, (M) monitor thermocouple.

## 4.2 Experimental setup for Measurement of Magnetization

### 4.2.1 The Principle of Vibrating Sample Magnetometer

All magnetization measurements have been made on EG and G Princeton Applied Research Co. makes vibrating sample magnetometer (V.S.M)<sup>(4.2-4.3)</sup>. The principle of V. S. M is as follows: when the sample of a magnetic material is place in a uniform magnetic field, a dipole moment proportional to the product of the sample susceptibility

times the applied field is induced in the sample. If the sample is made to undergo a sinusoidal motion, an electrical signal is induced in suitably located stationary pick-up coils. This signal, which is at the vibrating frequency, is proportional to the magnetic moment, vibration amplitude with vibration frequency. In order to obtain the reading of the moment only, a capacitor is made to generate another signal for comparison which varies in its moment, vibration amplitudes and vibration frequency in the same manner as does the signal from the pick-up coil. These two signals are applied to the two inputs of a differential amplifier, and because the differential amplifier passes only difference between the two signals, the effect of vibration amplitude and frequency changes are cancelled. Thus only the moment determines the amplitude of the signal at the output of the differential amplifier. This signal is in turn applied to a Lock-in amplifier, where it is compared with the reference signal which is at its internal oscillator frequency and is also applied to the transducer which oscillates the sample rod. Thus the output of the Lock-in amplifier is proportional to the magnetic moment of the sample only avoiding any noise of frequency other than that of the signal. The Lock-in action yields an accuracy of 0.05% of full scale. The absolute accuracy of this system is better than 2% and reproducibility is better than 1%. Least measurable moment is  $5 \times 10^{-4}$  emu.

Variable magnetic field is achieved with a Newport Electromagnet Typen 177 with 17.7cm diameter pole pieces. The magnet is mounted on a graduated rotating base. The standard model is modified to provide an adjustable pole gap in order that the highest possible field strength is available. The field can be varied from 0 to 9KG. The field is measured directly by using Hall probe.

#### **4.2.2 Mechanical Design of the V.S.M**

The various mechanical parts of the magnetometer are shown in detail in the Fig-4.4. The base B of the V.S.M is a circular brass plate of 8mm thickness and 250mm diameter. A brass tube T of 25mm outer diameter and 0.5mm thickness runs normally through the base such that the axis of the tube and the center of the plate coincide. The base and the tube are joined together by soft solder. The tube extends 60mm upward and 24mm downward from the base. There is a vacuum port on the lower part of the tube 120mm below.



Electrical connections from the audio amplifier to the speaker and from the reference coil system to the phase-shifter are taken via the Perspex feed-through. By connecting the vacuum port of the tube T to a vacuum pump the sample environment can be changed. The speaker SP is fitted 25mm above the tube T with the help of our brass stands. The lower ends of stands are screwed to the base plate while the rim of the speaker is screwed on the tops of the stands. The speaker has a circular hole of 10mm diameter along the axis of it. An aluminum disc having female threads in it is fitted to the paper cone with araldite. The aluminum connector having male threads on it and attached to the drive rod assembly fits in the aluminum disc and thus the drive rod assembly is coupled to the speaker. The drive rod assembly consists of two detachable parts which are joined together by means of aluminum threaded connectors. Each the part is a thin pyrex glass tubing of 4mm diameter. The upper part has a small permanent magnet P situated 100mm below the aluminum connector attached to it. At the lower end of the drive rod assembly perspex sample holder having quite thin wall can be fitted tightly with the sample in it. A few perspex spears are also attached to the driver rod throughout its length. The spacers guide the vibration of the sample only in the vertical direction and stops sidewise vibration or motion. The total length of the drive rod assembly is 920mm up to base. The lower end of the tube T is joined to a brass extension tube L by a threaded coupling and an o'ring seal. Another thin tube K made of german silver and of 8mm inner diameter runs through the extension tube L from the compiling point C to about 50mm below the sample position. Above the base there is a hollow brass cylinder M of 180mm length and 130mm inner diameter, having 40mm wide collars at its both ends. The lower collar seats on an o'ring seal which is situated in a circular groove in the base plate. On the upper collar, there rests an aluminum top N with an o'ring seal. The brass cylinder M has a side port VP. This is again a brass tube of 41mm diameter and 43mm length. The port has a collar at the end away from the cylinder. A perspex vacuum feed through is fitted at its end with o'ring seal. This port is connected to the cylinder by soft solder.

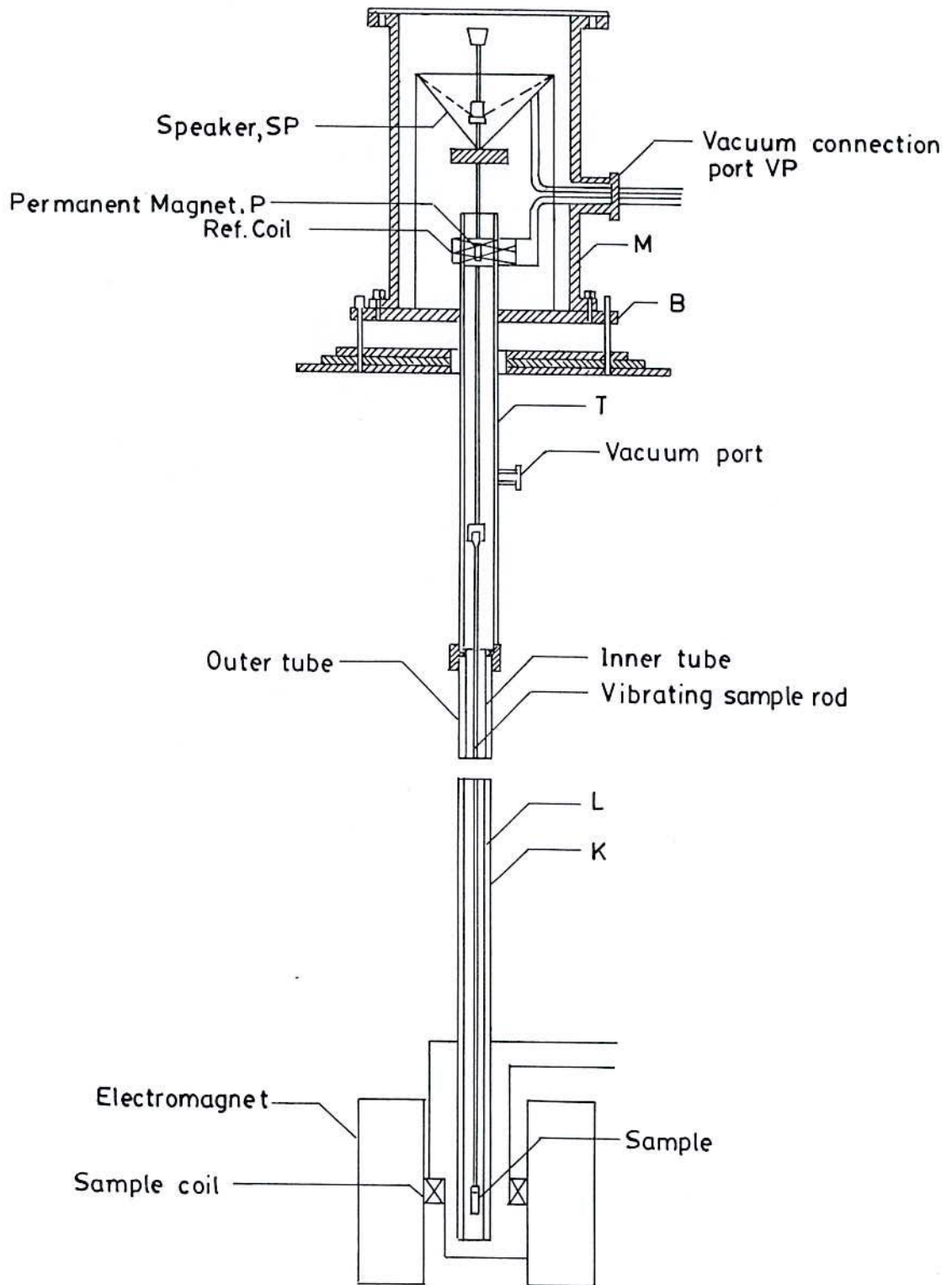


Fig- 4. 4. Mechanical construction of the vibrating sample magnetometer.

The base plate of the V.S.M. rests on three leveling screws above a brass frame which in turn rests on an iron angle bridge. The bridge is rigidly fitted to the sidewall of the room. The brass frame is provided with arrangements with the help of which it can be moved in two perpendicular in the horizontal plane.

The levelling screws are used to make the drive rod vertical and to put the sample at the centre of the pole-gap between the sample coils. The sample can be moved up and down by the leveling screws.

### **4.2.3 Electronic Circuits of the V. S. M.**

The function of the associated electronic circuits are

- i) To permit accurate calibration of the signal output obtained from the detection coils.
- ii) To produce a convenient ac output signal which is directly related to the input and which can be recorded.
- iii) To produce sufficient amplification for high sensitivity operation.

The block diagram of the electronic circuit used for the V.S.M. consists of a mechanical vibration, a sine wave generator, an audio amplifier, a ratio transformer, a phase-shifter, a lock-in amplifier, a pick-up coil system, a reference coil system and an electromagnet as shown in Fig.-4.5.

The sample magnetization by the electromagnet generates an e.m.f. in the pick-up coils PC. The strength of this signal is proportional to the magnetization of the sample. The vibrating permanent magnet also generates an e.m.f. of fixed amplitude in the surrounding reference coils. This reference signal is stepped down with the help of a ratio transformer so that its amplitude is equal to that the sample signal. The two signals are then brought in phase and put to the lock-in amplifier.

The Lock-in amplifier works as a null detector. The ratio transformer reading is to be calibrated using spherical shape sample S of 99.99% pure nickel.



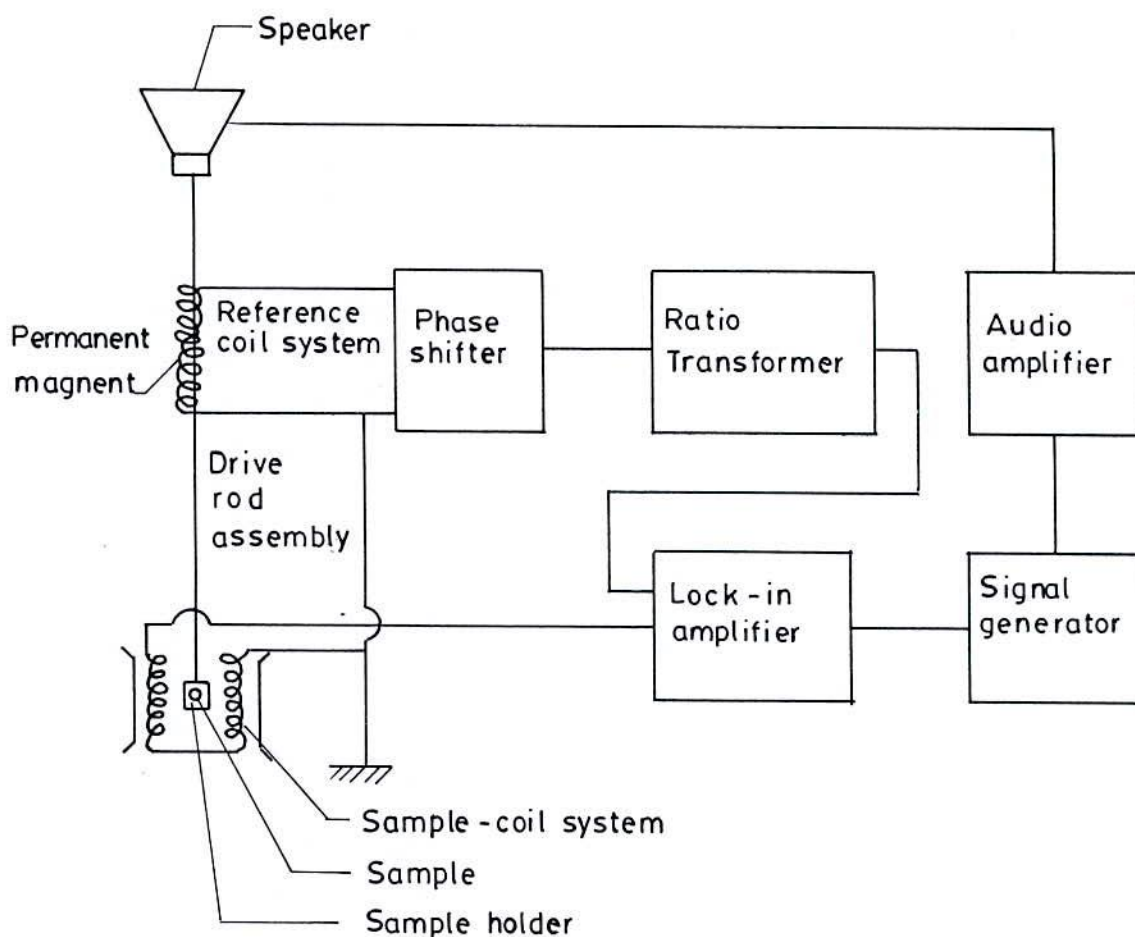


Fig- 4.5. Schematic diagram of the electronic system of the V.S.M.

#### 4.2.3.1 Sensitivity limits

Limits of sensitivity are determined by signal to noise ratio at the input circuit, where noise is defined as any signal not arising from the magnetic moment of the sample. The major sources of noise are the Johnson noise of the wire used for the pick-up coils, and the magnetic responses of the sample holder, which superimposes undesired signals in phase with the wanted signal. Use of a minimum mass of weakly diamagnetic material for a sample holder, carefully checked to contain no ferromagnetic impurities, is essential to minimize this coherent noise contribution. Corrections for the small magnetic

contribution of the sample holder can then be made by measurements with the sample removed. This correction is much less than the equivalent case with a moving coil system.

Our standard sample used for calibration was spherical shaped specimens of mass 0.0584 gm. The differential field susceptibility  $\Delta\chi \cong 5 \times 10^{-10}$  could be observed after synchronous phase detection with band width  $\cong 2 \times 10^{-2}$  cps. The other tests used was small current at 81Hz or an alternating current 81Hz passed through the coil which remained stationary.

#### **4.2.3.2 Stability Tests Differential Measurements**

With only the lock-in amplifier and the oscilloscope as a null detector, it was found that the 0.0584gm Ni-sample signal could be balanced reproducibly. Such reproducibility indicated that the long time drifts caused by the combined effects of vibration, amplitude changes and frequency changes a bridge sample position and other effects were negligible. Chosen synchronous phase detector added differential changes about one-tenth the size that could be recorded reproducibly.

#### **4.2.3.3 Vibration Amplitude**

The pick-to-pick vibration amplitude has been varied from less than 0.1mm upto 1.0mm in order to examine errors caused by amplitude changes. Such tests show that the measured magnetic moment varied by less than  $\pm 0.5\%$  over these range of amplitude, although at higher variation of amplitudes, because of the larger signals involved.

#### **4.2.3.4 Image Effects**

Image effects were also examined with a small vibrating coil carrying a dc current. The image effect was no greater than  $\pm 1\%$  for fields upto 5KG produced in an air gap of 3.6cm. Undoubtedly, there is an image induced in the magnet poles. It appears

however, that when the sample is vibrated, the effective image vibration is reduced by eddy current shielding.

#### **4.2.3.5 Vibration Frequency**

The Vibration frequency is not critical. High frequency operation is limited by the driving mechanism and capacitive shunting in the detection coils. Frequencies of 100Hz or less permit the use of inexpensive components and minimize eddy current shielding by the vacuum chamber. The measurements are completely independent of eddy currents in the surrounding parts, if measurements and calibration are made at the same temperature. The thickness of conducting parts has been minimized, so that the temperature dependence of penetration depth is less than 1%.

#### **4.2.3.6 Vibration Problems**

Mechanical coupling between the vibrating system and the fixed detection coils must be avoided. Although the coils are arranged for minimum sensitivity to external vibration, a noticeable background signal is obtained when the vacuum chamber contacts the direction coils. Such mechanical effects are difficult to eliminate electronically, because the spurious background signal has the same frequency as the sample signal and maintains a constant phase differences with respect to the sample signal. Usually the magnetometer and detection coils are both supported by the magnetic coupling. So that some mechanical coupling may be noticed at highest sensitivity.

#### **4.2.4 X-Y Recorder**

All the measurements of magnetizations were plotted using LISEIS make X-Y Recorder model LY18100. The Magnetic moment from V.S.M. form the potential differences in volts taken from panel meter are plotted on X-Y recorder. Magnetic moment can also be plotted as a function of time. A graph paper remains struck on an electrically charged plate during the plotting in X and Y scales are calibrated and can be reduced or enlarged as per need.



#### 4.2.5 Calibration of the V.S.M.

There are usually two methods of calibration of a vibrating sample magnetometer (V.S.M.)

- i) by using a standard sample and
- ii) by using a coil of small size whose moment can be calculated from the magnitude of the dc current through it.

We have calibrated our V.S.M. using a 0.0584gm spherical sample of 99.99% pure nickel. The sample was made spherical with the help of a sample shaping device. The saturation magnetic moment of the sample has been calculated using available data. The ratio transformer reading is obtained by actual measurement from the relation

$$M = KK', \quad (4.1)$$

where  $M$  is magnetic moment,  $K'$  is saturation ratio transformer reading and  $K$  is V.S.M. calibration constant. But

$$M = m\sigma, \quad (4.2)$$

where  $\sigma$  is the specific magnetization and  $m$  is the mass of the sample. From eq" (4.1) and eq" (4.2) calibration constant is given by

$$K = \frac{m\sigma}{K'} \quad (4.3)$$

The accuracy of this calibration, however, depends on the reliability of the standard nickel sample; the accuracy of the ratio transformer and the gain of amplifier. The equipment has been operated repeatedly with the same standard sample and stability has been found to be within 1 part in 100.

The absolute accuracy of the instrument depends on the knowledge of the magnetic properties of the calibration standard and reproducibility of sample position. When the substitution method of calibration is used, the major error  $\pm 1\%$  is introduced by the estimation of standard nickel sample. The relative accuracy of this instrument depends on accurate calibration of the precision resistor divider net work.

The total error here can be kept less than 0.5%. A typical calibration curve of magnetic field versus ratio transformer reading is shown in Fig.-4.6

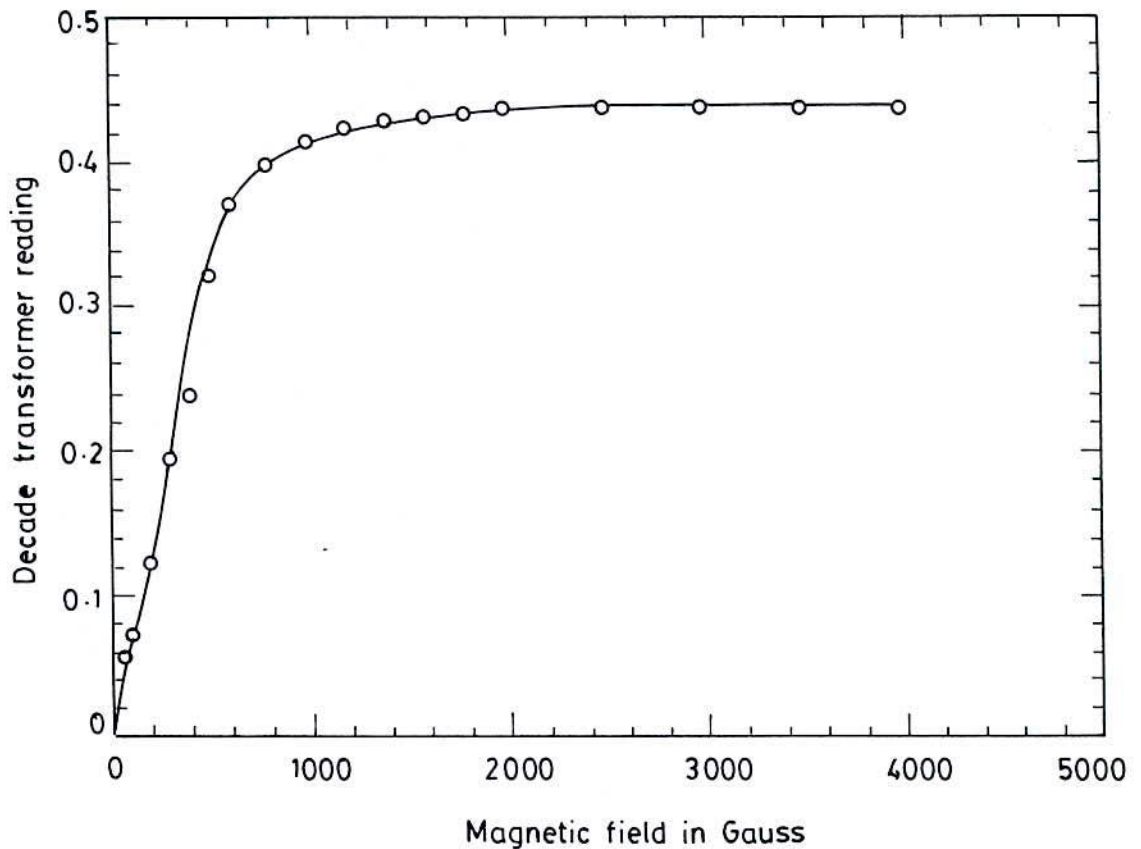


Fig -4.6. Calibration curve of magnetic field Vs. decade transformation reading (V.S.M.).

### 4.2.6.1 Calibration Data

- (i) Reference signal with phase shifter and decade transformer in connection.

$$V_{ref_1} = \frac{1}{0.01} \times \frac{10\mu V}{20} \times 19$$
$$= 9.5\mu V \times 100 = 0.95mV$$

- (ii) Reference signal with decade transformer in connection:

$$V_{ref_2} = \frac{1}{0.01} \times 11\mu V = 1.1mV$$

- (iii) Reference signal with direct connection:

$$V_{ref_3} = 13 \times 0.1mV = 1.3mV$$

Saturation decade transformer reading for pure Ni at 20° C is given as  $K' = 0.4386$ .

Specific magnetization for pure Ni at 20°C is given by  $\sigma_s = 54.75 \text{ Am}^2/\text{Kg}$

Mass of the pure Ni -sample  $m = 0.0584 \times 10^{-3} \text{ Kg}$

Magnetic moment  $M = m\sigma = 3.1975 \times 10^{-3} \text{ Am}^2$

and hence V.S.M. calibration constant is found as

$$K = \frac{m\sigma}{K'} = 7.29 \times 10^{-3} \text{ Am}^2$$



## 4.3 Experimental Techniques for Measuring Complex Permeability

### 4.3.1 Real and Imaginary Components of Complex Permeability

Determination of permeability normally involves the measurements of the change in self-inductance of a coil in presence of the magnetic core. Methods of measurement those are commonly used are

- i) The LCR bridge method
- ii) Resonance circuits and
- iii) The standing wave method

The behaviour of a self-inductance can now be described as follows. If we have an ideal lossless air coil of inductance  $L_0$ , on insertion of magnetic core with permeability  $\mu$ , the inductance will become  $\mu L_0$ . The complex impedance  $Z$  of this coil then be expressed as

$$\begin{aligned} Z &= R + iX = i\omega L_0\mu \\ &= i\omega L_0\mu (\mu' - i\mu'') \end{aligned} \quad 4.4$$

where the resistive part is

$$R = \omega L_0\mu'' \quad 4.5$$

and the reactive part is

$$X = \omega L_0\mu' \quad 4.6$$

The r.f. permeability can be derived from the complex impedance of a coil in eq<sup>n(4.4)</sup>. The core has taken in the toroidal form to avoid demagnetization effects. The quantity  $L_0$  is derived geometrically as shown in section 4.3.3.

### 4.3.2 Preparation of the samples for permeability measurements

The amorphous ribbons were wound into toroidal cores having outer and inner diameters within 13 to 15 mm and with the ratio of outer and inner diameter always kept less than 1.2 in order to improve the homogeneity of the applied field, as also to reduce the possibility of an inhomogeneous inductance response. A low capacitance coil with 8 to 10 turns was wound around the toroids to allow the application of magnetic fields over a wide range of amplitudes. While measuring the permeability of the amorphous ribbon cores at high frequency, the high electric resistance of these materials generally precludes the trouble some skin effect found with ribbons. However, the cross section of the amorphous ribbon core to be measured may have to be kept small in order to avoid dimensional resonance phenomena. To avoid an increase in resistance owing to skin effect, braided copper wire is used at frequencies higher than 100 KHz. The thickness of the separate wire stands being adapted in the measuring frequency of up to about 13 MHz. The thumb rule is that, the wire thickness in microns must be smaller than the wavelength in meters.

At higher frequencies the capacitance arising from the winding gives inaccurate values R and  $L_s$ . It is, therefore, necessary to kept the capacitance of the winding as low as possible. Frequency response characteristics were then investigated on these ring shaped specimens as a function of frequency.

### 4.3.3 Frequency Characteristics of Amorphous Materials

The frequency characteristics of the amorphous ribbon samples, i.e. the permeability spectra, were investigated using an Agilent Impedance Analyzer model No.- 4192 ALF. The measurement of inductances were taken in the frequency range 0.5 KHz to 13MHz. The values of measured parameters obtained as a function of frequency and the real and imaginary parts of permeability and the loss factor.  $\mu'$  is calculated by using following formula

$$L_s = L_o \mu' \quad 4.7$$

$$\mu' = \frac{L_s}{L_o}$$

and

$$\tan \delta = \frac{\mu''}{\mu'} \quad 4.8$$

$$\mu'' = \mu' \tan \delta ,$$

where  $L_s$  is the self inductance of the sample core and

$$L_o = \frac{\mu_o N^2 S}{\pi d} , \quad 4.9$$



whose  $L_o$  is the inductance of the winding coil without the sample core and  $N$  is the number of turns of coil (here  $N=8$ ),  $S$  is the area of cross-section as given bellow

$$S = dh \text{ where } d = \frac{d_2 - d_1}{2} ,$$

and  $h$  = height

and  $\bar{d}$  is the mean diameter of the sample given as follows

$$\bar{d} = \frac{d_1 + d_2}{2}$$

The relative quality factor is determined for the ratio  $\mu_i / \tan \delta$ .



## CHAPTER 5: RESULTS AND DISCUSSIONS

- 5.1. Differential Thermal Analysis
  - 5.1.1. DTA Results of amorphous Co-B-Si and Co-Fe-B-Si as affected by Fe-substitution
  - 5.1.2. Activation energy of Co- and Co-Fe- based amorphous ribbons
  - 5.1.3. Annealing effects on the kinetics of structural relaxation of Co-B-Si and Co-Fe-B-Si amorphous ribbons studied by DTA
- 5.2. Effects of two- step annealing time on Magnetization
  - 5.2.1 Specific Magnetization measurements on as cast Co- and Co-Fe- based amorphous ribbons
  - 5.2.2. Specific magnetization measurements on two step time annealed Co- and Co-Fe-based amorphous ribbons
- 5.3. Dynamic Magnetic Properties of Co- and Co-Fe- based amorphous ribbons
  - 5.3.1. Initial Permeability of as cast Co-and Co-Fe- based amorphous ribbons
  - 5.3.2. Complex Permeability of as cast the Co- and Co-Fe- based amorphous ribbons
  - 5.3.3 Frequency Dependence of the real part of the complex permeability of Co- and Co-Fe- based amorphous ribbon with different annealing Temperature and two step annealing time
  - 5.3.4. Frequency dependence of the Imaginary part of the complex permeability of Co- and Co-Fe- based amorphous ribbon with different annealing Temperature and two step annealing time
  - 5.3.5. Relative quality factor
  - 5.3.6. Two-step annealing time effects on frequency spectra of Co and Co-Fe-based ribbons at constant annealing temperature 390°C
  - 5.3.7. Annealing temperature dependence of initial permeability at constant low field for two step annealing time with composition  $\text{Co}_{80-x}\text{Fe}_x\text{B}_{10}\text{Si}_{10}$

## 5.1 Differential Thermal Analysis Results

The kinetics of crystallization of different crystalline phases of  $\text{Co}_{80-x}\text{Fe}_x\text{B}_{10}\text{Si}_{10}$  has been studied by differential thermal analysis (DTA). A calorimetric study of amorphous alloys provided substantial fundamental information concerning the kinetics of crystallization and structural relaxation effects. The kinetics of the onset of crystallization has been studied calorimetrically by Clements W.G. and Cantor B. <sup>(5.1)</sup> and both calorimetrically and magnetically by Luborsky F.E. <sup>(5.2)</sup> in a variety of amorphous magnetic alloys. Co- and Co-Fe-based amorphous ribbons with composition  $\text{Co}_{80-x}\text{Fe}_x\text{B}_{10}\text{Si}_{10}$  [ $x = 0, 2, 4, 6$  &  $8$ ] are of special interest because, these magnetic systems with high Co content and small amount of Fe content can help us to understand why the magnetostriction of amorphous 3d metals differ so markedly from that of their crystalline counterparts. Amorphous ribbons prepared by rapid quenching method have been subjected to DTA using a DT analyzer model TG/DTA 6300, manufactured by Seiko Instruments Inc, Japan.

### 5.1.1 DTA Results of Amorphous Co-B-Si and Co-Fe-B-Si as Affected by Fe- Substitution

DTA trace of a as cast amorphous sample recorded in a nitrogen atmosphere with a heating rate  $20^\circ\text{C}/\text{min}$  is presented in representative Fig- 5.1. Two exothermic peaks are aligned which correspond to  $T_g$  and  $T_x$  phases respectively. DTA is a direct and effective technique for analyzing kinetics of the amorphous ribbons in respect of phase transitions. In Fig- 5.1  $T_g$  and  $T_x$  correspond to observed exothermic peaks of the ribbon with composition  $\text{Co}_{80}\text{B}_{10}\text{Si}_{10}$ . Two anomalies observed in the DTA curve are at  $393.7^\circ\text{C}$  and  $549.1^\circ\text{C}$  respectively. Both the anomalies showed peaks, which corresponds to the release of heat at these temperature due to change in the ordering of the atoms. We identify the first peak as  $T_g$ , when the ribbon was transforming from amorphous state to crystalline state. The second peak is considered to be due to the formation of crystalline phase  $T_x$ . No obvious endothermic heat flow event due to  $T_g$  is observed in the DTA traces.

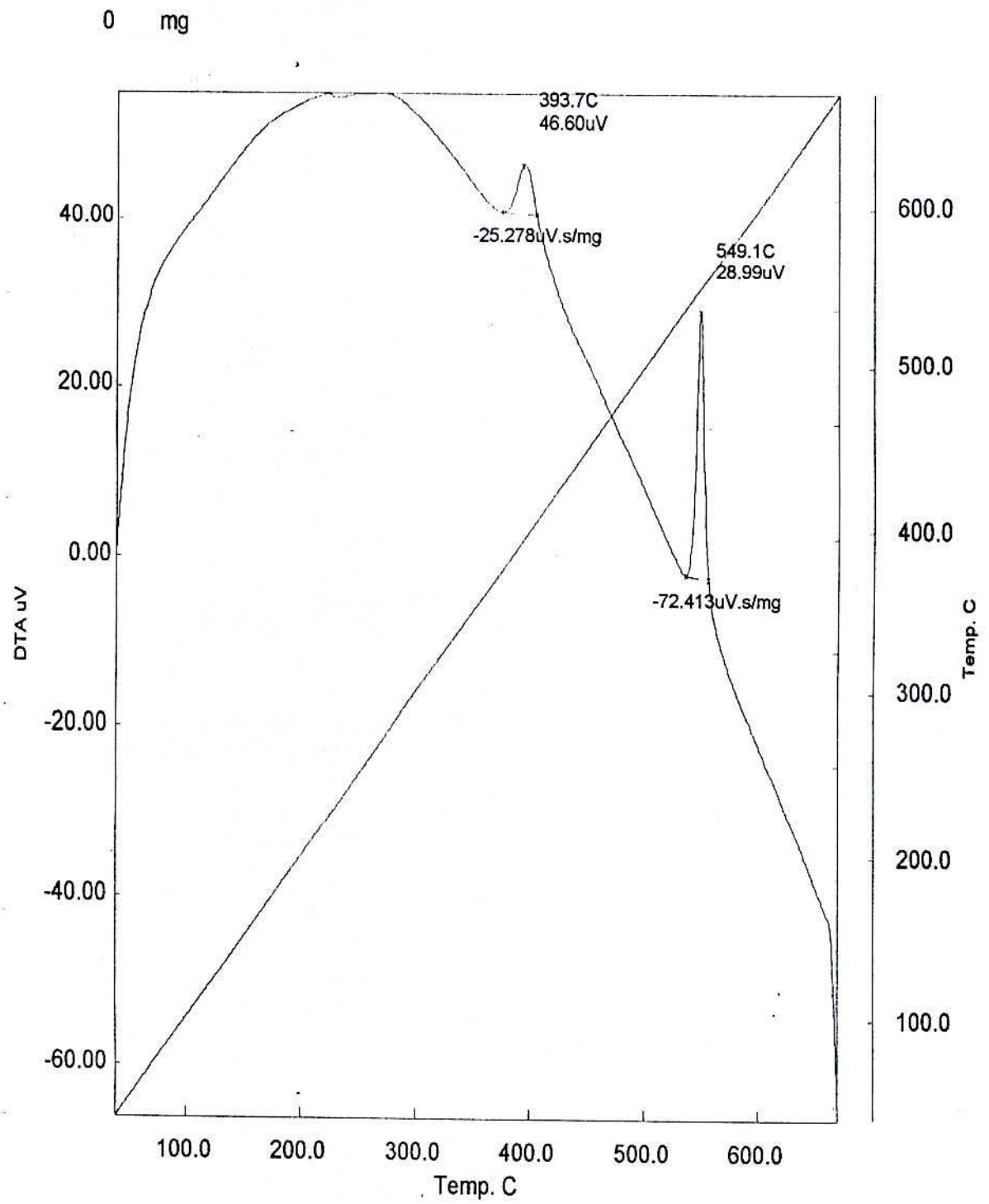


Fig- 5.1. DTA trace of the amorphous ribbon with composition  $\text{Co}_{80}\text{B}_{10}\text{Si}_{10}$ .



The compositional dependence of  $T_g$  and  $T_x$  of amorphous  $Co_{80-x}Fe_xB_{10}Si_{10}$  [ $x = 0, 2, 4, 6 \text{ \& } 8$ ] alloys were also studied. It has been observed that the crystallization temperature of these alloys, with constant Si and B changes with Fe content as measured by DTA when the heating rate is maintained at  $20^\circ C/ \text{min}$ . The results are presented in a summarized from Fig- 5.2 for comparison between samples of different compositions. For all the samples the eutectic points remain unchanged. This shows that all the compositions are equally favorable for producing amorphous ribbons. The values of  $T_g$  and  $T_x$  for all the samples are noted in table- 5.1.  $T_g$  of  $Co_{80-x}Fe_xB_{10}Si_{10}$  alloys increases slowly but monotonically with the increase of Fe-content. The values of  $T_x$ , which are higher than those of  $T_g$ , remain practically constant for all the compositions shown in Fig- 5.3.

Table 5.1:  $T_g$  and  $T_x$  of amorphous ribbons with compositions  $Co_{80-x}Fe_xB_{10}Si_{10}$  at constant heating rate  $20^\circ C/\text{min}$ .

$Co_{80-x}Fe_xB_{10}Si_{10}$	$T_g^\circ C$	$T_x^\circ C$
X=0	394	549
X=2	411	550
X=4	414	536
X=6	424	535
X=8	435	538

And the second stage of crystallization ( $T_x$ ) corresponds to the sharp exothermic peak may be due to the temperature when the hexagonal  $\alpha$ -Co changes into f.c.c.  $\beta$ -Co phase<sup>(5.3)</sup>.

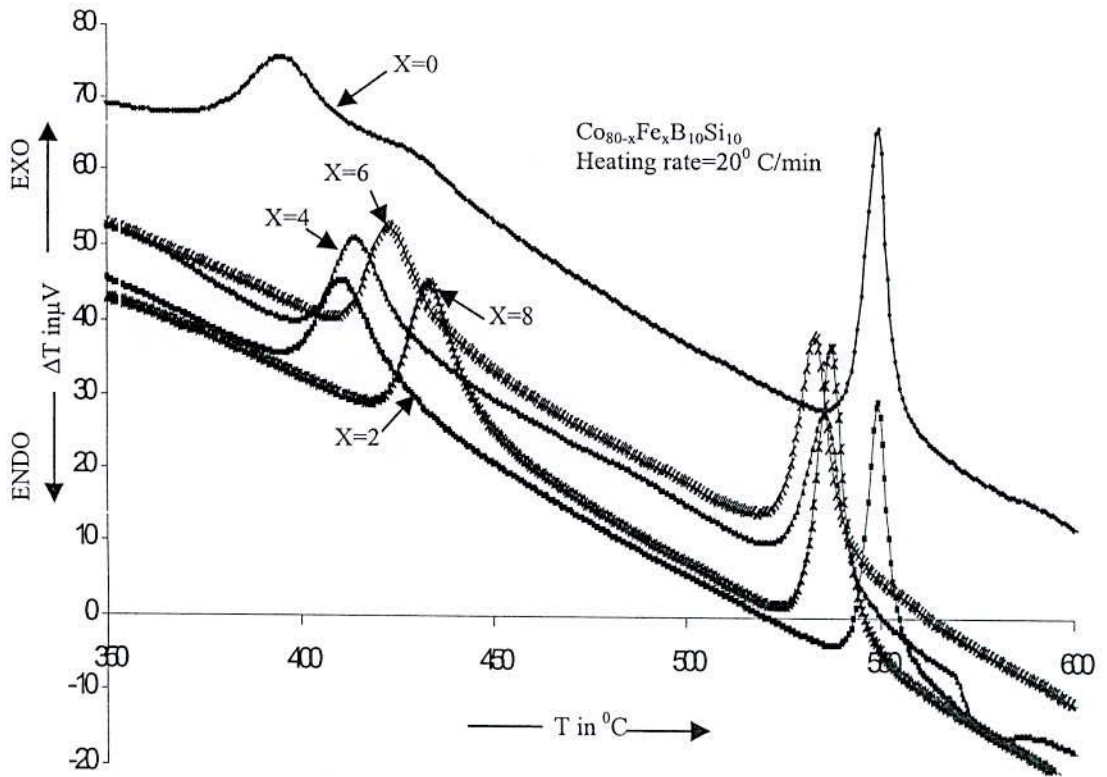


Fig-5.2: DTA traces of amorphous ribbons with composition  $\text{Co}_{80-x}\text{Fe}_x\text{B}_{10}\text{Si}_{10}$ .

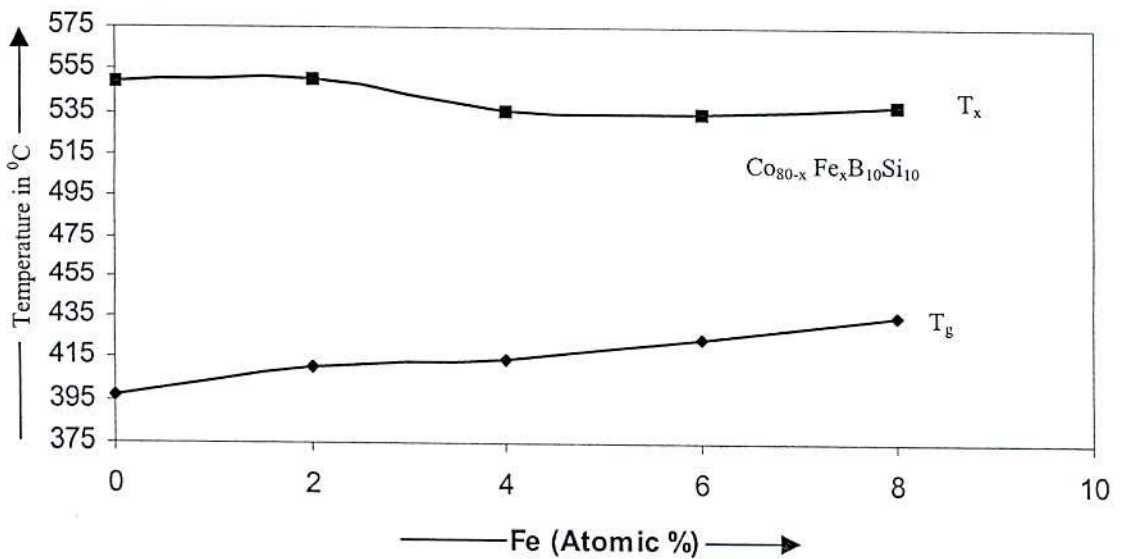


Fig-5.3 Variation of  $T_g$  and  $T_x$  due to change in the Fe- content in  $\text{Co}_{80-x}\text{Fe}_x\text{B}_{10}\text{Si}_{10}$  amorphous ribbons.

### 5.1.2 Activation energy of Co- and Co-Fe- based amorphous ribbons

The kinetics of structural relaxation is virtually known at this time, and in view of the change of speed available data may be thermally activated. As cast amorphous ribbons predominantly takes place through a low activation energy mechanism, presumably via the movement of high mobility “defects”. These defects may through to be driven out by stabilization. The latter describes the transition to  $T_g$  and  $T_x$  and this process requires an activation energy. Turnbull D.<sup>(5.3)</sup> proposed that the reduced glass transition temperature,  $T_{rg}$ , defined as the glass transition temperature  $T_g$  divided by the liquidus temperature  $T_l$ , could be regarded as a measure to evaluate the glass forming ability of an alloy<sup>(5.3)</sup>. This correlation has been confirmed in many experiments<sup>(5.4)</sup>. Inoue A. and Masumoto T. adopted the temperature difference  $\Delta T_x$  between  $T_g$  and the first crystallization  $T_x$  upon heating at constant rate as a measure of stability of the super cooled liquid above  $T_g$ <sup>(5.5)</sup>.  $T_g$  clarify the thermal stability of the Co-and Co-Fe-based amorphous ribbon is important for the following reasons. The crystallization phase activation energies products are determined and are shown in table-2. Energy products linearly increase with increasing Fe content in the amorphous ribbon.

Table 5.2: Energy products for  $T_g$  and  $T_x$  of amorphous ribbons with composition  $Co_{80-x}Fe_xB_{10}Si_{10}$  at constant heating rate 20°C/min.

$Co_{80-x}Fe_xB_{10}Si_{10}$	Energy products	
	$T_g$ ( $\mu V\text{-s/mg}$ )	$T_x$ ( $\mu V\text{-s/mg}$ )
X=0	25.28	72.41
X=2	39.18	63.60
X=4	43.64	62.60
X=6	57.42	87.58
X=8	73.56	93.57

Representative Fig- 5.4. and Fig- 5.5 show DTA traces of Co- and Co-Fe- based amorphous ribbons taken in nitrogen atmosphere with continuous heating rate of 10-50°C/min at a step of 10°C.

It is observed that the crystallization of each phase has occurred over a wide range of temperatures and that the peak temperature shifts to higher values with the increase of heating rate. The crystallization of each phase occurs over a wide range of temperature.



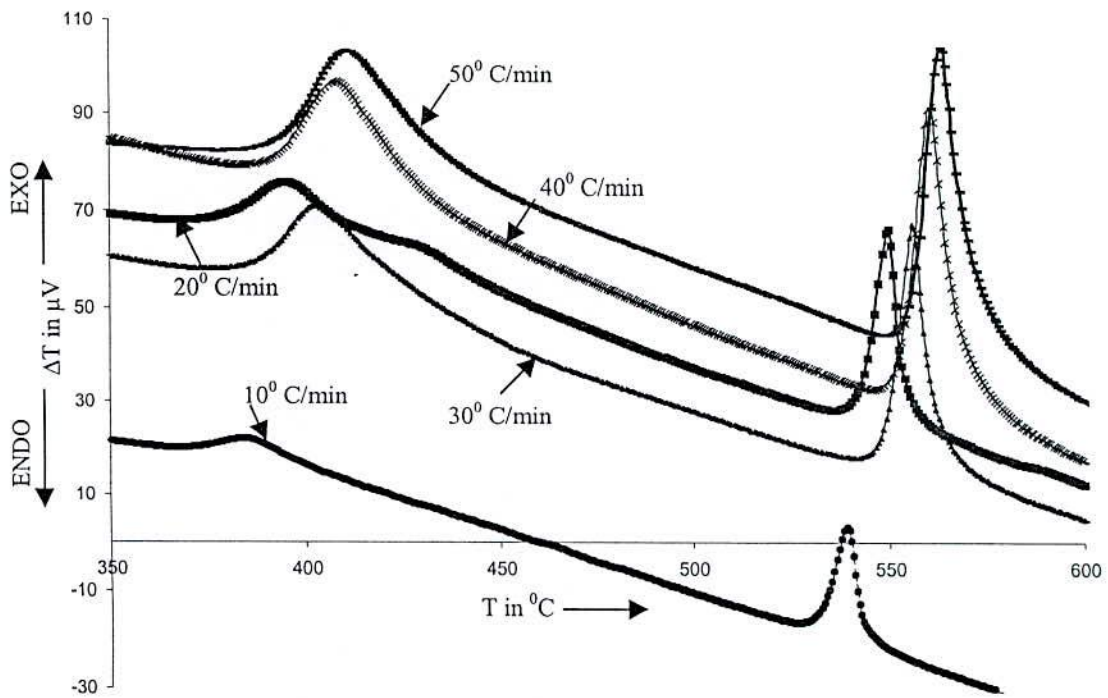


Fig-5.4 Effects of heating rate on DTA traces of the amorphous ribbon with composition  $\text{Co}_{80}\text{B}_{10}\text{Si}_{10}$ .

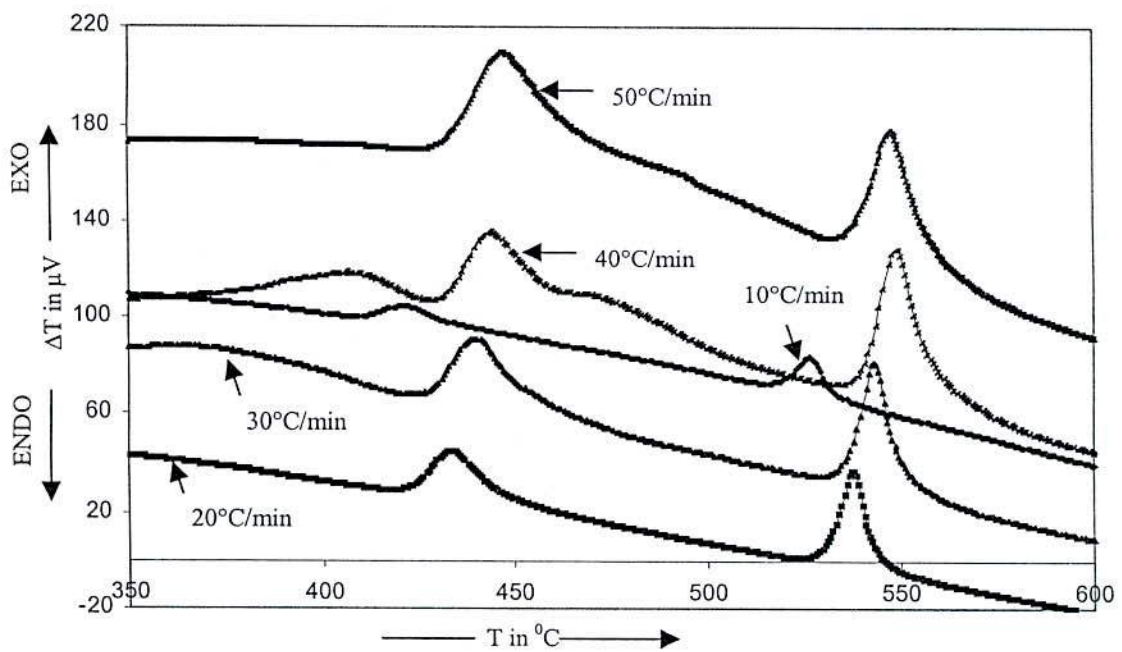


Fig-5.5 Effects of heating rate on DTA traces of the amorphous ribbon with composition  $\text{Co}_{72}\text{Fe}_8\text{B}_{10}\text{Si}_{10}$ .

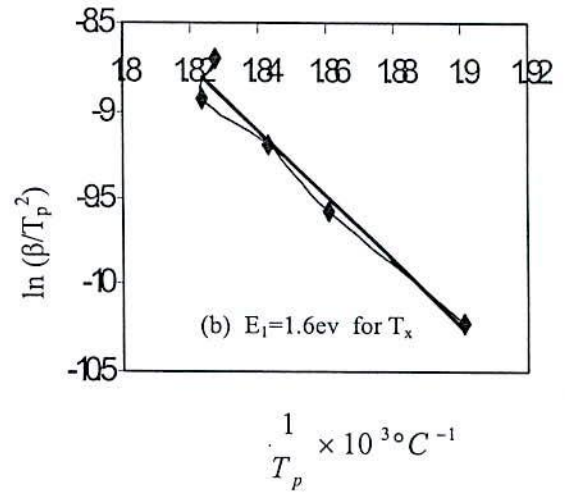
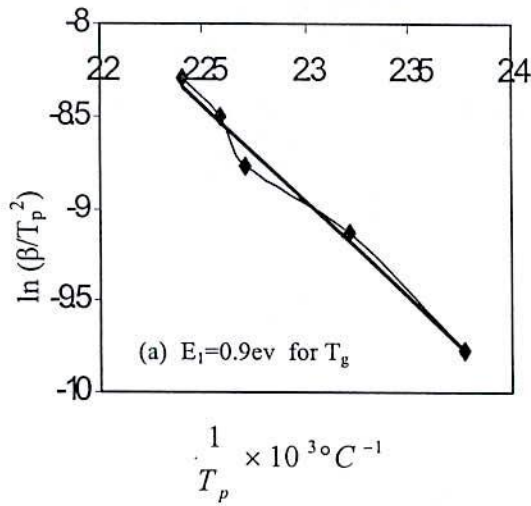


Fig: 5.6  $\frac{1}{T_p} \times 10^3$  versus  $\ln(\beta/T_p^2)$  curve for  $T_g$  and  $T_x$  phases of the amorphous ribbon with composition  $\text{Co}_{72}\text{Fe}_8\text{B}_{10}\text{Si}_{10}$

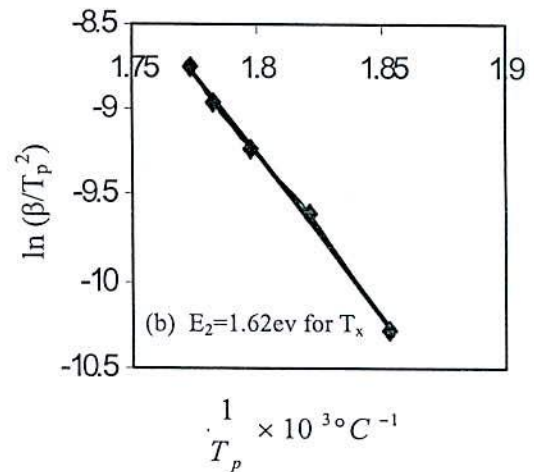
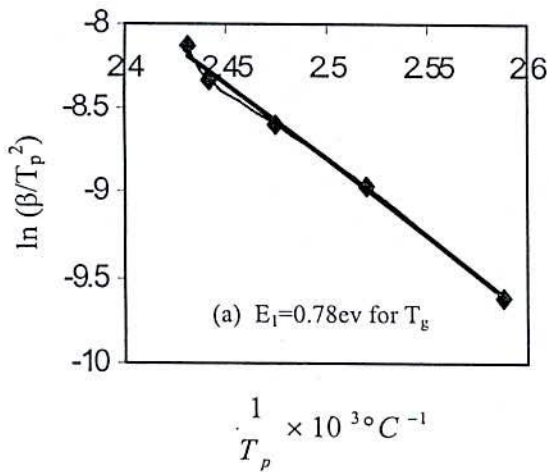


Fig: 5.7  $\frac{1}{T_p} \times 10^3$  versus  $\ln(\beta/T_p^2)$  curve for  $T_g$  and  $T_x$  phases of the amorphous ribbon with composition  $\text{Co}_{80}\text{B}_{10}\text{Si}_{10}$ .

The activation energy of crystallization of  $T_g$  and  $T_x$  phases have been calculated using Kissinger equation <sup>(3.8)</sup>.

$$\beta = T_p^2 e^{-E/kT_p}$$

$$\ln\left(\frac{\beta}{T_p^2}\right) = -\frac{E}{kT_p}$$

$$E = -kT_p \ln\left(\frac{\beta}{T_p^2}\right)$$

where  $\beta$  is the heating rate,  $T_p$  is the crystallization peak temperature,  $E$  is the crystallization activation energy and  $k$  is the Boltzmann constant. The activation energy of  $T_g$  and  $T_x$  calculated from the plots shown in Fig- 5.6.(a,b) and Fig- 5.7. (a,b) and are depicted in table 5.3. It is seen that the first thermal crystallization activation energy  $E_1$  for  $T_g$  phases slightly increase with increasing Fe content in the amorphous ribbon.

The second crystallization activation energy  $E_2$  for  $T_x$  phases initially slightly decreases with increasing Fe up to 4 atomic percent and then slightly increases with the increase of the Fe- content. We obtained an  $E_2$  value close to  $1.54\text{eV} \pm 0.076\text{eV}$  a Kissinger plot gives the same result. It appears that alloying does change the activation energy significantly and the first step of crystallization is achieved, the remaining amorphous layer presents a low ferromagnetism induced by a change in Fe of the composition.

Table 5.3: Activation energies for  $T_g$  and  $T_x$  of amorphous ribbons with composition  $\text{Co}_{80-x}\text{Fe}_x\text{B}_{10}\text{Si}_{10}$

$\text{Co}_{80-x}\text{Fe}_x\text{B}_{10}\text{Si}_{10}$	$E_1$ for $T_g$ in eV	$E_2$ for $T_x$ in eV
X=0	0.78	1.62
X=2	0.79	1.53
X=4	0.82	1.45
X=6	0.87	1.49
X=8	0.91	1.61



### 5.1.3 Annealing effects on the kinetics of structural relaxation of Co-B-Si and Co-Fe-B-Si amorphous ribbons studied by DTA

The experimental data have been interpreted in terms of two step time annealing effects of DTA traces at constant temperature 200°C. Fig- 5.8 shows the anneal effects on DTA graph of Co<sub>80</sub>B<sub>10</sub>Si<sub>10</sub> amorphous ribbon. And Fig- 5.9 shows anneal effects on DTA traces of Co<sub>72</sub>Fe<sub>8</sub>B<sub>10</sub>Si<sub>10</sub>. It is observed that the T<sub>g</sub> and T<sub>x</sub> practically unchanged. The general consensus seems to be that the local structural state of the amorphous ferromagnetic alloys with annealing. An even though the over all amorphous state is maintaining through out less then Curie temperature of amorphous ribbons. Activation energy products increases with increasing and decreasing annealing time is shown in table 5.4 and table 5.5.

Table 5.4: Two step annealing time effects on energy products of the amorphous ribbon with composition Co<sub>80</sub>B<sub>10</sub>Si<sub>10</sub> at constant heating rate 20°C/min.

Co <sub>80</sub> B <sub>10</sub> Si <sub>10</sub>	T <sub>g</sub> °C	Energy products for T <sub>g</sub> μV-s/mg	T <sub>x</sub> °C	Energy products for T <sub>x</sub> μV-s/mg
As cast	393.7	25.28	549.1	72.41
10 minute annealed at 200°C	395.3	32.73	550	79.78
100 minute annealed at 200°C	396.8	42.67	549.2	85.02

Table 5.5: Annealing time effects on energy products of the amorphous ribbon with composition Co<sub>72</sub>Fe<sub>8</sub>B<sub>10</sub>Si<sub>10</sub> at constant heating rate 20°C/min.

Co <sub>72</sub> Fe <sub>8</sub> B <sub>10</sub> Si <sub>10</sub>	T <sub>g</sub> °C	Energy products for T <sub>g</sub> μV-s/mg	T <sub>x</sub> °C	Energy products for T <sub>x</sub> μV-s/mg
As cast	435	73.56	538.5	93.57
100 minute annealed at 200°C	440.4	70.11	542.6	84.14

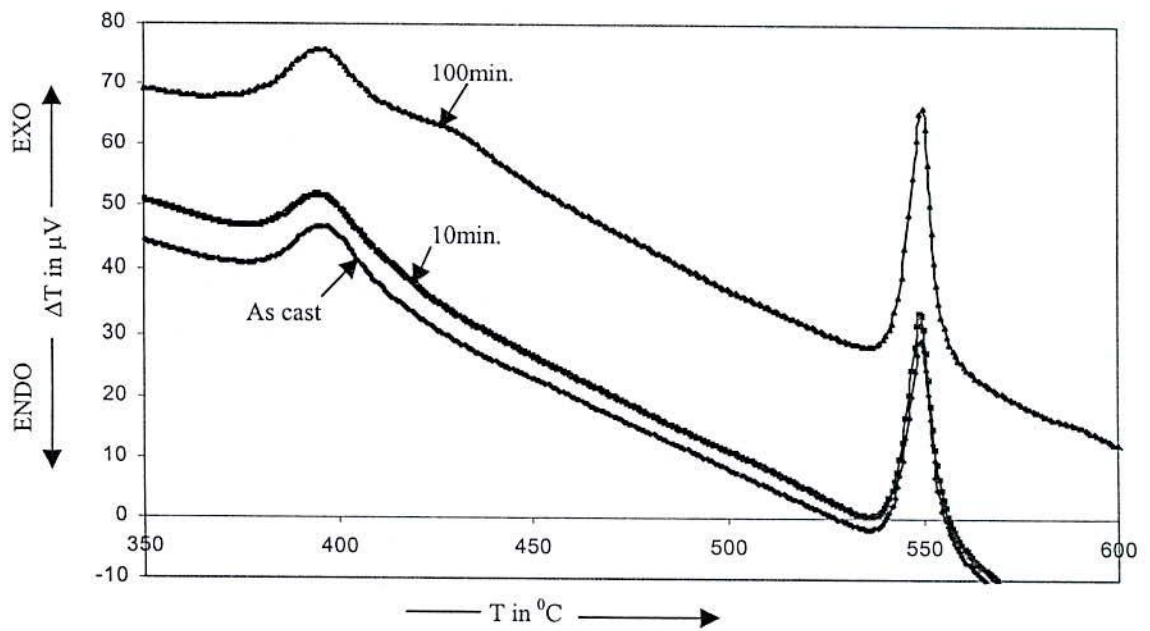


Fig-5.8 Effects on DTA trace of as cast and different annealing time at 200°C on the amorphous ribbon with composition  $\text{Co}_{80}\text{B}_{10}\text{Si}_{10}$ .

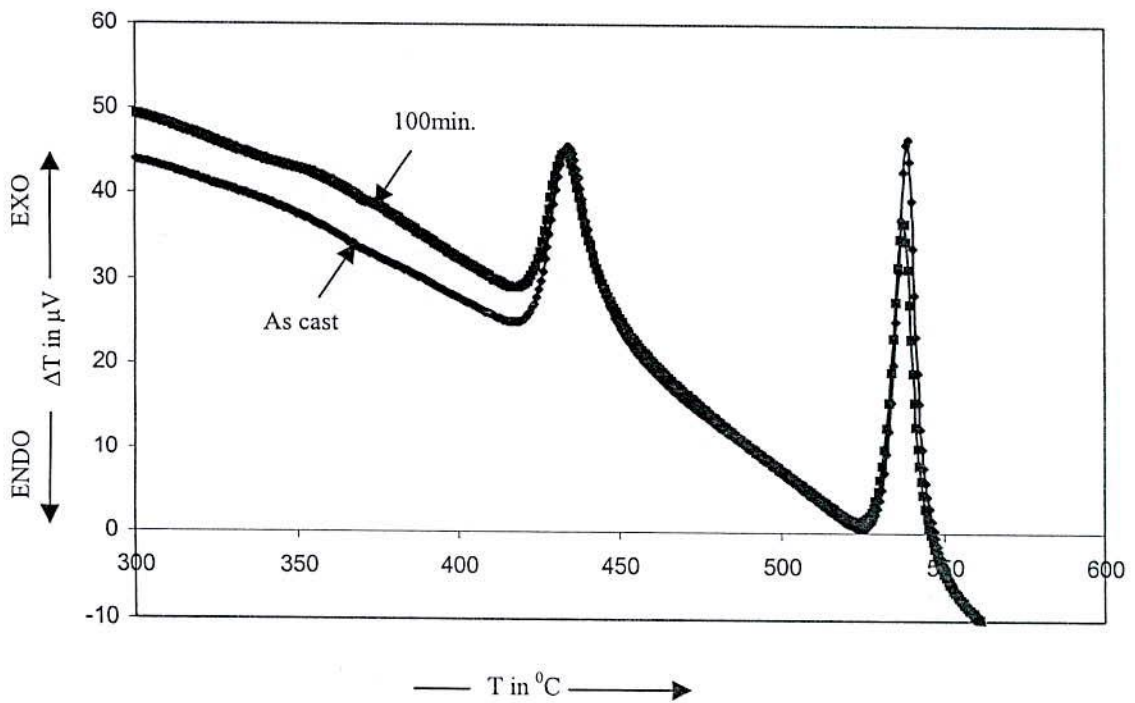


Fig-5.9 Effects on DTA trace of as cast and time annealed at 200°C on the amorphous ribbon with composition  $\text{Co}_{72}\text{Fe}_8\text{B}_{10}\text{Si}_{10}$ .

The kinetics of structural relaxation is virtually shown at this time annealing. These kinetics anisotropy reorientation depends on the instantaneous structural state and may be described in terms of activation energy products. It may qualitatively be said that the activation energy products for anisotropy reorientation increases upon time annealing. Further time annealing, the low range values of activation energy products are similar in magnitude to that found structural phase in amorphous ferromagnetic ribbons.





## 5.2 Effects of Two- Step Annealing Time on Magnetization

The present work is mainly aimed at studying the magnetization process of Co-B-Si and Co-Fe-B-Si ribbons as affected by two step annealing time at constant temperature 390°C. This provides information about the nature of residual strains in as prepared melt spun ribbons and their effects on domain wall pinning. This study also provides important technical information about the possibility of using these Co- and Co-Fe- based ribbons at elevated annealing time and the optimum operating points of these ribbons, when they are used as soft magnetic materials under varying fields. The detailed quantitative analysis of the situation is, therefore, very complex and present understanding of the problem of magnetization process as affected by these defects is not yet clear. The present work therefore aims at experimental determination of two step time annealing effect on relaxation of strains and corresponding change in the field dependence of the magnetization. We can distinguish reversible and irreversible types of relaxation due to annealing. Irreversible types of relaxation are those which are connected with thermally initiated microscopic jumps of defects or ordering atomic pairs which corresponds to irreversible domain wall movements under external fields <sup>(5.6-5.8)</sup>. Thus reversibility of magnetization is not possible in these cases by reversing the external field. The reversible relaxation on the other hand means micro structural atomic rearrangement with in the domain wall potential in a way that allows the reversal of the magnetic domain wall movements through reversing of the direction of the magnetic field. The present work will be confined to the later situation only. The relaxation process of a quenched amorphous ribbon can again be distinguished into three characteristic temperature ranges. These are lower temperature ranges, where tunneling cannot reverse micro structural rearrangement takes place by the two level Anderson model <sup>(5.9-5.10)</sup>. This is a quantum mechanical process and is independent of the type of heat treatment used.

Second relaxation process corresponds to overcoming energy peaks due to residual strains, which depends sensitively on the type of heat treatment used. The high temperature range which corresponds to the so-called Hopkinson effect that results from the magnetic transition and is irreversible.

The present results are interpreted interms of conventional domain theory of ferromagnetism, where it is postulated that the effect of time annealing in the selected

temperature is to partially remove the pinning centers of the domain walls and thereby improving the magnetic softness of these ribbons.

### 5.2.1 Specific Magnetization Measurements on as cast Co- and Co-Fe-Based Amorphous Ribbons

The specific magnetization of Co-and Co-Fe-based amorphous ribbons with composition  $\text{Co}_{80-x}\text{Fe}_x\text{B}_{10}\text{Si}_{10}$  [ $x=0, 2, 4, 6 \& 8$ ] in the as cast condition was measured using a vibrating sample magnetometer (VSM).

The saturation specific magnetization ( $\sigma_s$ ) have been calculated using formula

$$\sigma_s = \frac{KK'}{m} \text{emu / gm}$$

where  $K$ =V.S.M. calibration constant

$m$ = weight of the sample and

$K'$ = Decade transformer reading

The specific magnetization process as a function of field is shown in Fig- 5.10. The saturation specific magnetization ( $\sigma_s$ ) for these ribbons have higher values for increasing replacement of Co by Fe. In the case of saturation specific magnetization it is observed that while ribbon with composition  $\text{Co}_{80}\text{B}_{10}\text{Si}_{10}$  reaches its saturation value at around 3.5KG field,  $\text{Co}_{78}\text{Fe}_2\text{B}_{10}\text{Si}_{10}$  requires 2.8KG,  $\text{Co}_{76}\text{Fe}_4\text{B}_{10}\text{Si}_{10}$  requires 2.7KG,  $\text{Co}_{74}\text{Fe}_6\text{B}_{10}\text{Si}_{10}$  requires 2.6 KG and  $\text{Co}_{72}\text{Fe}_8\text{B}_{10}\text{Si}_{10}$  requires 2.7KG.  $\sigma_s$  values for different samples obtained from Fig 5.10 are shown in table-5.6.

Fig- 5.11 shows that  $\sigma_s$  increases with increasing values of Fe-content in the amorphous alloy with composition  $\text{Co}_{80-x}\text{Fe}_x\text{B}_{10}\text{Si}_{10}$  [ $x= 0, 2, 4, 6 \& 8$ ]. With increasing values of Fe in the amorphous ribbon the magnetization increases, which is quite similar to the results of crystalline Co-Fe-alloys and is explained as due to higher magnetic moment of iron atoms. A simple approach is to replace a randomly varying local field at the moment site of Co by that of Fe. The results indicate that the average moment of the transition metal alloy increases with the replacement of Co by Fe. However, the rigid band model is not strictly applicable.

## 5.2.2 Specific Magnetization Measurements on two step time annealed Co- and Co-Fe- Based Amorphous Ribbons

In order to find the effect of two step annealing time on magnetic softness of the ribbons, elaborate experiments were done in amorphous ribbons with composition  $\text{Co}_{80-x}\text{Fe}_x\text{B}_{10}\text{Si}_{10}$  [ $x= 0, 2, 4, 6 \& 8$ ] by annealing time 10 minutes and 100 minutes. The annealing temperature was kept constant as  $390^\circ\text{C}$ . These results are presented Fig-5.12 to Fig- 5.16. It is observed that saturation specific magnetization increase slightly with increasing annealing time but has much larger effect on the domain wall movements, which is reflected in the easyness of magnetization of samples annealed for longer time. This is explained due to relaxation of defects in the as cast ribbons. Since domain walls are pinned at the defect centers, the annealing process thermally relaxes the sample to lower energy states. The annealing temperature, however, has to be kept below the temperature, where re- crystallization or growth of crystalline nuclei may happen. Thus coercivity of the magnetic ribbons would be increased due to annealing time.





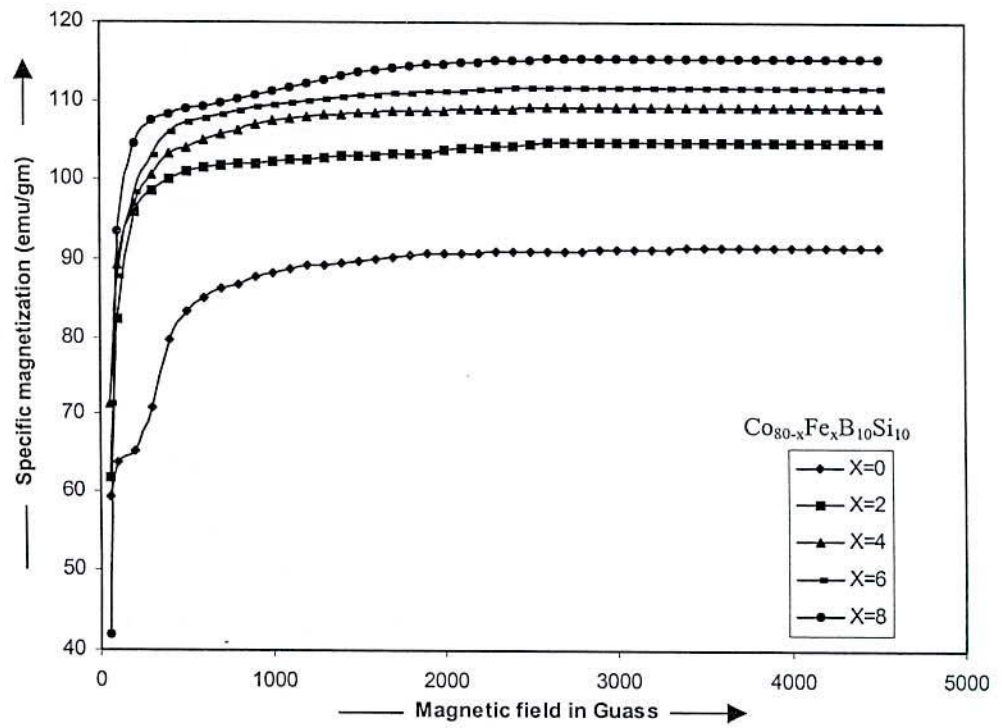


Fig.5.10 Specific magnetization versus magnetic field of as cast amorphous ribbons.

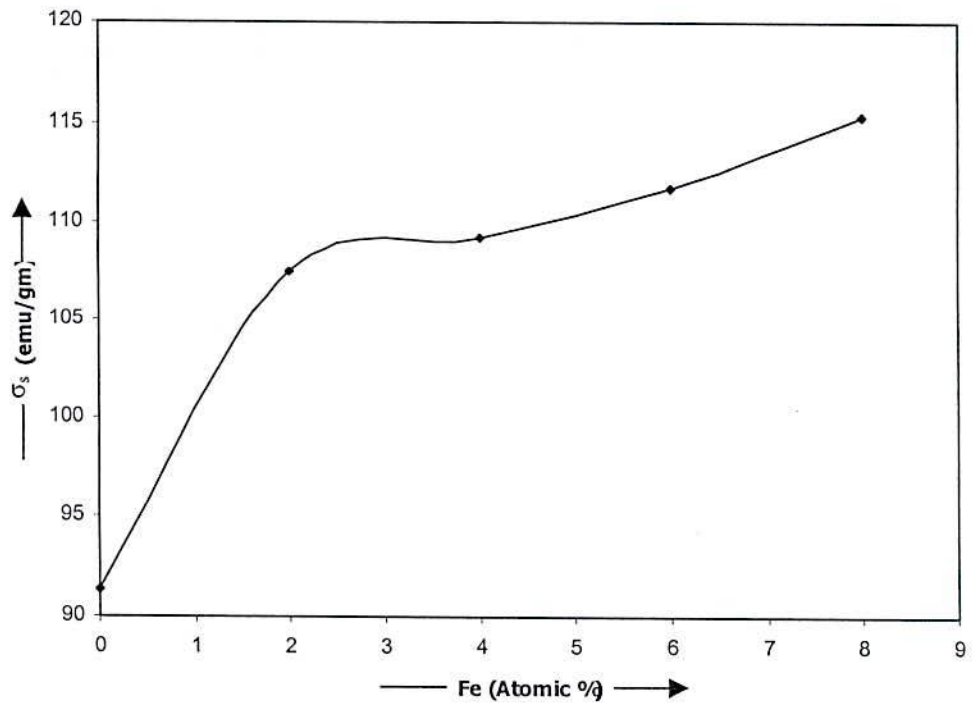


Fig.5.11 Variation of saturation specific magnetization due to change in the Fe-content.

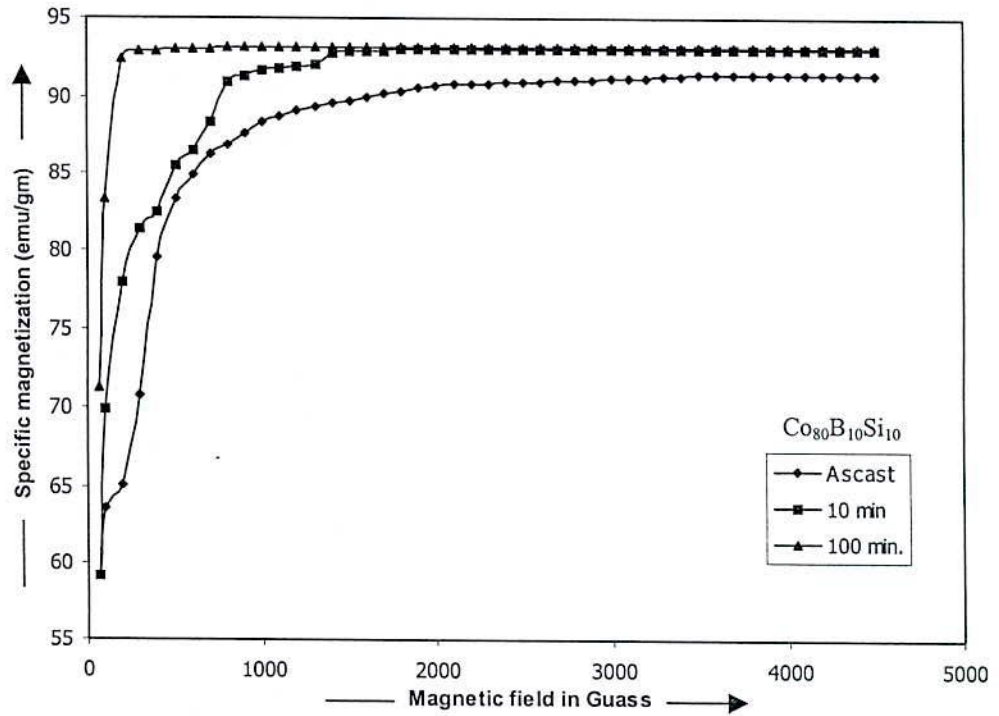


Fig.5.12 Magnetization versus magnetic field for different annealing time annealed at temperature  $390^{\circ}\text{C}$  of amorphous ribbon.

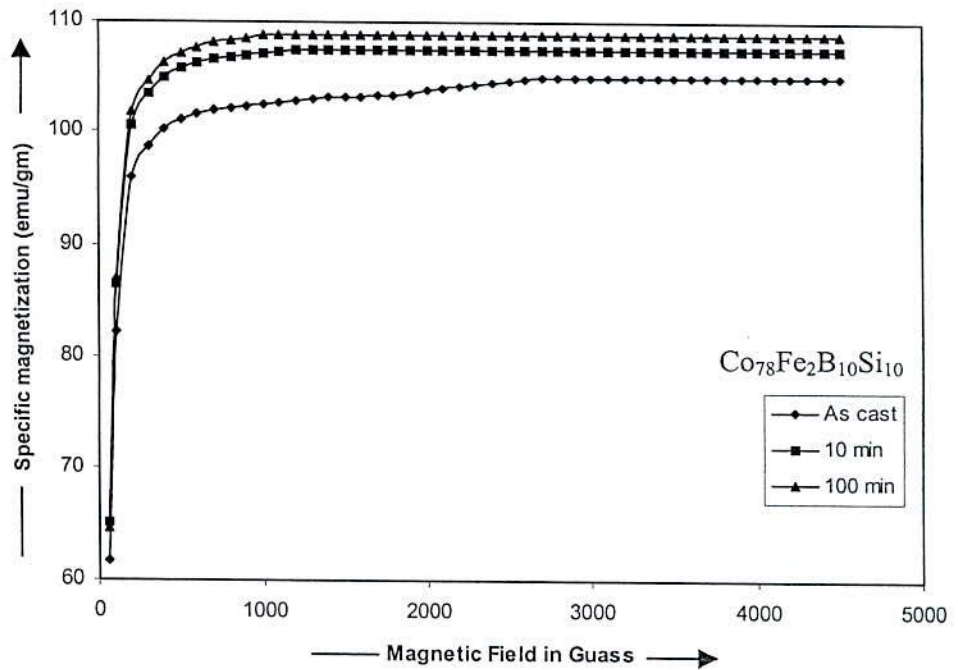


Fig.5.13 Magnetization versus magnetic field for different annealing time annealed at temperature  $390^{\circ}\text{C}$  of amorphous ribbon.

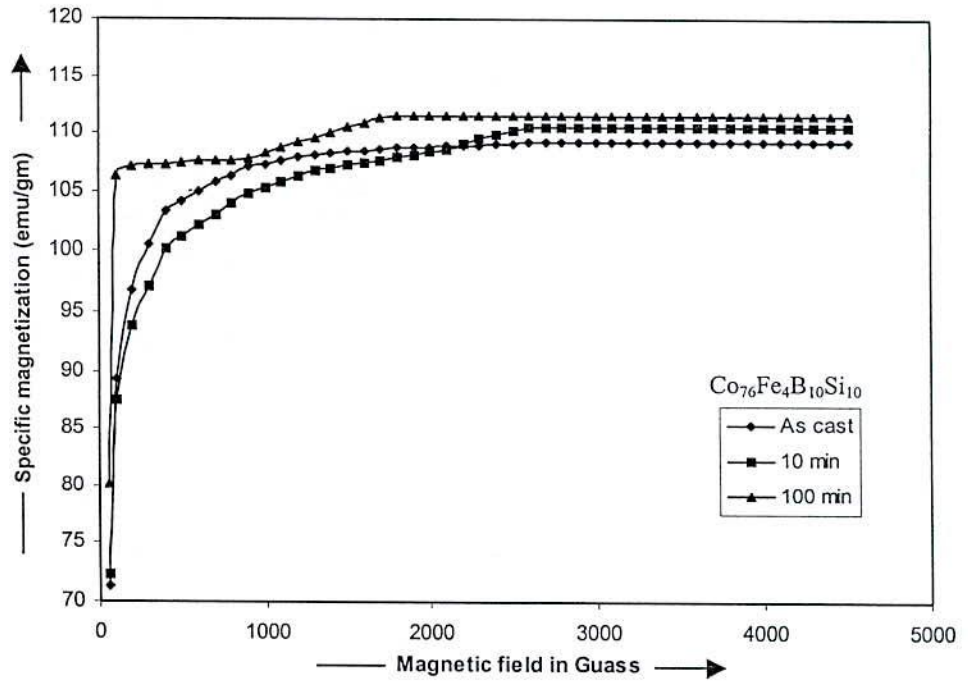


Fig.5.14 Magnetization versus magnetic field for different annealing time annealed at temperature 390°C of amorphous ribbon.

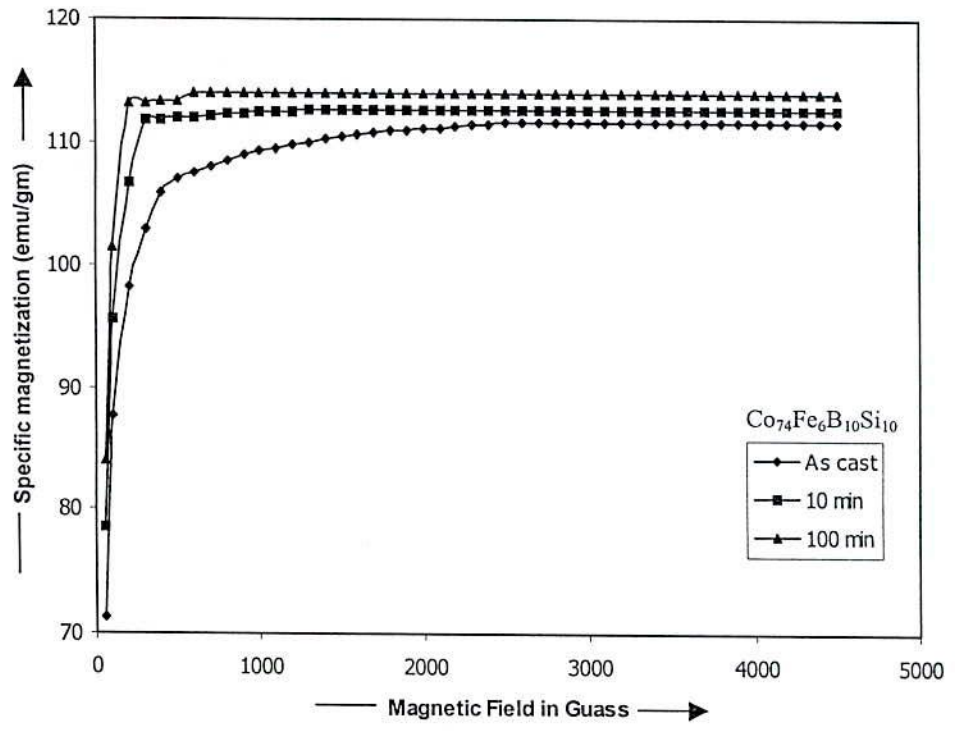


Fig.5.15 Magnetization versus magnetic field for different annealing time annealed at temperature 390°C of amorphous ribbon.



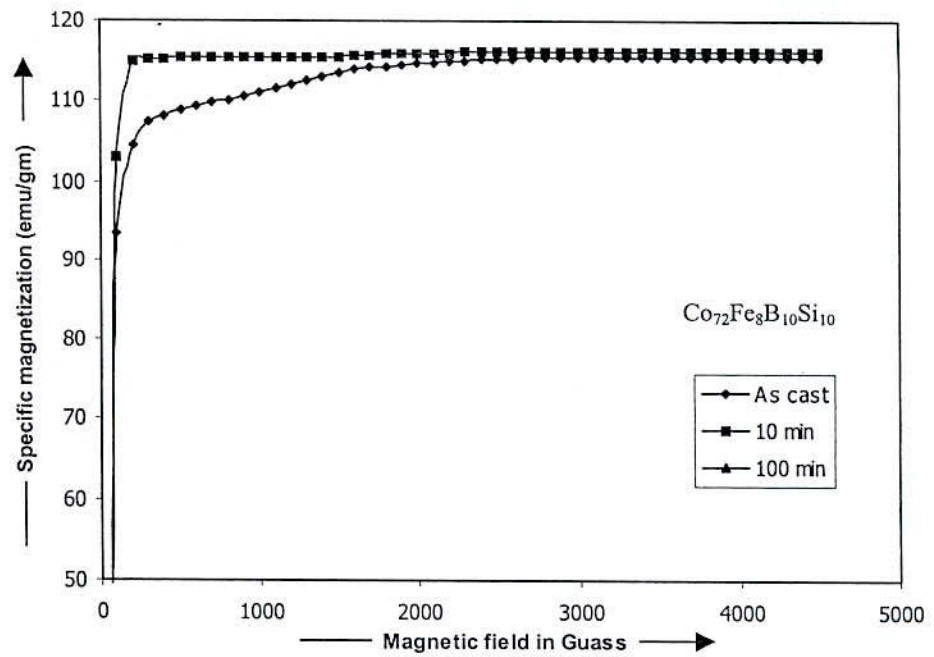


Fig.5.16 Magnetization versus magnetic field for different annealing time annealed at temperature  $390^{\circ}\text{C}$  of amorphous ribbon.

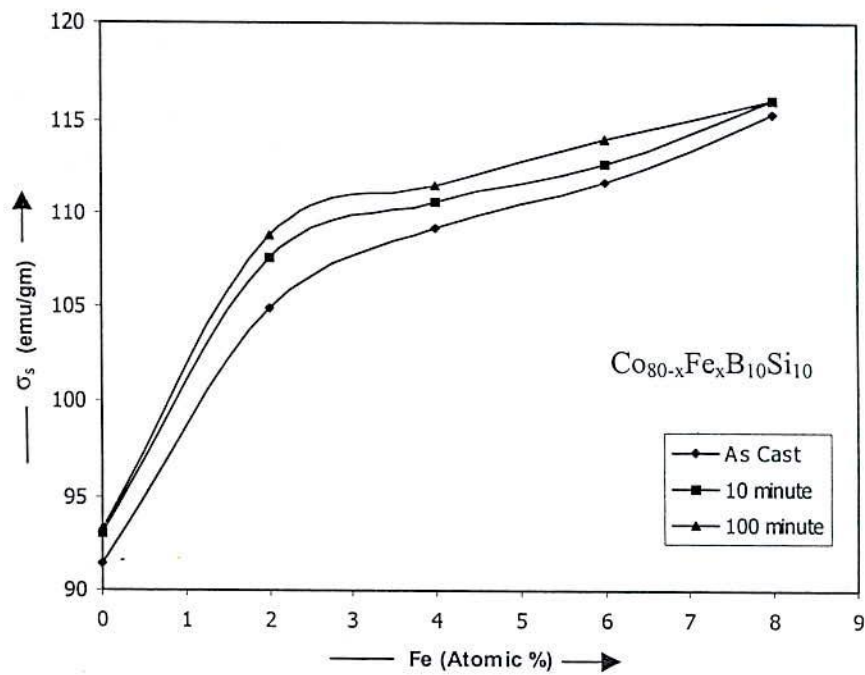


Fig.5.17 Variation of saturation specific magnetization due to change in the Fe-content of two step time annealing at  $390^{\circ}\text{C}$  of amorphous ribbon.

Fig- 5.17 Shows that the  $\sigma_s$  of Co-Fe-B-Si amorphous system increases with increasing Fe content and that also increases with increasing annealing time at constant annealing temperature 390°C. An increase of  $\sigma_s$  for the annealing time at 10 minute and 100 minute at 390°C compared with the amorphous state is due to the structural relaxation and changing the degree of chemical disorder of the amorphous state. The increase in  $\sigma_s$  is evidently caused by the irreversible relaxation.  $\sigma_s$  are given table- 5.6

Table 5.6: Two step annealing time effects on saturation specific magnetization of amorphous ribbons with composition  $\text{Co}_{80-x}\text{Fe}_x\text{B}_{10}\text{Si}_{10}$  at constant annealing temperature 390°C.

$\text{Co}_{80-x}\text{Fe}_x\text{B}_{10}\text{Si}_{10}$	$\sigma_s$ (emu/gm)		
	as cast	10 minute	100 minute
X=0	91.38	93.04	93.21
X=2	104.86	107.53	108.79
X=4	109.23	110.59	111.56
X=6	111.73	112.70	113.98
X=8	115.35	116.09	116.09

Thus the effects of annealing is explained in term of domain reorganization and domain wall movements. As is expected theoretically this annealing time changes the initial magnetization curves, due to the change in domain wall stiffness, but does not effective change in the saturation magnetization is slightly increased and observed.

### 5.3 Dynamic Magnetic Properties of Co- and Co-Fe- Based Amorphous Ribbons

Dynamic magnetic properties of as cast Co-Fe-B-Si system with composition  $\text{Co}_{80-x}\text{Fe}_x\text{B}_{10}\text{Si}_{10}$  [X=0, 2, 4, 6 & 8] have been determined using LF impedance analyzer (LF impedance analyzer, 4192A, Range 5Hz- 13MHz, Agilent Technologies, Japan limited, Japan). Permeability measurements were performed on toroidal samples at frequency of 1KHz to 13MHz and an applied ac driving field ( $\approx 0.11A/m$ ) low enough to ensure the measurements of initial permeability. The measurement has been done both in the as cast, two step annealing time with different annealing condition. In order to

avoid the experimental error due to fluctuation in ribbon thickness and thermal treatments, just one piece of each ribbon has been measured at room temperature after subsequent annealing temperature and annealing time. The compositional dependence of initial permeability is determined for different values of x and their frequency dependence of complex magnetic characteristics, like real and imaginary parts of initial permeability, loss factor and relative quality factor are analyzed.

### 5.3.1 Initial Permeability of as cast Co- and Co-Fe- Based Amorphous Ribbons

Frequency measurements were performed with an impedance analyzer in the frequency 1KHz at room temperature and with various applied field. The initial permeability ( $\mu'$ ) of the ribbons with composition  $\text{Co}_{80-x}\text{Fe}_x\text{B}_{10}\text{Si}_{10}$  calculated from the low a.c magnetic field dependence of permeability in the limit of frequency 1KHz and vanishing magnetic field as shown in Fig-5.18. The results are shown in table 5.7. Initial permeability is controlled by the reversible part of the domain motion. The preparation technique determines the defects and the associated energy barriers to domain wall motion. As shown in Fig- 5.18,  $\mu'$  is independent of applied field for x= 0, 2, & 8 and  $\mu'$  increases with applied for x= 4 & 6.

Table 5.7: The initial permeability in the vanishing field region of the amorphous ribbon with composition  $\text{Co}_{80-x}\text{Fe}_x\text{B}_{10}\text{Si}_{10}$

$\text{Co}_{80-x}\text{Fe}_x\text{B}_{10}\text{Si}_{10}$	X=0	X=2	X=4	X=6	X=8
$\mu'$	472	1509	1714	1875	1070

Fig- 5.19 Shows that  $\mu'$  of Co-Fe-B-Si amorphous system increases almost monotonously with the replacement of Fe up to 6 At. % for Co, at which a maximum value of 1875 is observed for the relative permeability. This increase of  $\mu'$  with increased Fe- content is explained as due to the decrease of the net magnetostriction arising from the cancellation of the negative contribution of Co by the positive contribution of Fe. The maximum value of  $\mu'$  ribbons having 6 At. % iron is attributed to the minimum magnetostriction and low coercivity at this composition. When the proportion of Fe is increased further to 8 At.%  $\mu'$  decrease which is attributed to the increase of manetostriction, as the negative manetostriction of Co is more than compensated by the positive contribution of manetostriction of Fe atoms of this composition.



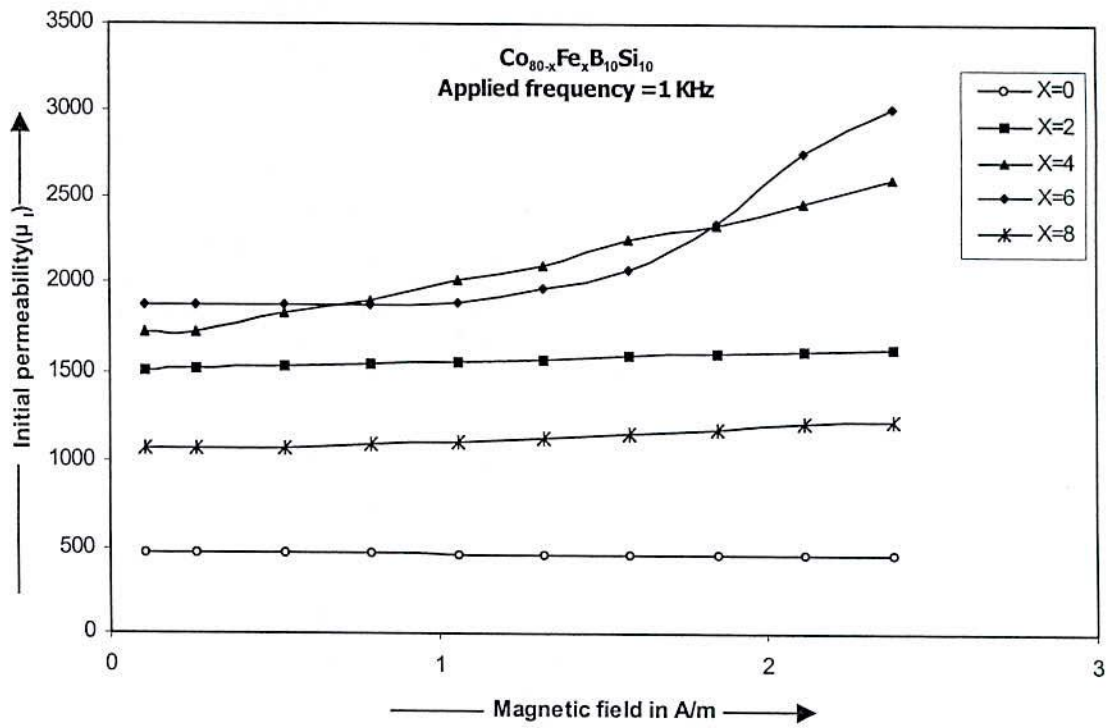


Fig 5.18 Permeability versus a.c. magnetic field of amorphous ribbons with composition  $\text{Co}_{80-x}\text{Fe}_x\text{B}_{10}\text{Si}_{10}$ .

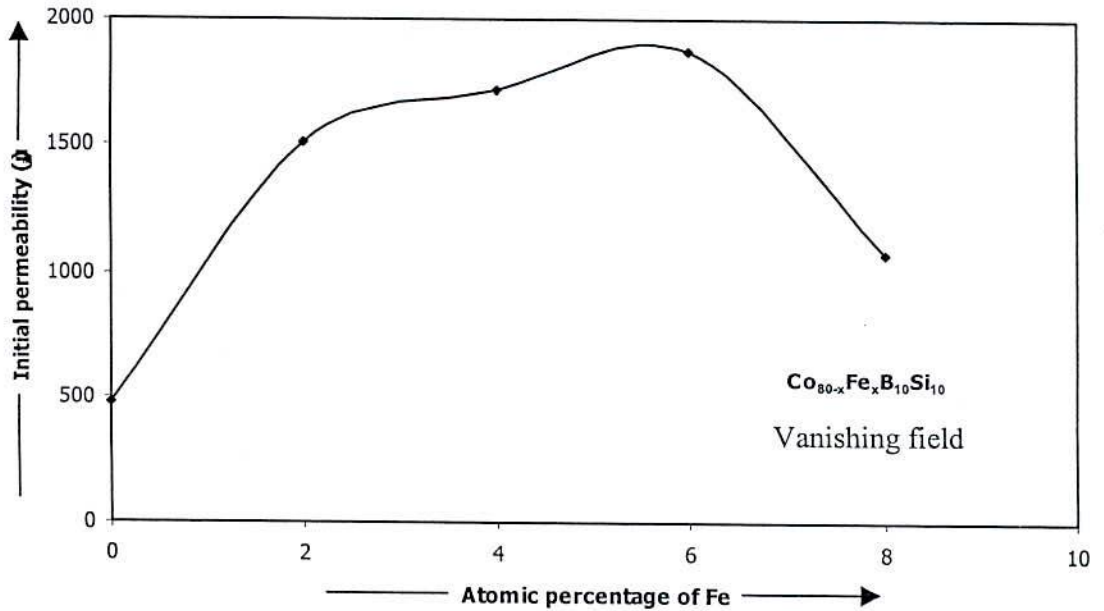


Fig 5.19 Variation of initial permeability with the change in the Fe-content in  $\text{Co}_{80-x}\text{Fe}_x\text{B}_{10}\text{Si}_{10}$  amorphous ribbons.

### 5.3.2 Complex Permeability of the as cast Co- and Co- Fe-Based Amorphous Ribbons

The compositional dependence of initial permeability of amorphous ribbons with composition  $\text{Co}_{80-x}\text{Fe}_x\text{B}_{10}\text{Si}_{10}$  were determined for different values of X and their frequency dependence of complex magnetic characteristics, like real and imaginary parts of initial permeability, loss factor and relative quality factor are analyzed. The frequency dependence of the real part of complex permeability is shown in Fig- 5.20. The flat region up to the frequency 700 KHz indicates that all the samples with different compositions are suitable as core materials at low fields. While the iron free sample shows a relative permeability of 472 and maintains almost a constant value even beyond 1MHz, the partly introduction of Fe, to partly replace Co, increase the permeability enormously. However, the maximum frequency ranges for which the permeability is maintained constant in order of  $10^5$  Hz to  $10^6$  Hz.

The imaginary part of the complex permeability and loss factor for different compositions over the frequency range 1 KHz to 13 MHz are shown in Fig- 5.21 and Fig- 5.22 respectively. The origin of the loss factor can be attributed to various domain defects<sup>(5.11)</sup>, which include non-uniform and non-repetitive domain wall motion, domain wall bowing, localized variation of flux density and nucleation and annihilation of domain walls. The frequency dependence of relative quality factor is shown in Fig- 5.23. The relative quality factors are controlled by the real part of the complex permeability, have quite high values in the range 10 KHz to 500 KHz for the three ribbons having composition  $\text{Co}_{78}\text{Fe}_2\text{B}_{10}\text{Si}_{10}$ ,  $\text{Co}_{76}\text{Fe}_4\text{B}_{10}\text{Si}_{10}$ ,  $\text{Co}_{74}\text{Fe}_6\text{B}_{10}\text{Si}_{10}$  and quite naturally, these samples have low loss factors. The other two samples having compositions  $\text{Co}_{80}\text{B}_{10}\text{Si}_{10}$  and  $\text{Co}_{72}\text{Fe}_8\text{B}_{10}\text{Si}_{10}$  have high loss factors and relatively low quality factors.

### 5.3.3 Frequency Dependence of the real Part of the Complex Permeability of Co- and Co-Fe- Based Amorphous Ribbons With Different Annealing Temperature and Two Step Annealing Time

Two step time annealing effect on complex permeability of Co and Co-Fe- based amorphous ribbons with composition  $\text{Co}_{80-x}\text{Fe}_x\text{B}_{10}\text{Si}_{10}$  [X= 0, 2, 4, 6 & 8] has been

measured as a function of frequency in the range 1 KHz to 13 MHz. The measurements has been done both in the as cast and annealed conditions. The annealing temperature was varied 25 to 450°C with constant annealing time 10 minute (1st step) and with constant annealing time 100 minute (2nd step). Fig- 5.24 to Fig- 5.33 show frequency dependence of the real part of initial permeability for constant 10 minute (1st step) time annealing and constant 100 minute (2nd step) time annealing. For samples annealed for 10 minutes, it is observed that there is consistent decrease in the initial permeability value with increasing annealing temperature. From these spectra observed that for initial permeability linearly decreases with increasing annealing temperature up to 390°C for Co- based ribbon and 425°C for Co-Fe- based ribbons. There is a drastic fall in permeability spectrum when the annealing temperature 425°C for  $\text{Co}_{80}\text{B}_{10}\text{Si}_{10}$  and 450°C for  $\text{Co}_{80-x}\text{Fe}_x\text{B}_{10}\text{Si}_{10}$  [ $X= 2, 4, 6 \text{ \& } 8$ ] at constant annealing time 10 minutes. The initial permeability spectrum (Fig- 5.24, Fig- 5.26, Fig- 5.28, Fig- 5.30 & Fig 5.32) compared as cast sample at 10 minute annealing time decreases with increasing 100 minute annealing time (Fig- 5.25, Fig- 5.27, Fig-5.29, Fig-5.31 & Fig- 5.33) at constant annealing temperature varied from 25°C to 450°C. The real part of complex permeability Co- and Co-Fe- based amorphous ribbon annealed at 100°C to 350°C have similar behavior with frequency through their values are different depending on the annealing temperature. It can be observed that the real part of the initial complex permeability enhancement with short time annealing is more effective then long time annealing at the same temperature. These studies of two step effect of annealing time on permeabilities provides information regarding the thermal stability of these material as a transformer core when used at an elevated temperature. From these results are evident that annealing temperature and annealing time are both important parameter in controlling the frequency response of permeability of samples. The best choice of these two parameters depends on the desired characteristics of the material in respect of permeability value and its frequency dependence. For the present work we were interested only in all the permeabilities measurement and therefore the applied field was kept constant and small in its value 0.11A/m.



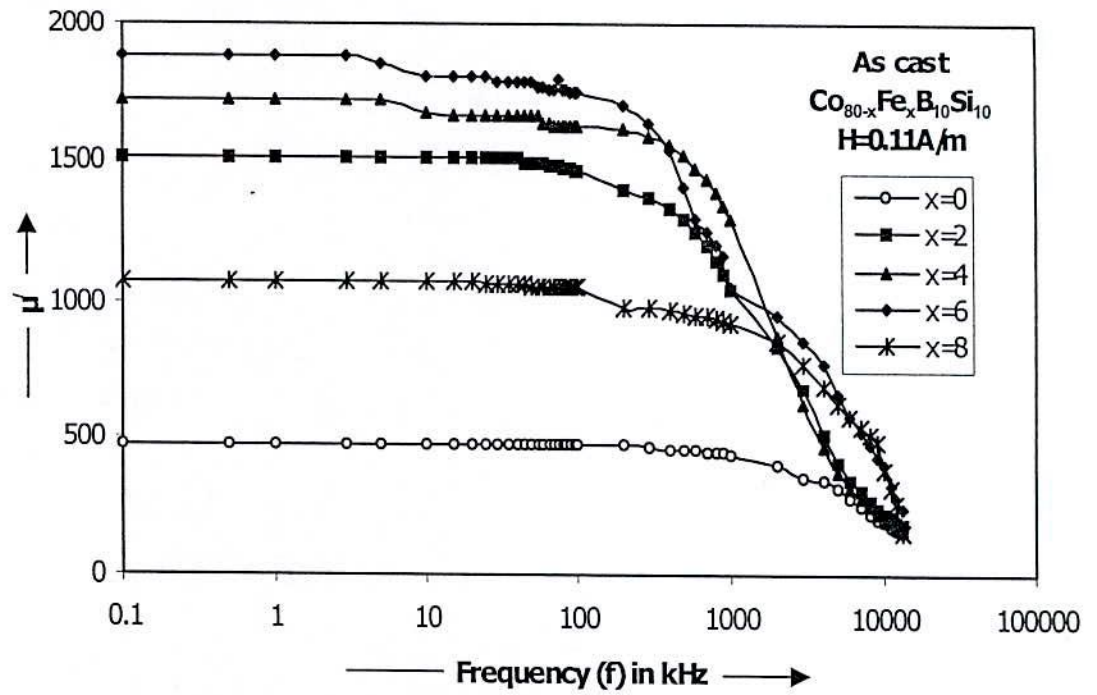


Fig 5.20 Frequency dependence of the real part of initial permeability of amorphous ribbons.

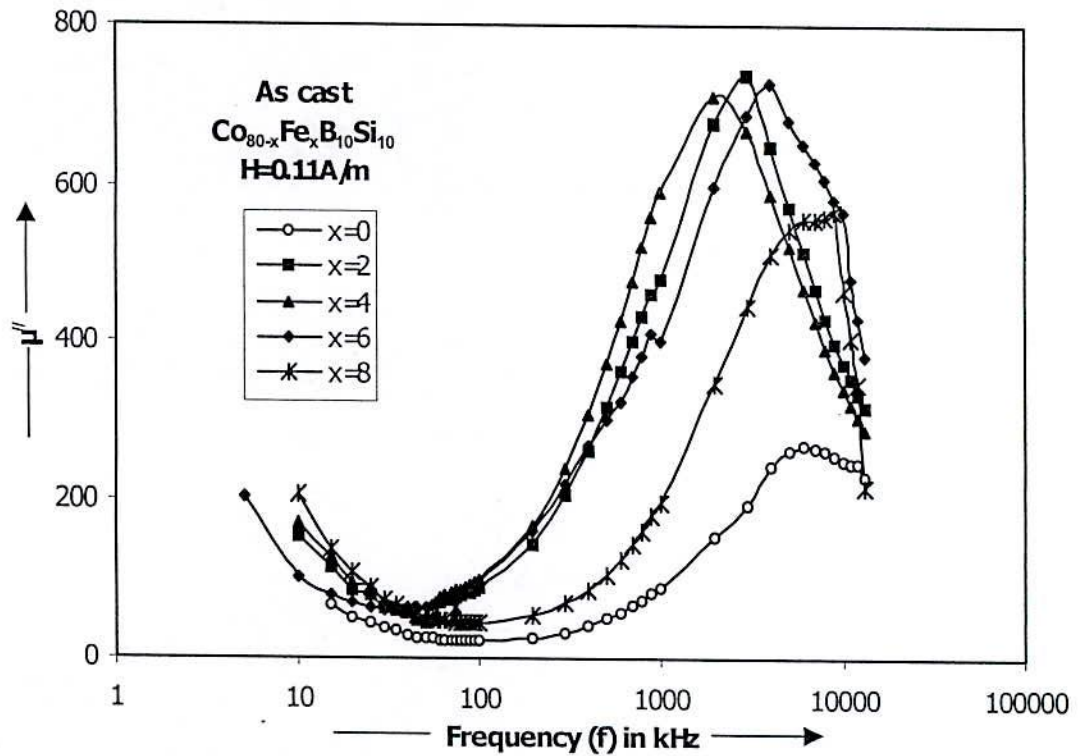


Fig 5.21 Frequency dependence of the imaginary part of initial permeability of amorphous ribbons.

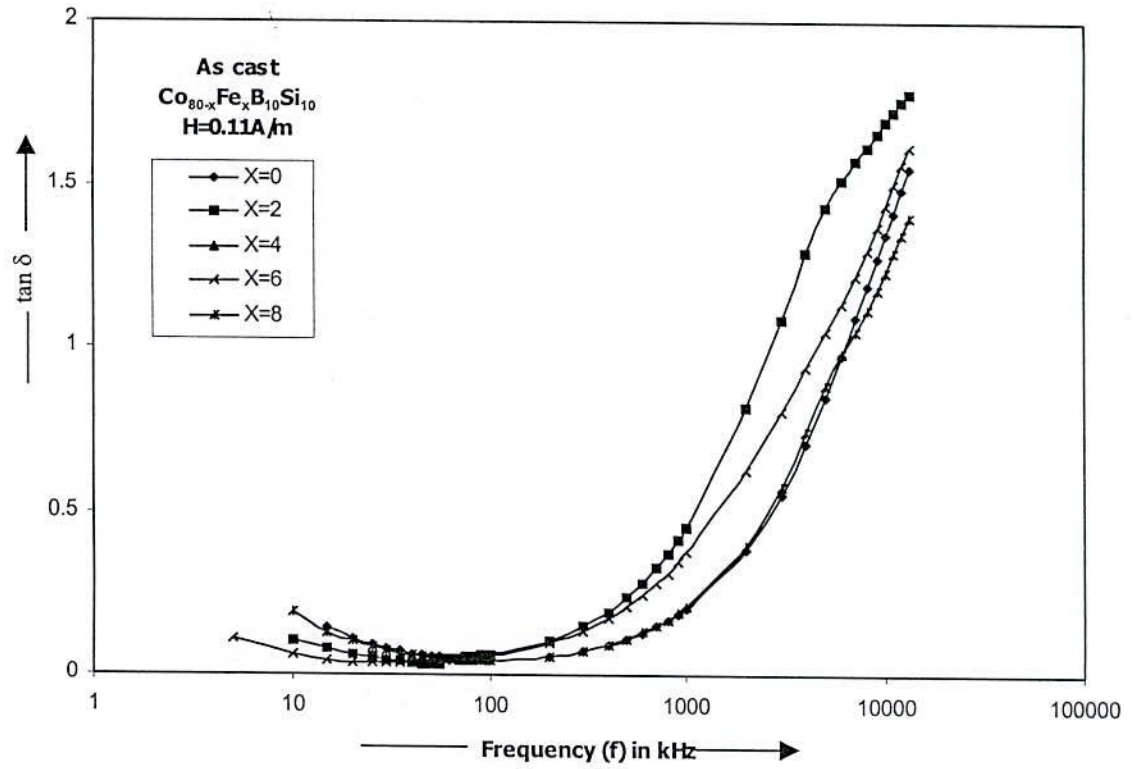


Fig 5.22 Frequency dependence of loss factor of amorphous ribbon.

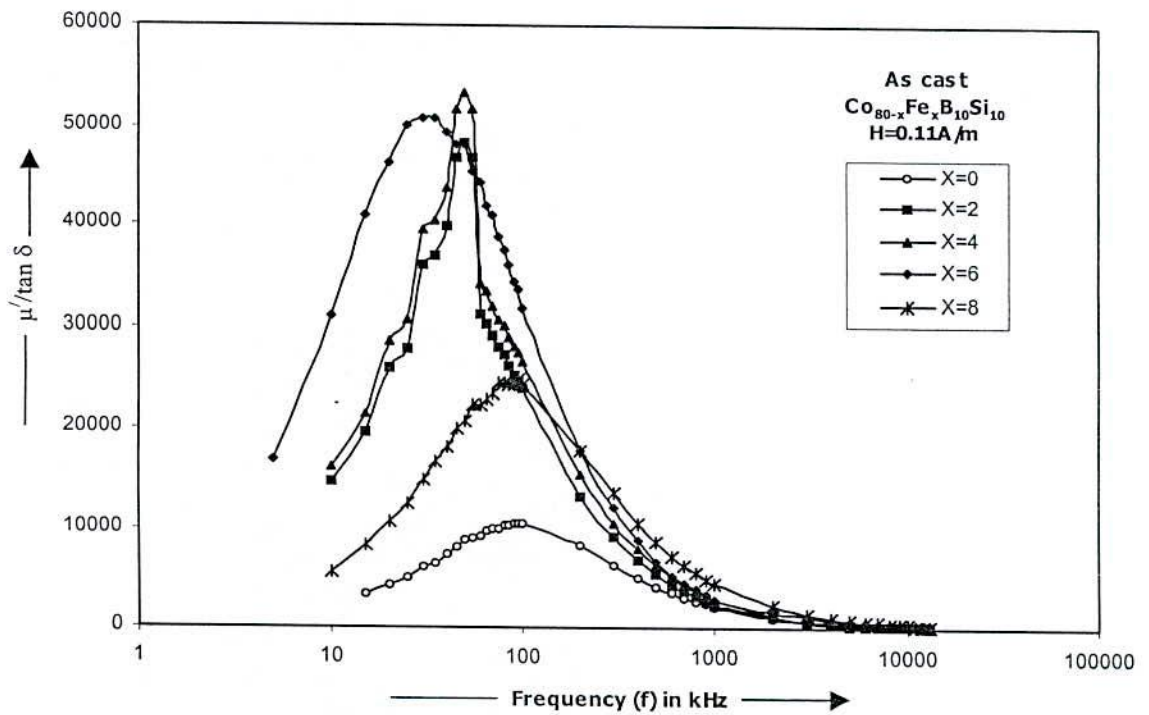


Fig 5.23 Frequency dependence of relative quality factor of amorphous ribbons.

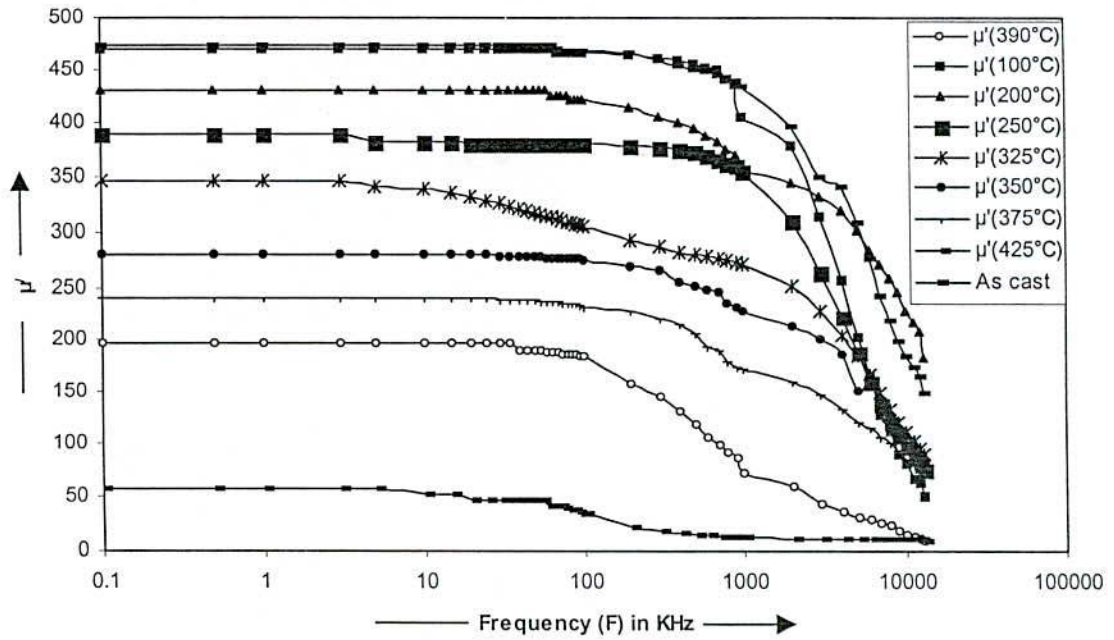


Fig-5.24 Frequency dependence of the real part of initial permeability of amorphous ribbon for different annealing temperature with composition  $\text{Co}_{80}\text{B}_{10}\text{Si}_{10}$  at constant 10minute annealing time ( $H= 0.11\text{A/m}$ ).

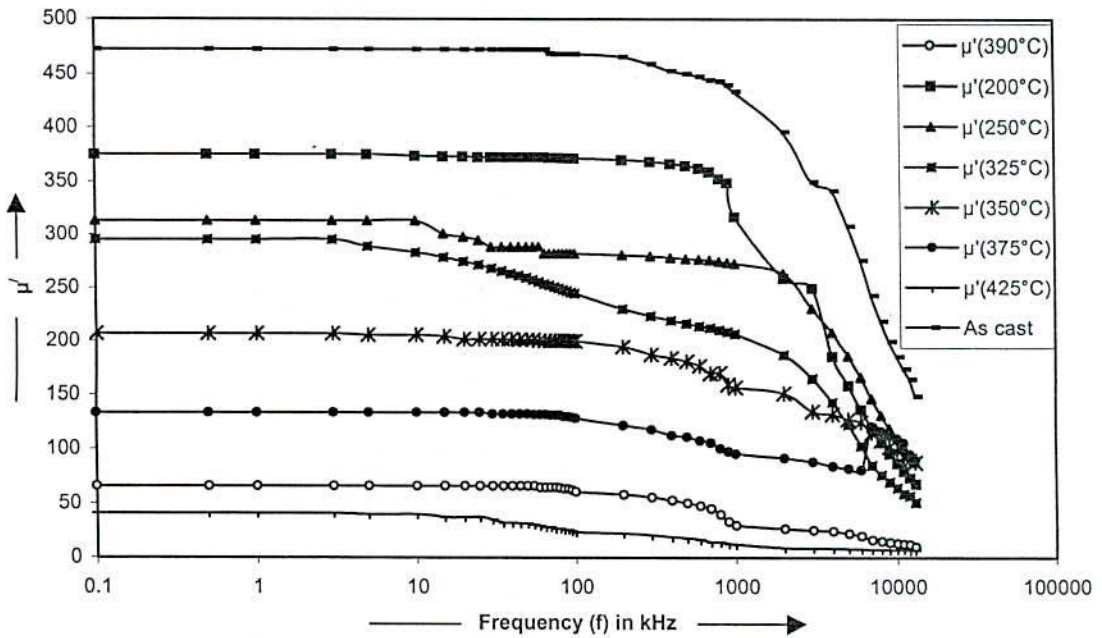


Fig-5.25 Frequency dependence of the real part of initial permeability of amorphous ribbon for different annealing temperature with composition  $\text{Co}_{80}\text{B}_{10}\text{Si}_{10}$  at constant 100 minute annealing time ( $H= 0.11\text{ A/m}$ ).



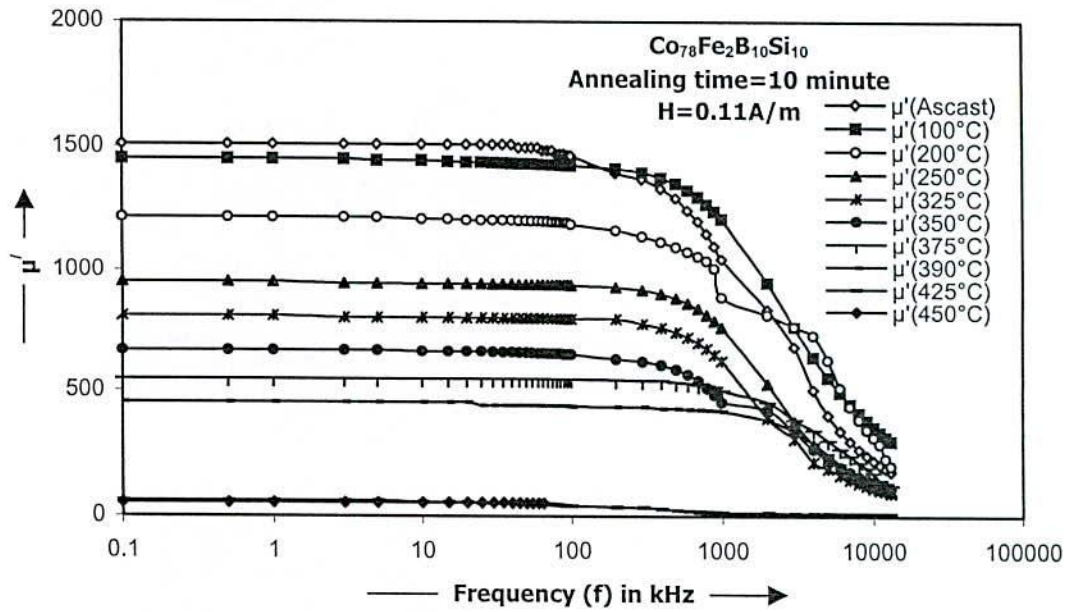


Fig 5.26 Frequency dependence of the real part of initial permeability of the amorphous ribbon for different annealing temperature.

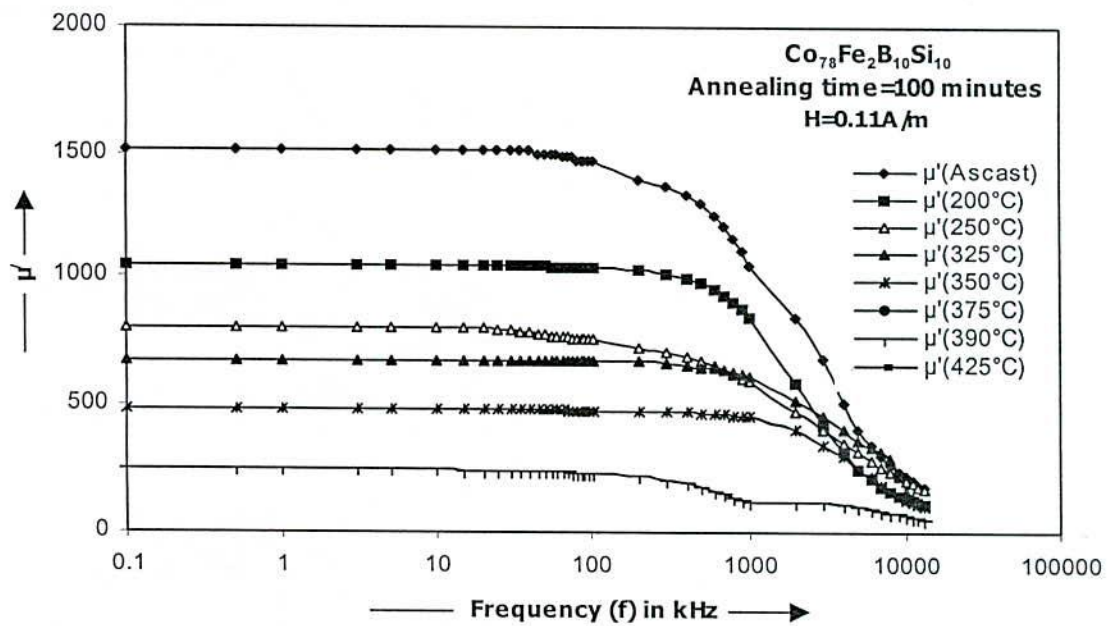


Fig 5.27 Frequency dependence of the real part of initial permeability of the amorphous ribbon for different annealing temperature.

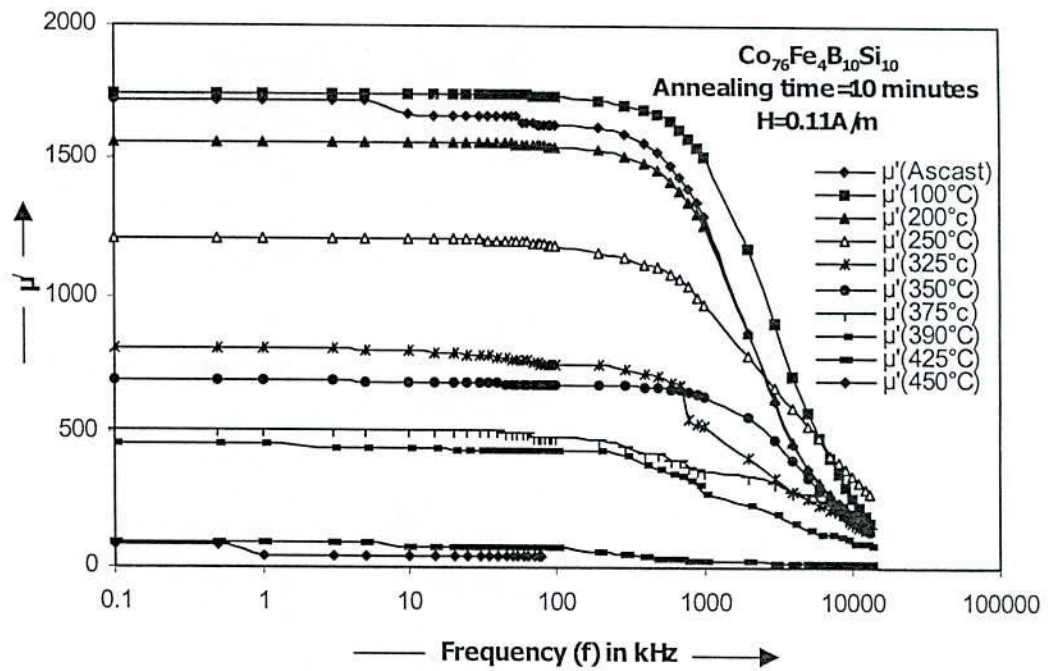


Fig 5.28 Frequency dependence of the real part of initial permeability of the amorphous ribbon for different annealing temperature.

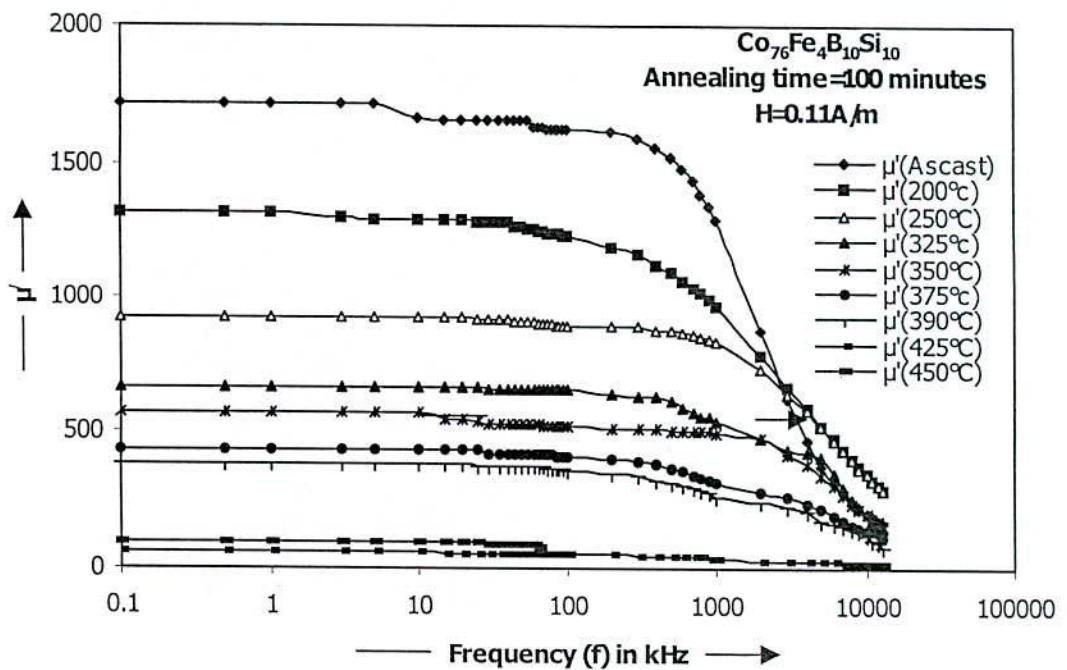


Fig 5.29 Frequency dependence of the real part of initial permeability of the amorphous ribbon for different annealing temperature.

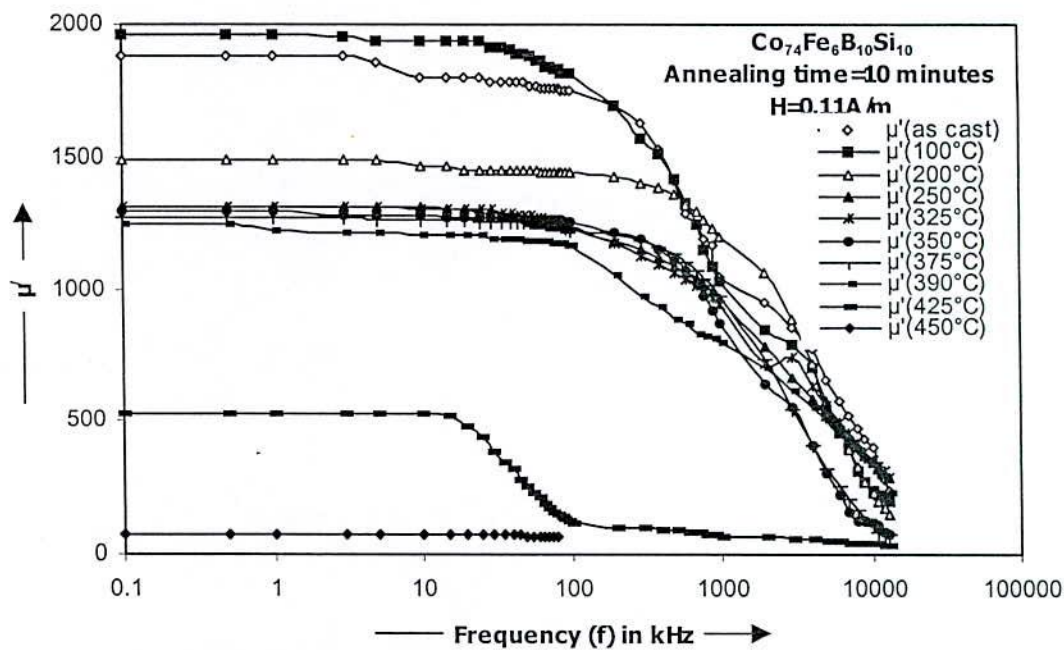


Fig 5.30 Frequency dependence of the real part of initial permeability of the amorphous ribbon for different annealing temperature.

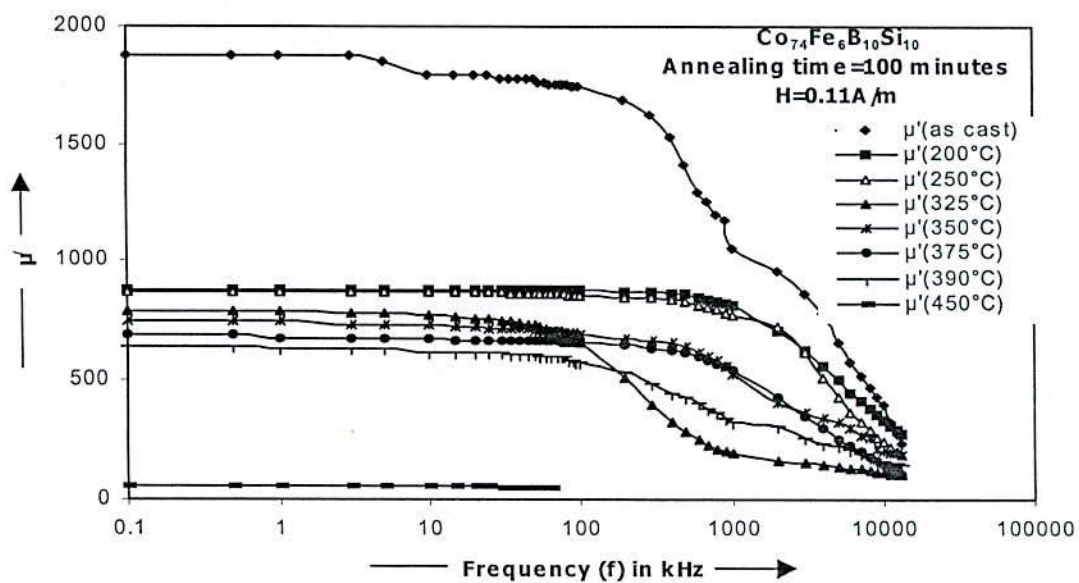


Fig 5.31 Frequency dependence of the real part of initial permeability of the amorphous ribbon for different annealing temperature.



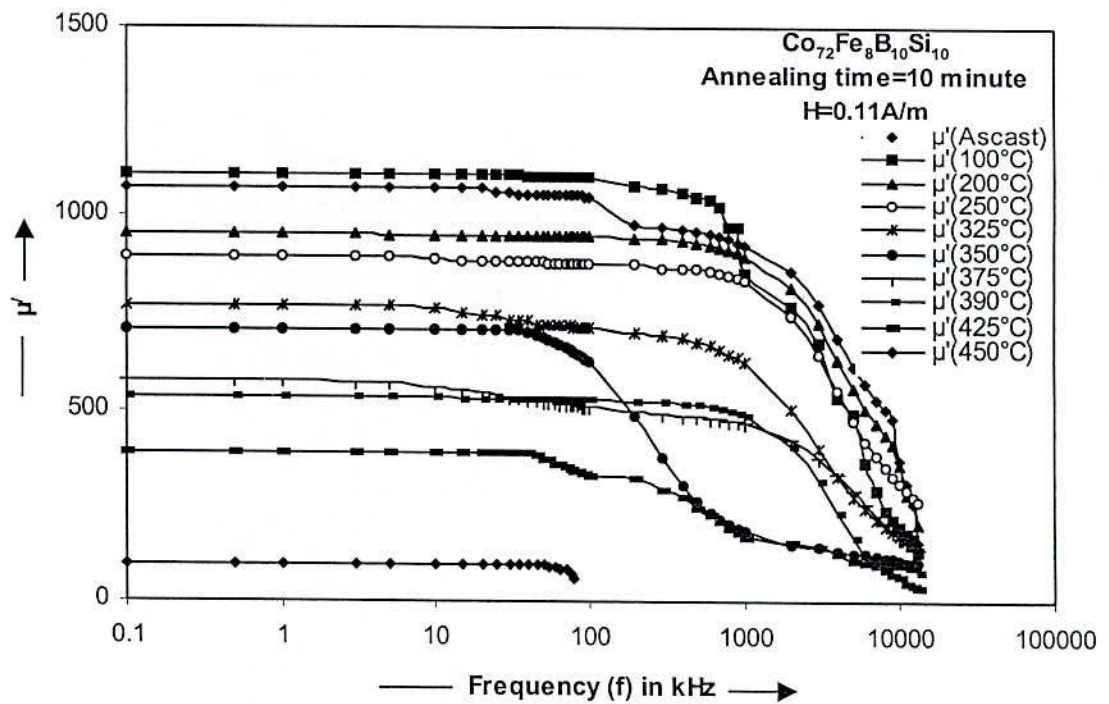


Fig 5.32 Frequency dependence of the real part of initial permeability of the amorphous ribbon for different annealing temperature.

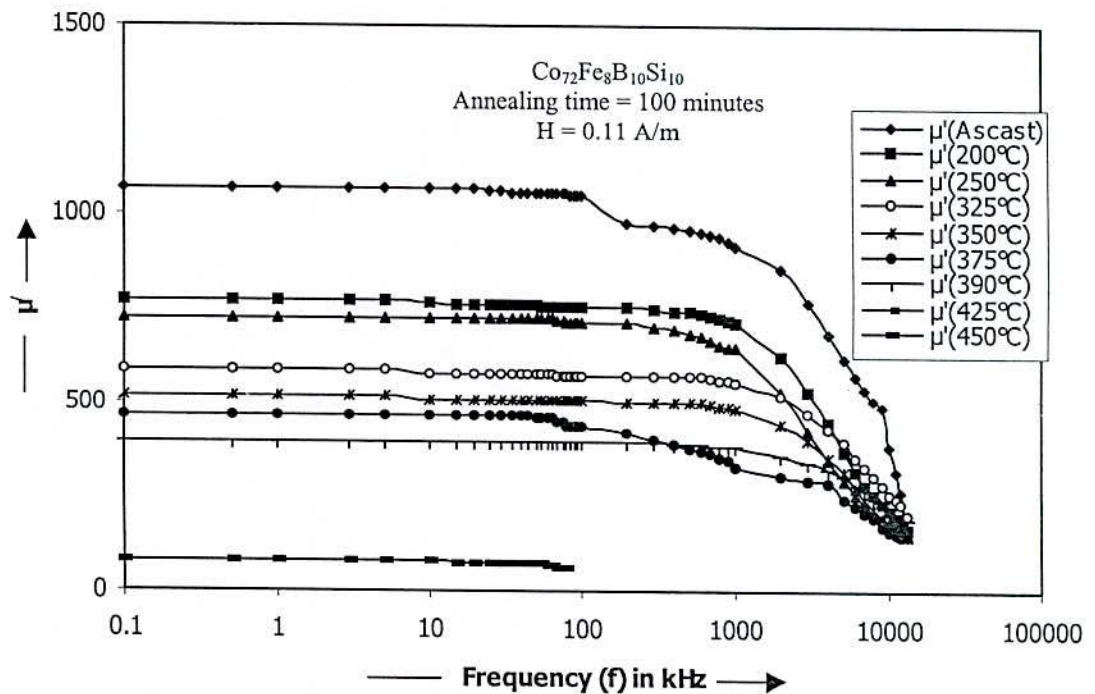


Fig 5.33 Frequency dependence of the real part of initial permeability of the amorphous ribbon for different annealing temperature.

### 5.3.4 Frequency Dependence of the Imaginary Part of the Complex Permeability of Co- and Co-Fe- Based Amorphous Ribbon With Different Annealing Temperature and Two Step Annealing Time

The imaginary part of the complex permeability ( $\mu''$ ) for two step annealing time (10 minutes & 100 minutes) with different annealed temperature over the frequency range 1 KHz to 13 MHz are shown in Fig- 5.34 to Fig 5.43. These results are quite complimentary to the results for the real part of the complex permeability of samples. The usefulness of the results of  $\mu''$  lie in the determination of the relative quality factor of these samples. The  $\mu''$  for all the samples at low frequencies has relatively low value and corresponds to low loss factor and high relative quality factor. The origin of the loss factor can be attributed to various domain effects<sup>(5.11)</sup>, which include non-uniform and non repetitive domain wall motion, domain wall bowing, localized variation of flux density and nucleation and annihilation of domain walls. The frequency dependence of  $\mu''$  of the samples annealed at different temperatures can be attributed to the growth and distribution of the crystallites. The increase in annealing time brings about smoothness in the variation of  $\mu''$  with frequency. These are explained as due to the stabilization of the crystallites.

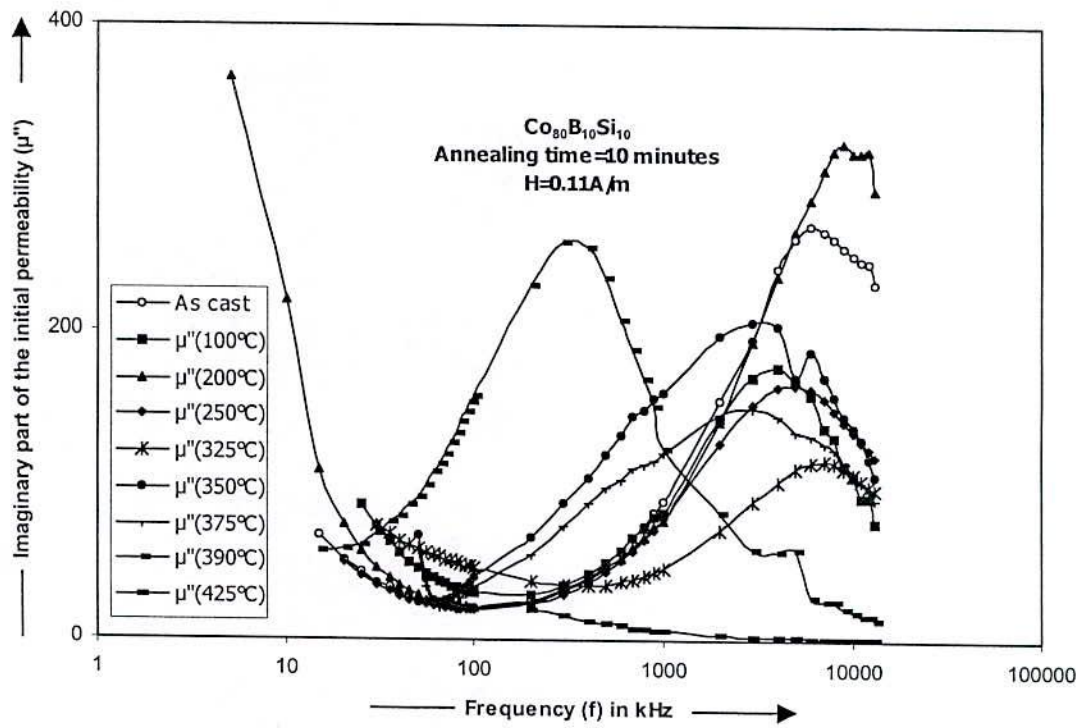


Fig 5.34 Frequency dependence of the imaginary part of the initial permeability of amorphous ribbons for different annealing temperature.

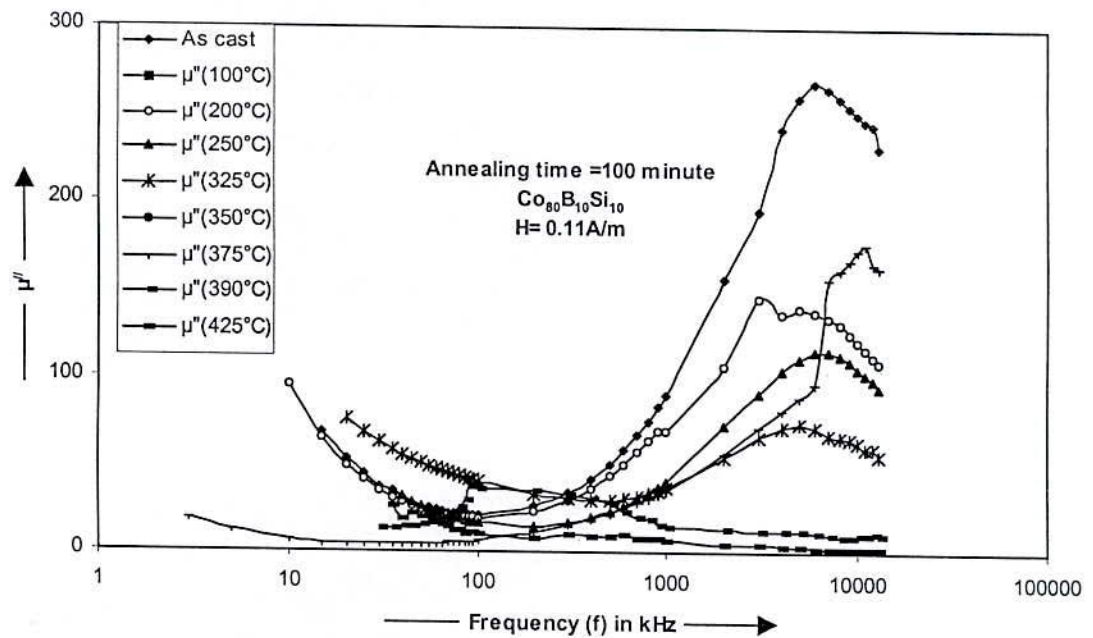


Fig 5.35 Frequency dependence of the imaginary part of the initial permeability of amorphous ribbons for different annealing temperature.



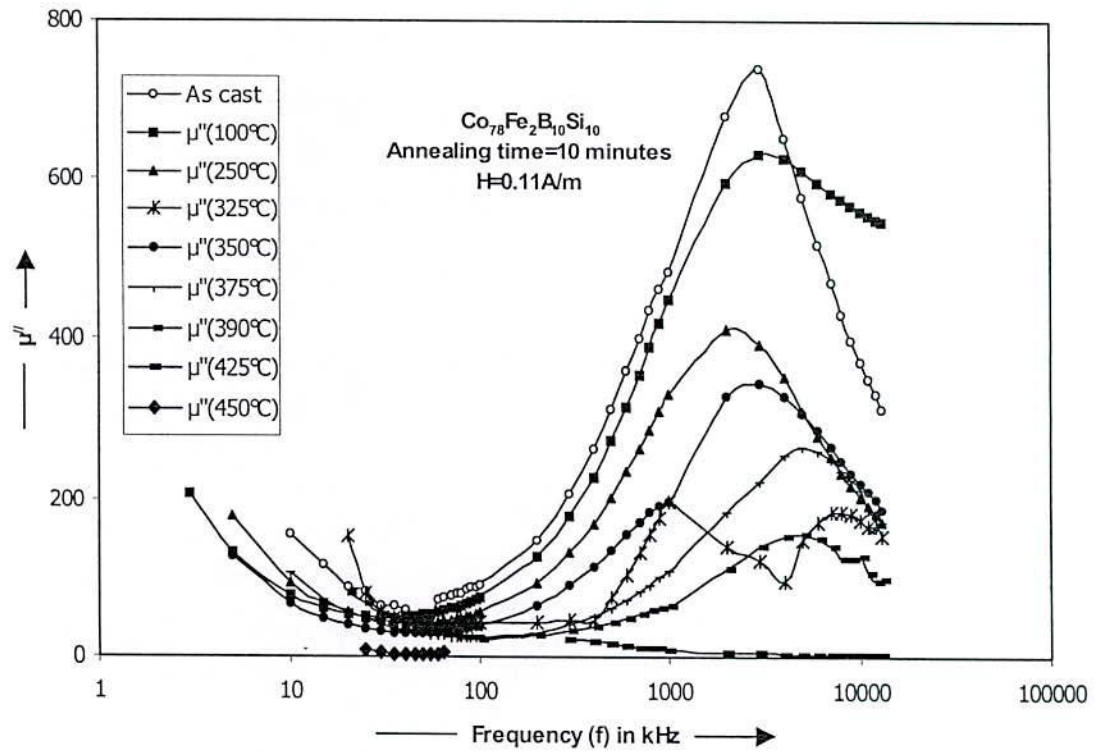


Fig 5.36 Frequency dependence of the imaginary part of the initial permeability of amorphous ribbons for different annealing temperature.

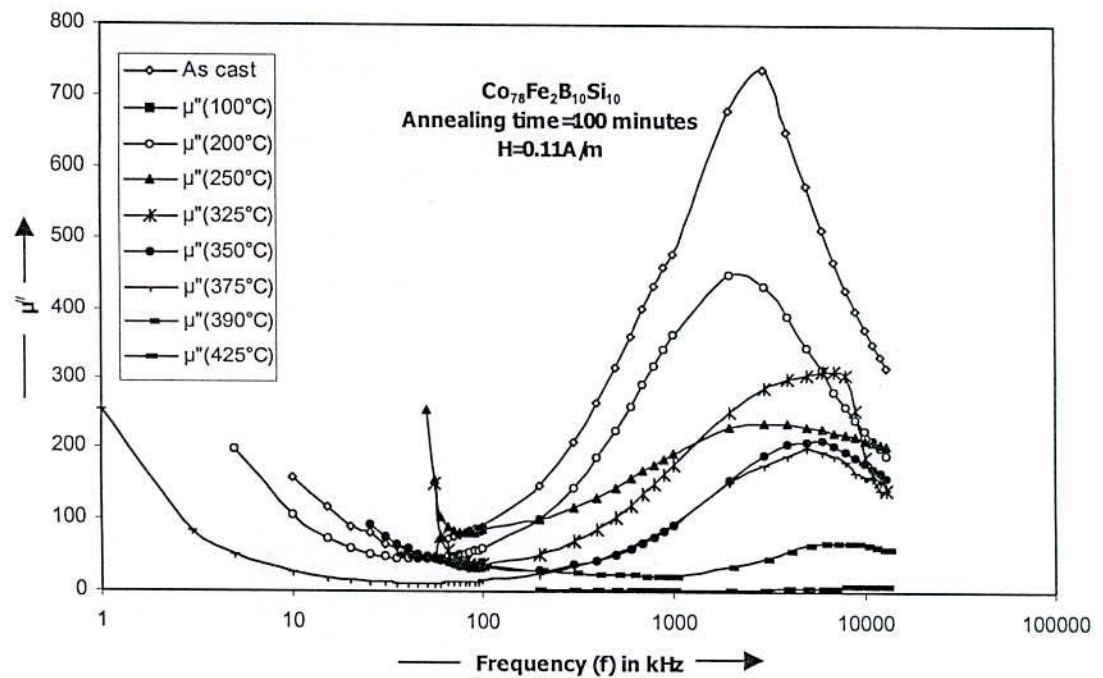


Fig 5.37 Frequency dependence of the imaginary part of the initial permeability of amorphous ribbons for different annealing temperature.

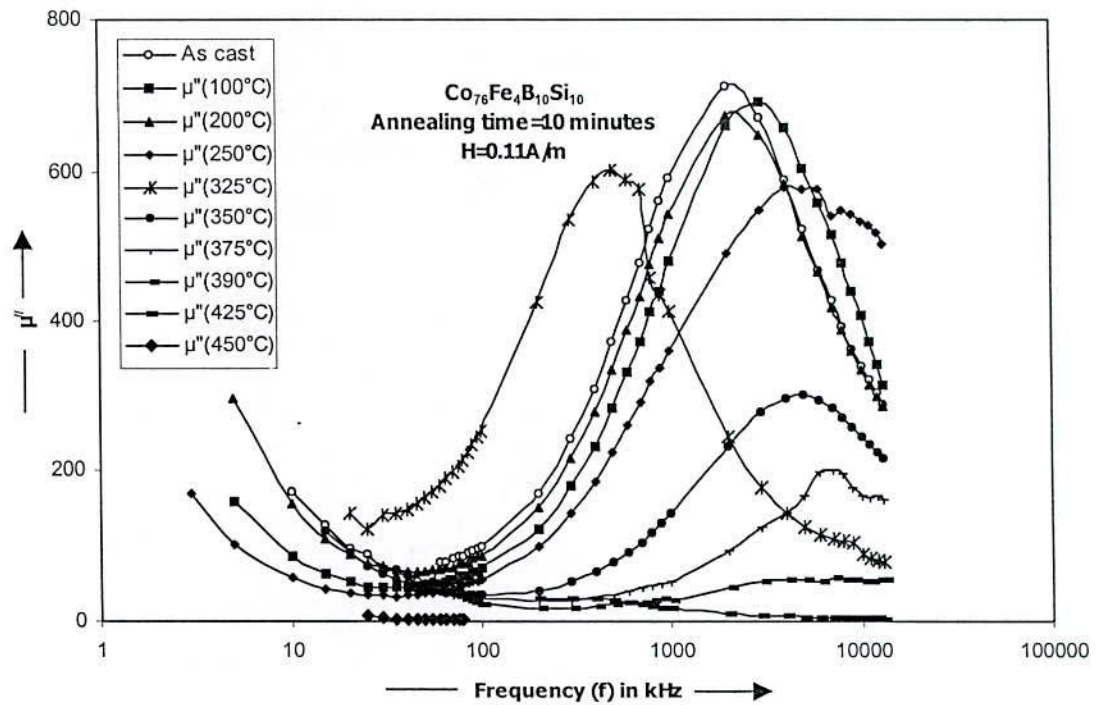


Fig 5.38 Frequency dependence of the imaginary part of the initial permeability of amorphous ribbons for different annealing temperature.

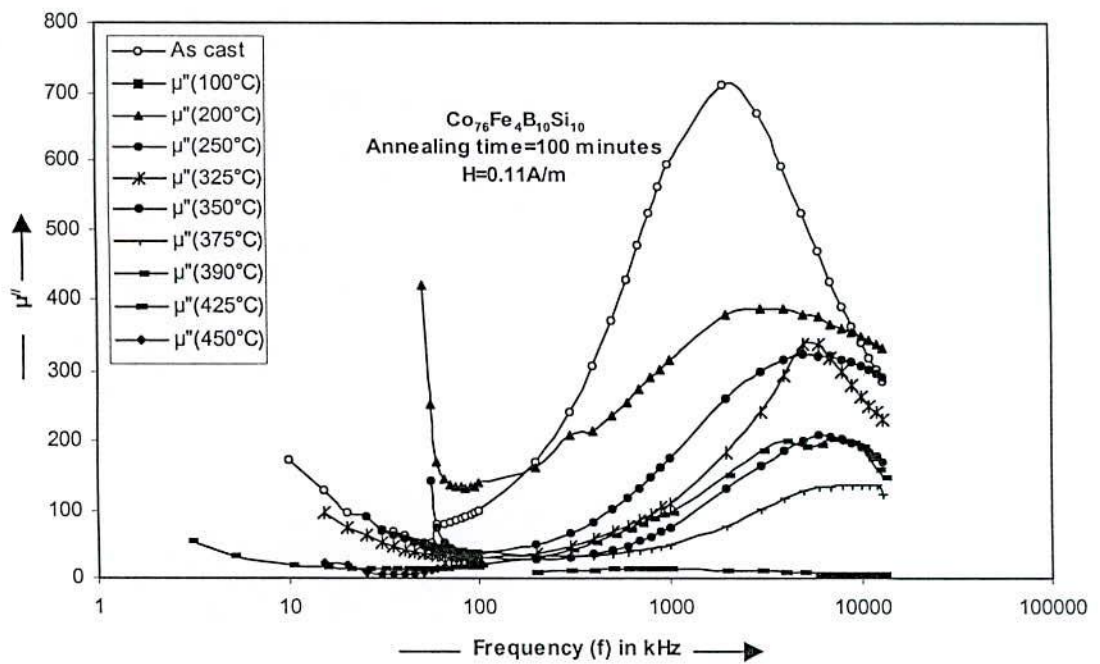


Fig 5.39 Frequency dependence of the imaginary part of the initial permeability of amorphous ribbons for different annealing temperature.

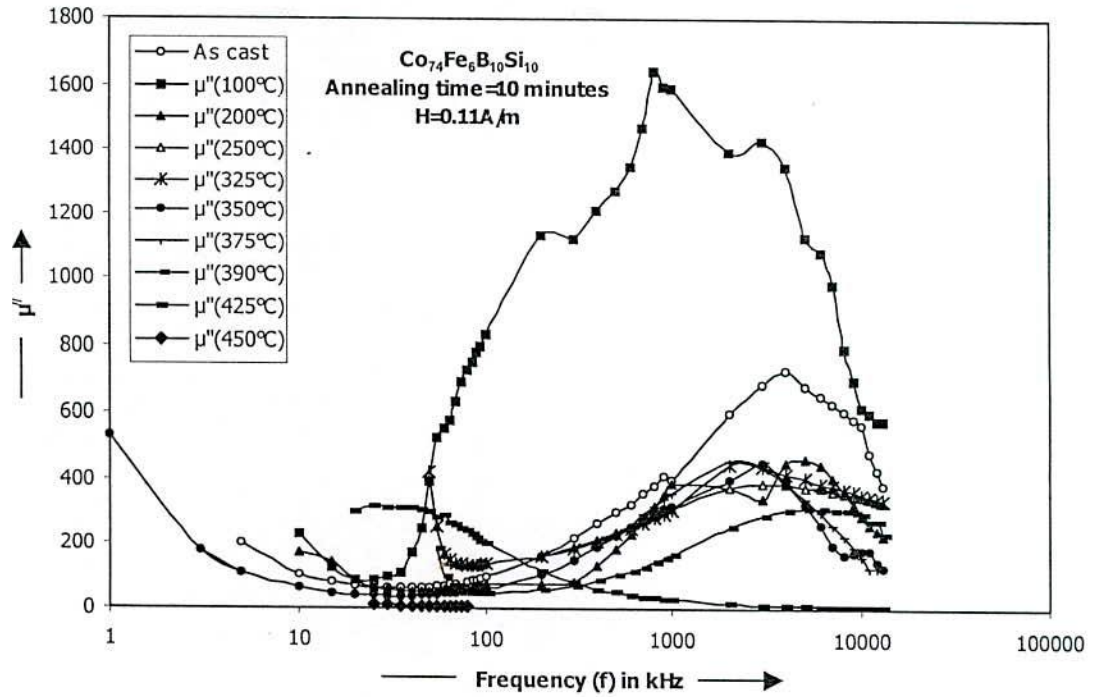


Fig 5.40 Frequency dependence of the imaginary part of the initial permeability of amorphous ribbons for different annealing temperature.

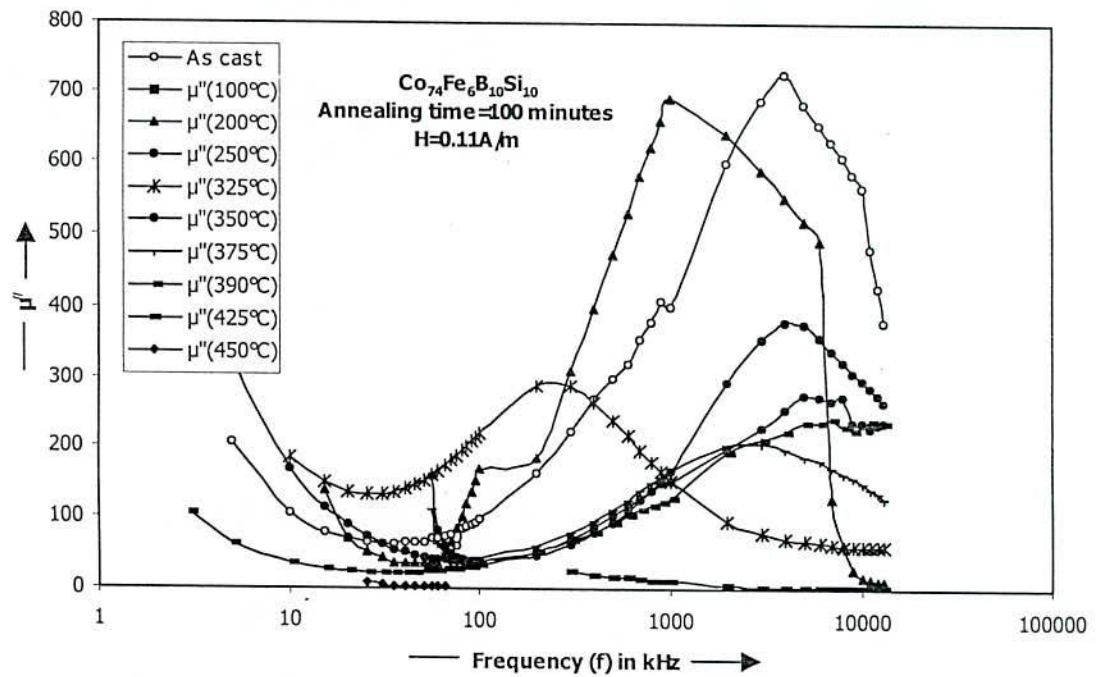


Fig 5.41 Frequency dependence of the imaginary part of the initial permeability of amorphous ribbons for different annealing temperature.



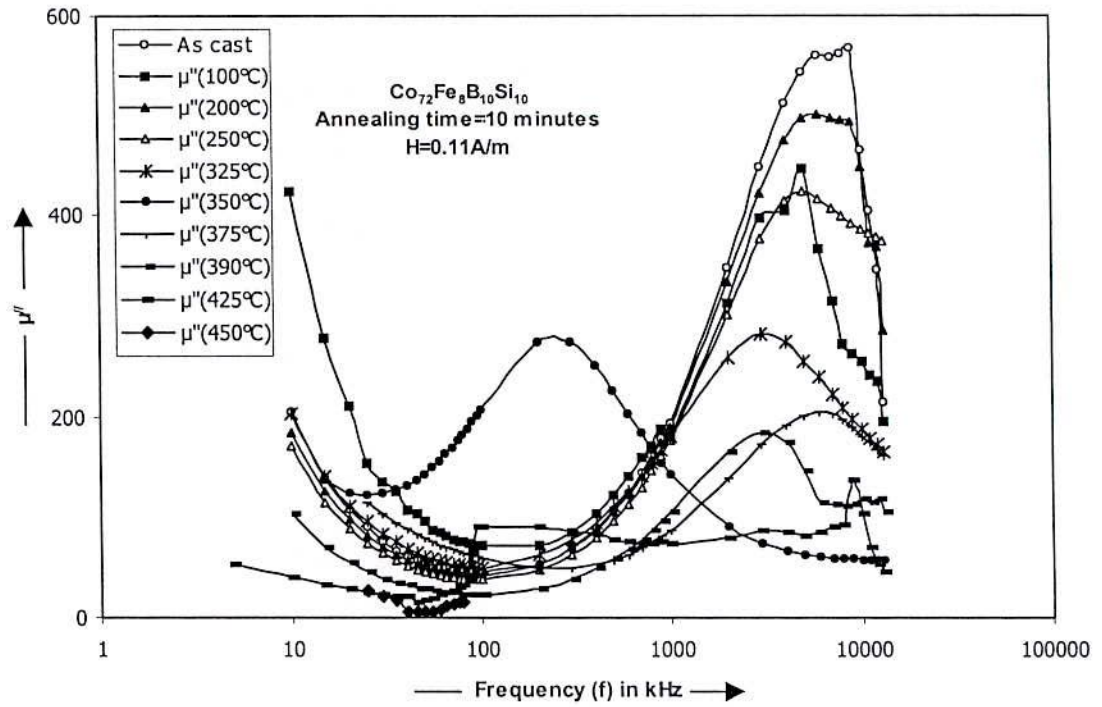


Fig 5.42 Frequency dependence of the imaginary part of the initial permeability of amorphous ribbons for different annealing temperature.

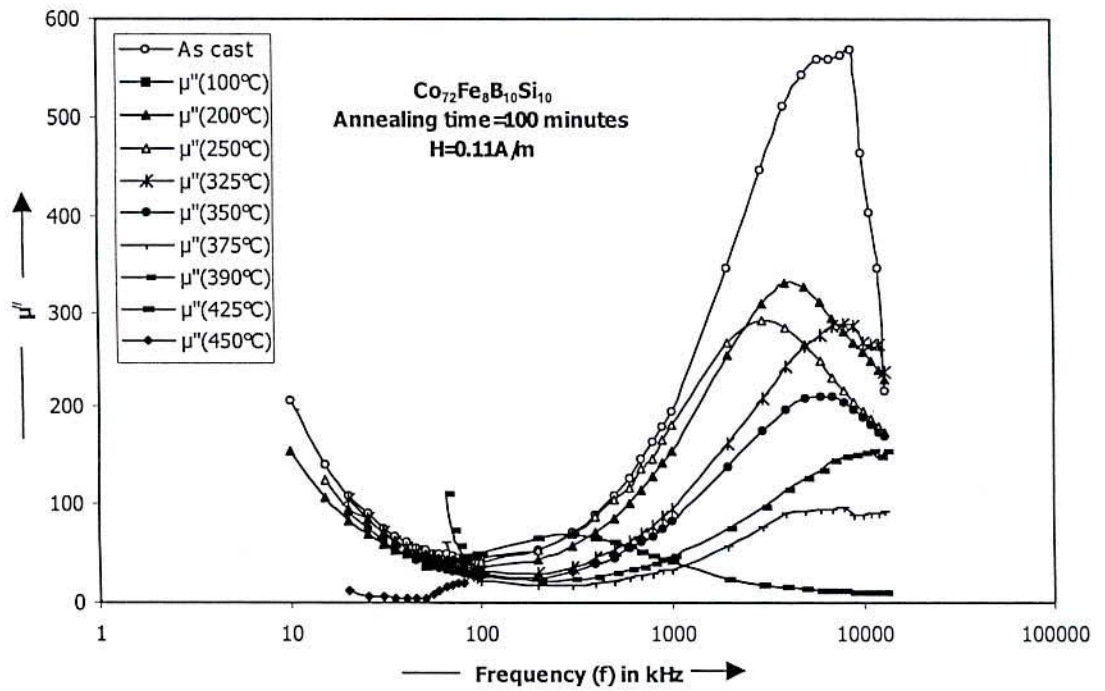


Fig 5.43 Frequency dependence of the imaginary part of the initial permeability of amorphous ribbons for different annealing temperature.

### 5.3.5 Relative Quality Factor

The frequency dependence of  $\mu'/\tan\delta$  for two step annealing time (10 minutes & 100 minutes) with different annealing temperatures are shown in fig- 5.44 to Fig- 5.53.  $\mu'/\tan\delta$  as controlled by the real part of the complex permeability, have very high values in the frequency range 10 KHz to 500 KHz for the ribbon having composition  $\text{Co}_{80}\text{B}_{10}\text{Si}_{10}$  (Fig- 5.44 & Fig- 5.45), 10 KHz to 300 KHz for two ribbons having compositions  $\text{Co}_{78}\text{Fe}_2\text{B}_{10}\text{Si}_{10}$  (Fig- 5.46 & 5.47) and  $\text{Co}_{76}\text{Fe}_4\text{B}_{10}\text{Si}_{10}$  (Fig- 5.48 & Fig- 5.49) and 10 KHz to 700 KHz for two ribbons having composition  $\text{Co}_{74}\text{Fe}_6\text{B}_{10}\text{Si}_{10}$  (Fig- 5.50 & 5.51) and  $\text{Co}_{72}\text{Fe}_8\text{B}_{10}\text{Si}_{10}$  (Fig- 5.52 & Fig- 5.53). This gives a choice of annealing temperature and time depending on the operating frequency of the specimen. Annealing for longer time reduces the relative quality factor in general. The maximum reduction for all samples occurs after annealing temperature  $350^\circ\text{C}$ . The values of the relative quality factor for all samples annealed after  $350^\circ\text{C}$  are very low and almost steady for the whole range of frequency. High relative quality factor and low loss factor of the ribbons indicate that these can be useful as a soft magnetic material. The loss factor in general is found to be high for all sample at low frequency as well as for high frequency. The loss factor arises due to eddy current loss as well as for the phase lag of the spin orientation with respect to the external field. Since these amorphous ribbons are conducting the net loss factor given by  $\tan\delta$  is quite complex. It is difficult to separate out the contribution from the eddy current loss and the phase of the spins with respect to the field. For all the ribbons minimum loss as well as maximum quality factors occurs around 100 KHz.

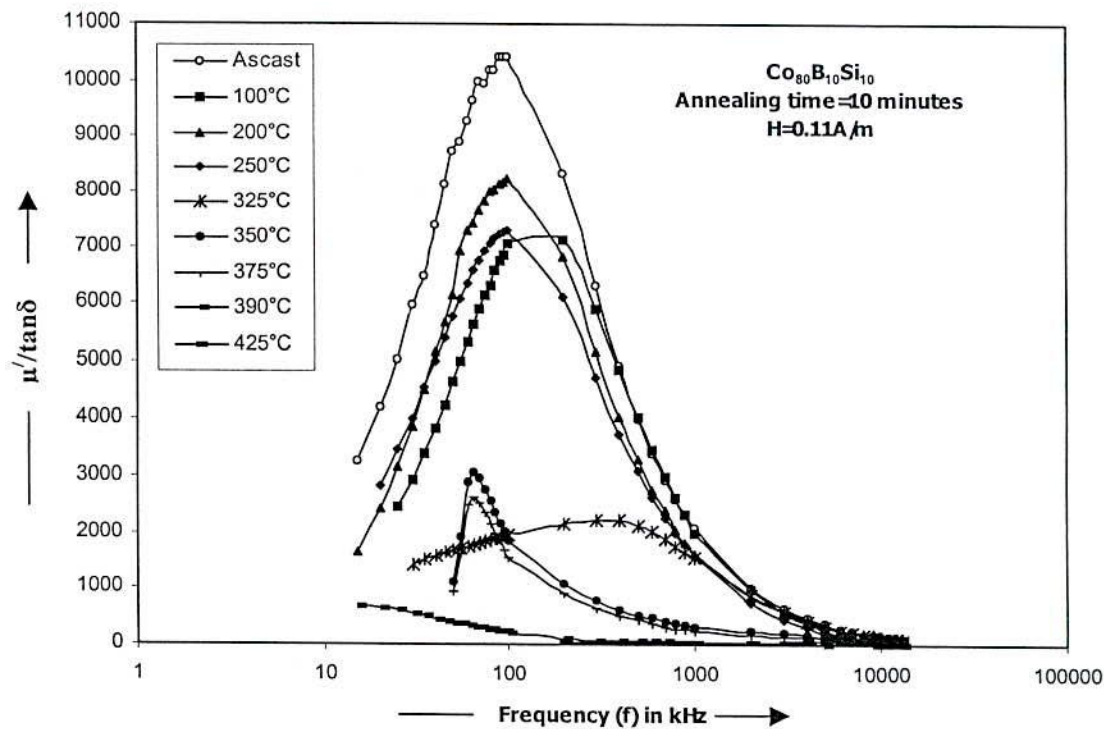


Fig 5.44 Frequency dependence of the relative quality factor of amorphous ribbons for different annealing temperature.

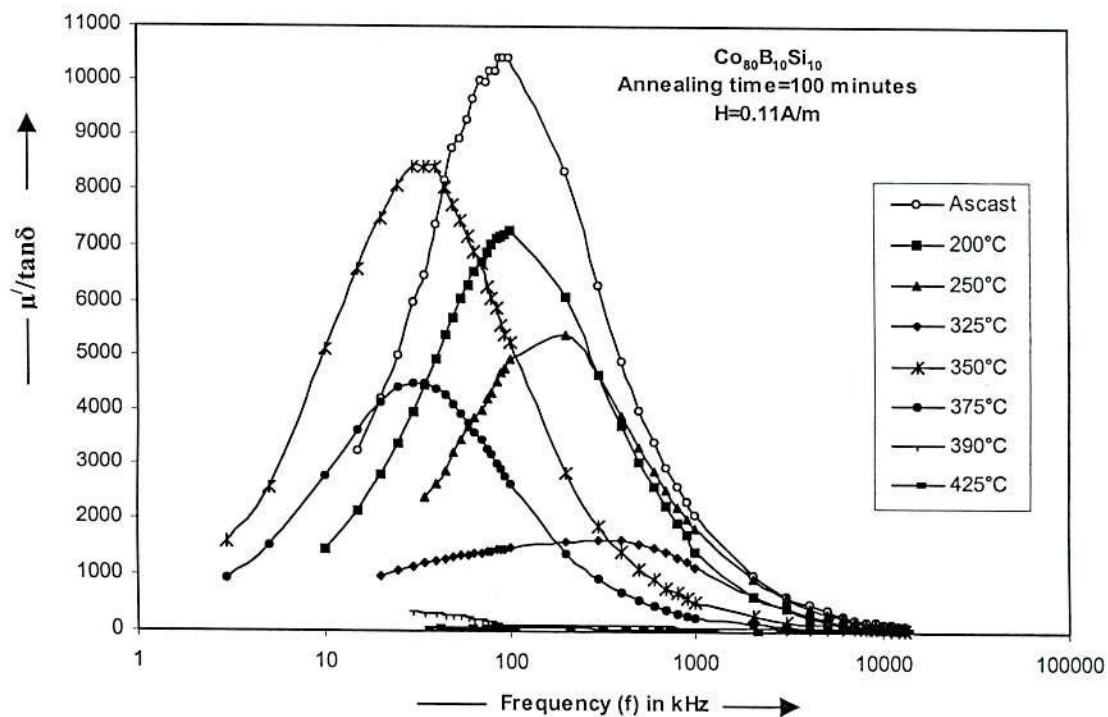


Fig 5.45 Frequency dependence of the relative quality factor of amorphous ribbons for different annealing temperature.



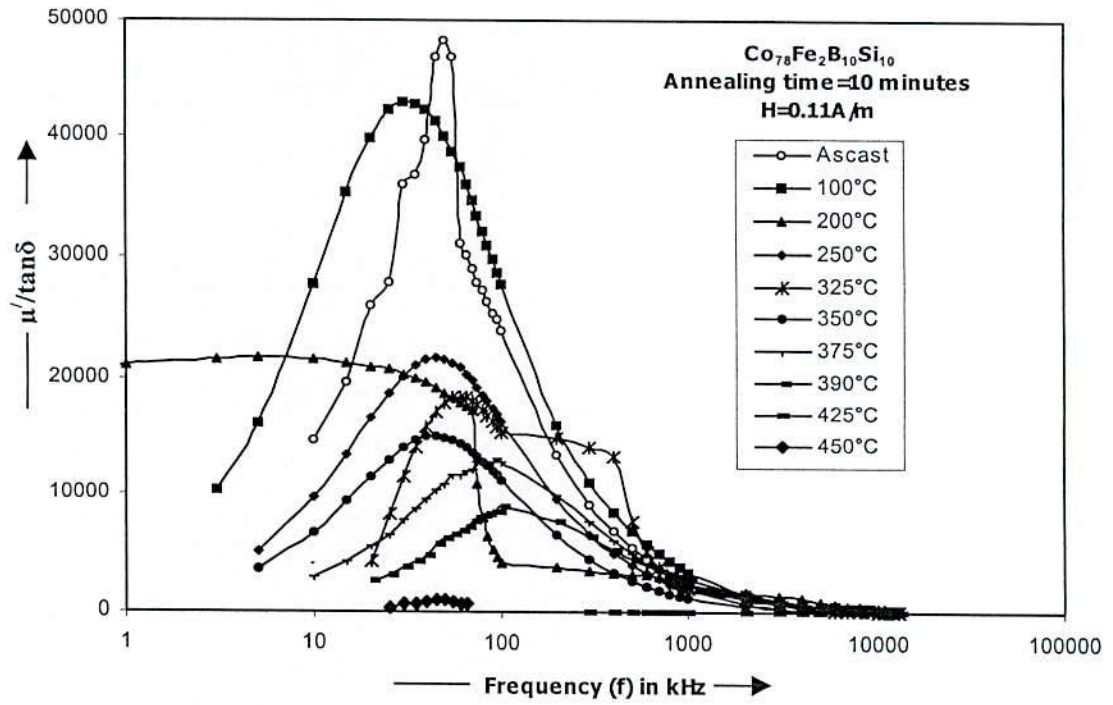


Fig 5.46 Frequency dependence of the relative quality factor of amorphous ribbons for different annealing temperature.

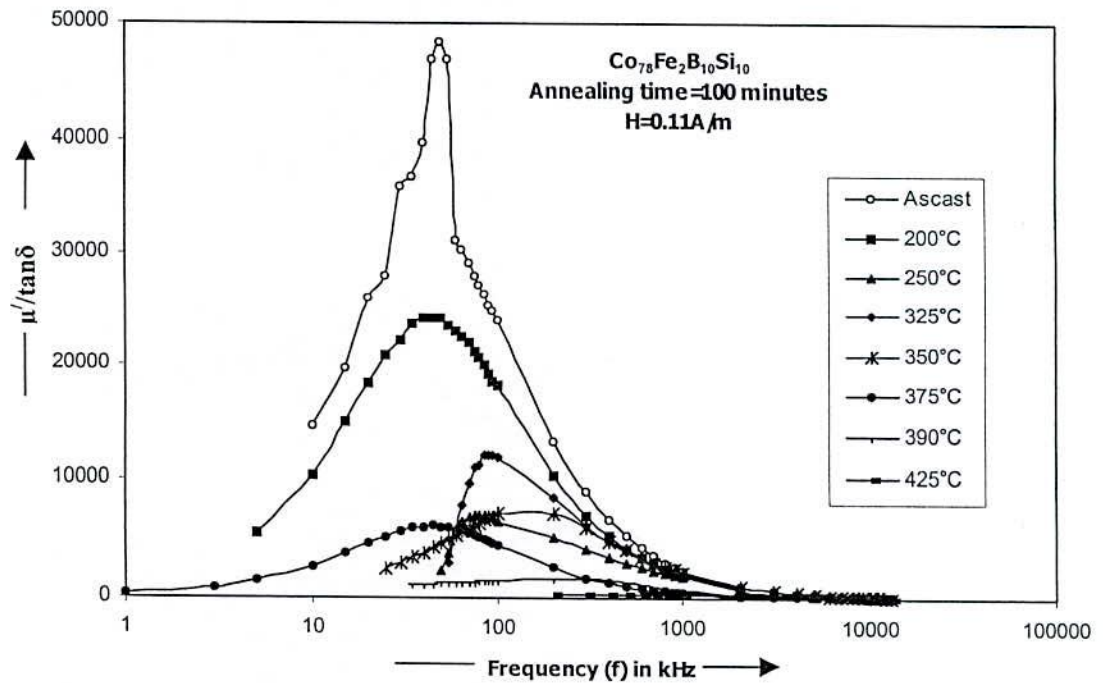


Fig 5.47 Frequency dependence of the relative quality factor of amorphous ribbons for different annealing temperature.

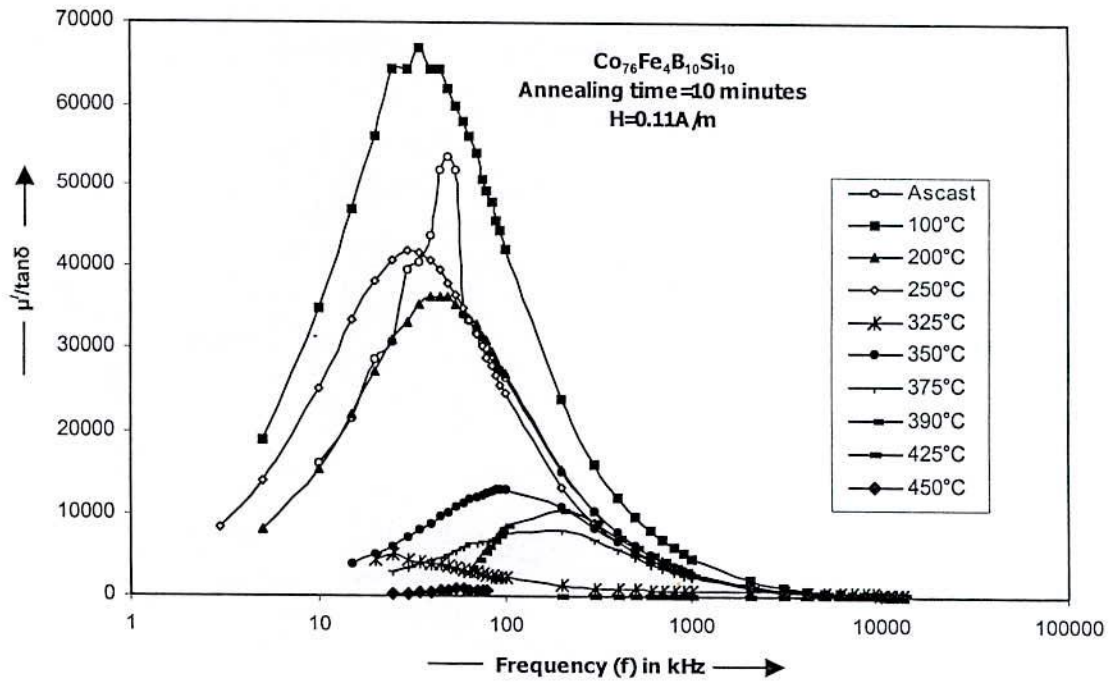


Fig 5.48 Frequency dependence of the relative quality factor of amorphous ribbons for different annealing temperature.

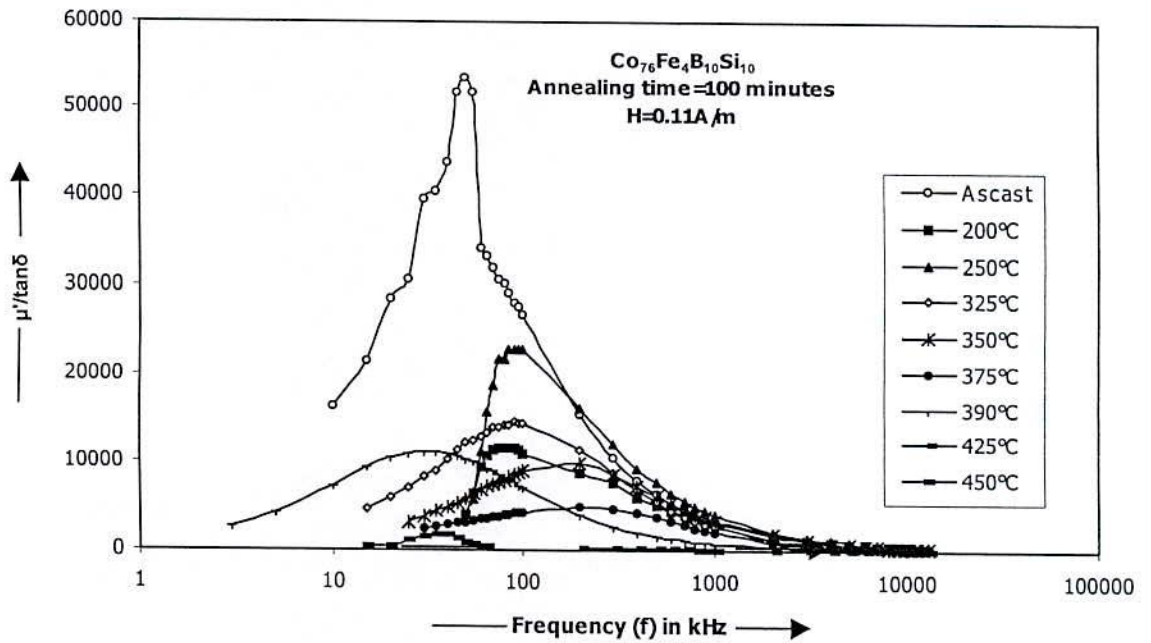


Fig 5.49 Frequency dependence of the relative quality factor of amorphous ribbons for different annealing temperature.

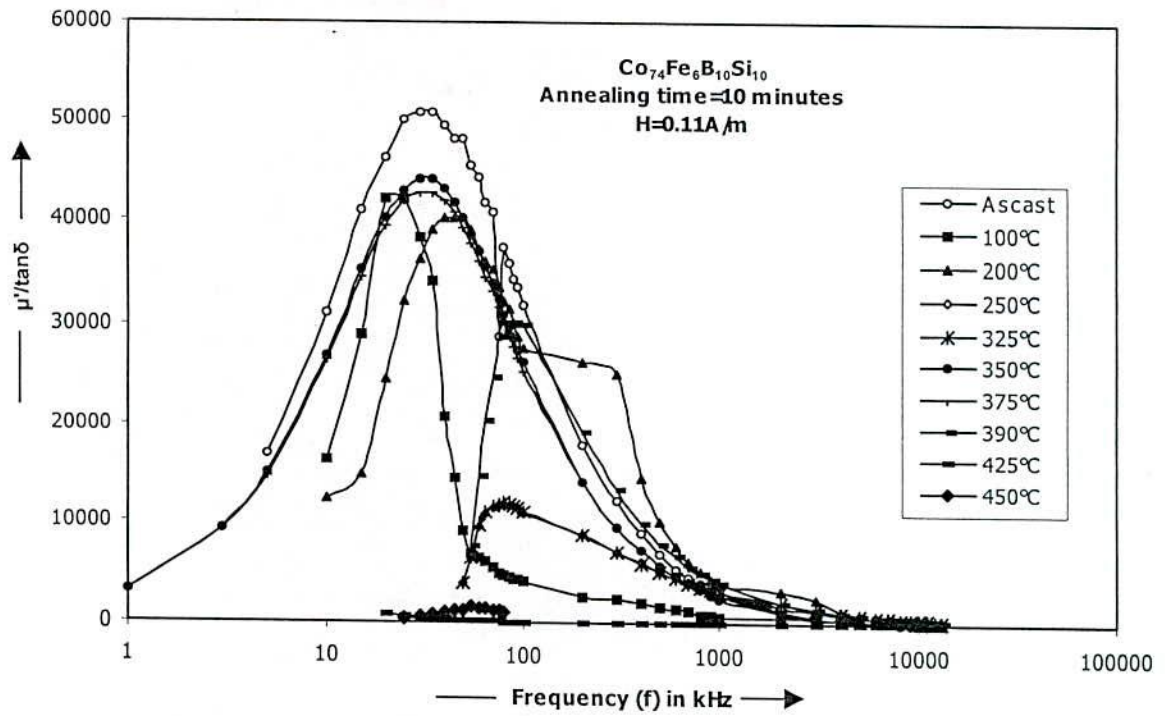


Fig 5.50 Frequency dependence of the relative quality factor of amorphous ribbons for different annealing temperature.

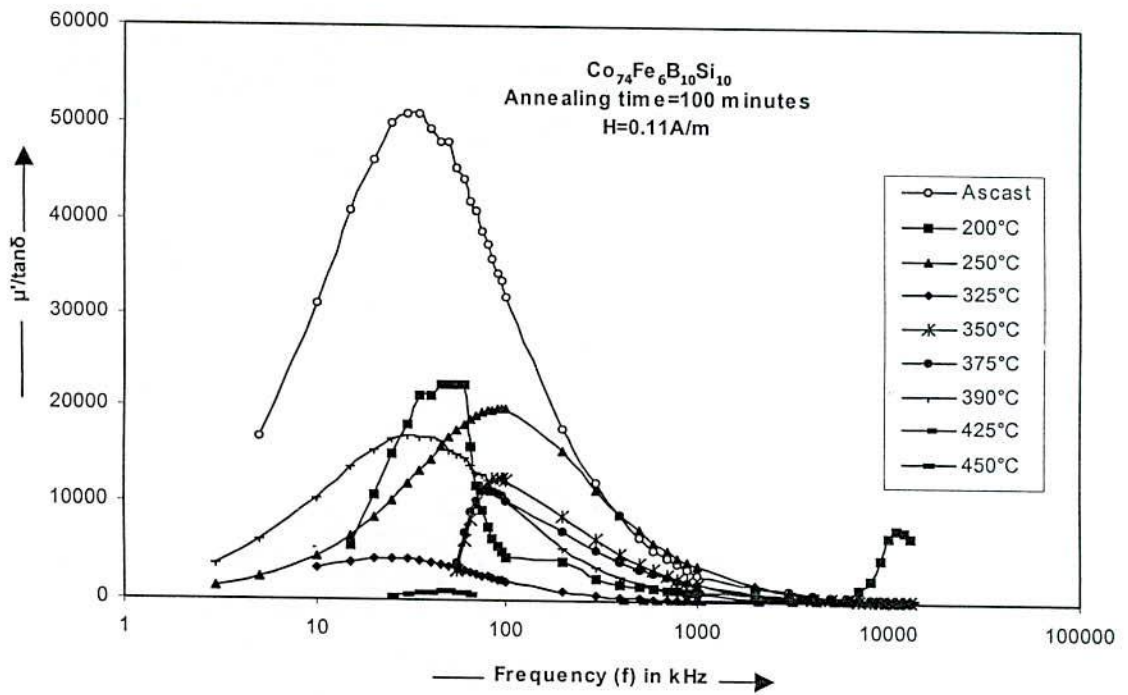


Fig 5.51 Frequency dependence of the relative quality factor of amorphous ribbons for different annealing temperature.



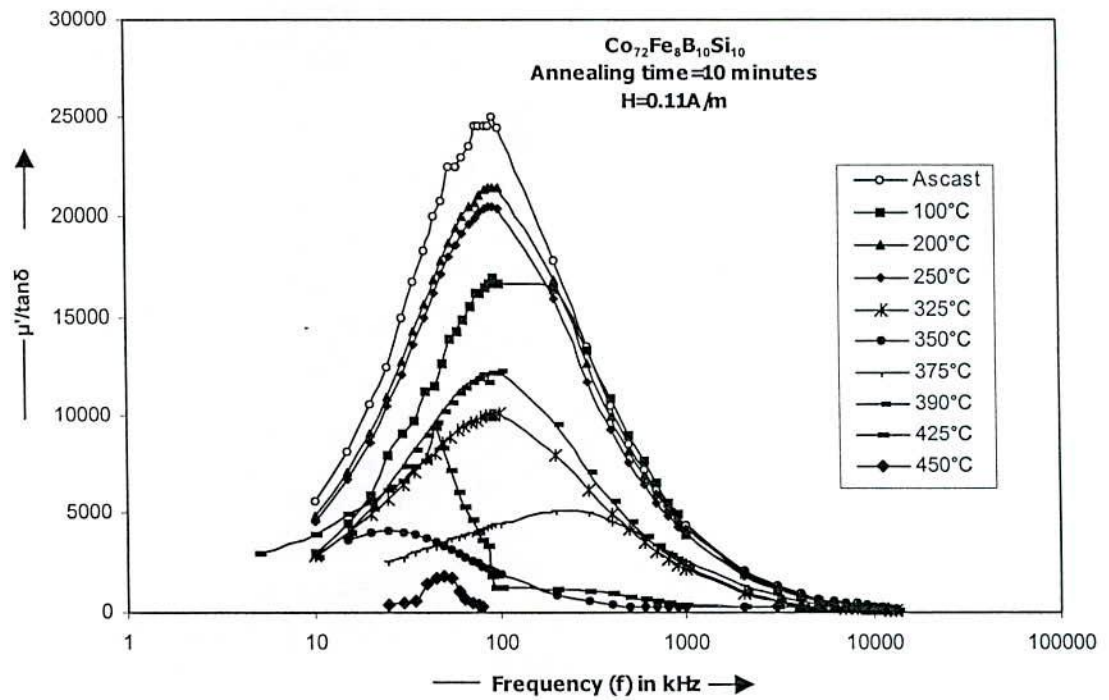


Fig 5.52 Frequency dependence of the relative quality factor of amorphous ribbons for different annealing temperature.

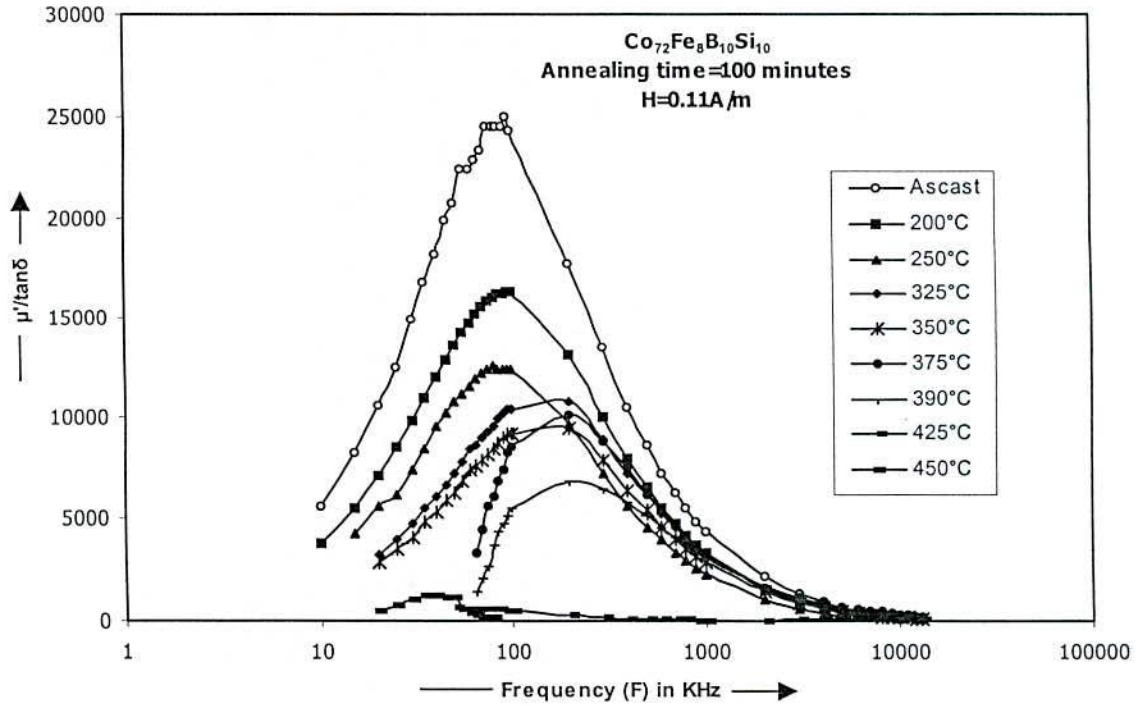


Fig 5.53 Frequency dependence of the relative quality factor of amorphous ribbons for different annealing temperature.

### **5.3.6 Two Step Annealing Time Effects on Frequency Spectra of Co- and Co-Fe-Based Ribbons at Constant Annealing Temperature 390°C**

Frequency dependence of  $\mu'$  for as-cast samples and sample of two step annealing time at constant annealing temperature 390°C are shown in Fig- 5.54 to Fig- 5.58 for comparison. It is seen from the figures that the  $\mu'$  decreases significantly after a long annealing for 10 minutes and further reduces to some extent after 100 minutes annealing. It is evident that annealing temperature and annealing time are both important parameters in controlling the frequency response of permeability of the sample. The best choice of these parameters depends on the desired characteristics of the material in respect of permeability value and its annealing time effects.

### **5.3.7 Annealing Temperature Dependence of Initial Permeability at Constant Low Field for Two Step Annealing Time with Composition $\text{Co}_{80-x}\text{Fe}_x\text{B}_{10}\text{Si}_{10}$**

The initial permeability of all sample as effected by annealing at different temperature with annealing time of 10 minutes (1st step) and 100 minutes (2nd step) in each case, is measured at low frequency (1 KHz) and in very low field ( $H= 0.11$  A/m). Fig- 5.59 and Fig- 5.60 show the effect of annealing temperature on the initial permeability of amorphous ribbons with compositions  $\text{Co}_{80-x}\text{Fe}_x\text{B}_{10}\text{Si}_{10}$  at annealing time 10 minutes and 100 minutes respectively. The initial permeability decreases monotonously with increasing annealing temperature. The values of the initial permeabilities at different annealing temperatures for the compositions  $\text{Co}_{80-x}\text{Fe}_x\text{B}_{10}\text{Si}_{10}$  are summarized in table 5.8 and table 5.9

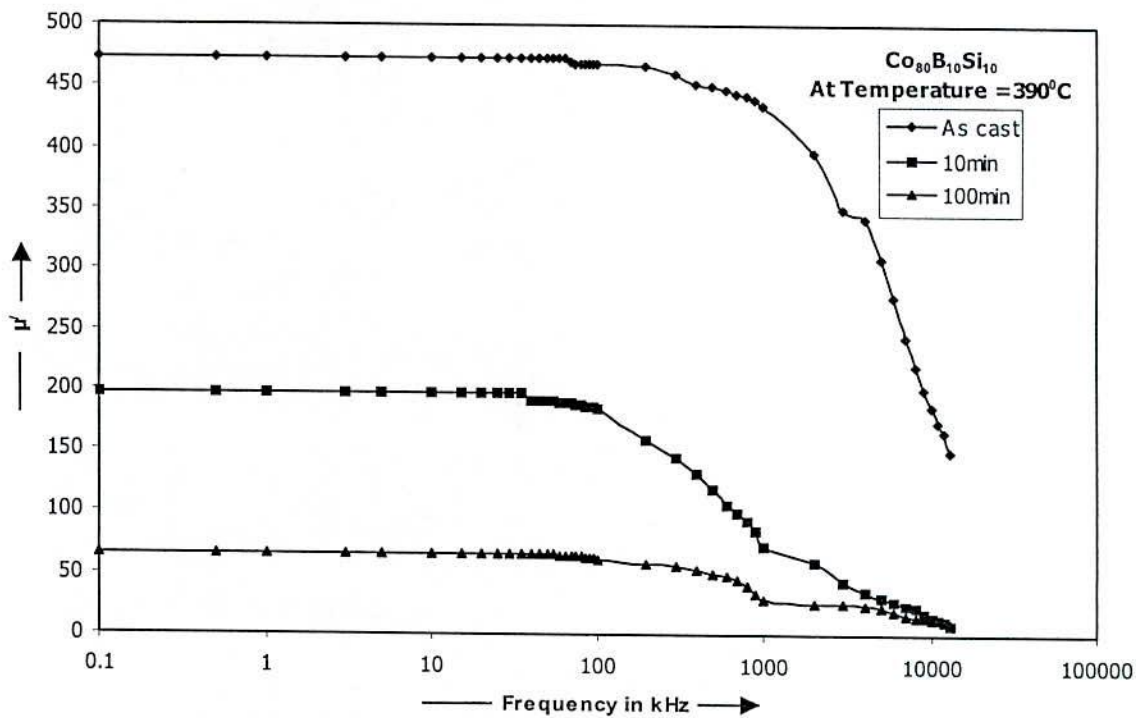


Fig 5.54 Frequency dependence of the real part of initial permeability of amorphous ribbons.

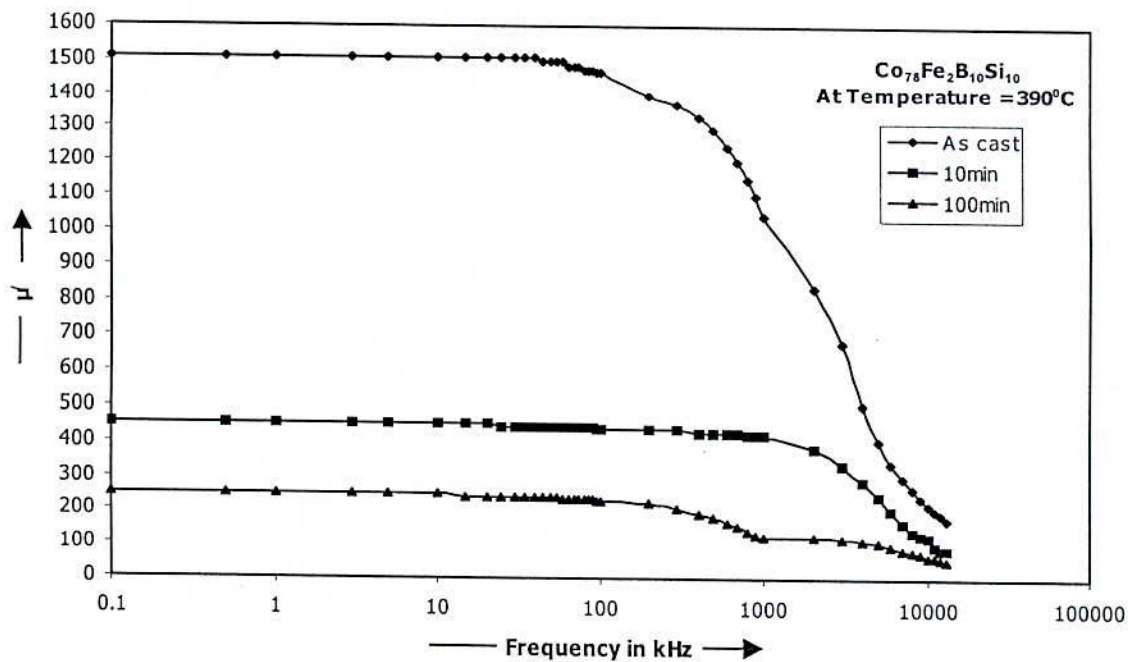


Fig 5.55 Frequency dependence of the real part of initial permeability of amorphous ribbons.



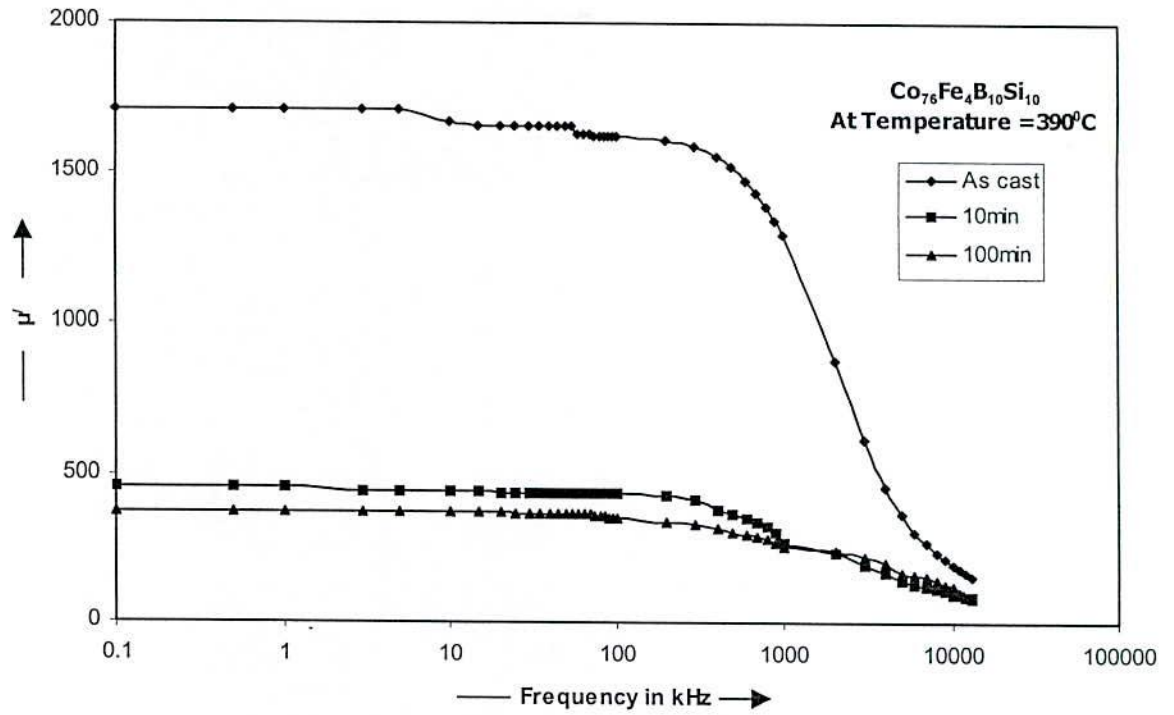


Fig 5.56 Frequency dependence of the real part of initial permeability of amorphous ribbons.

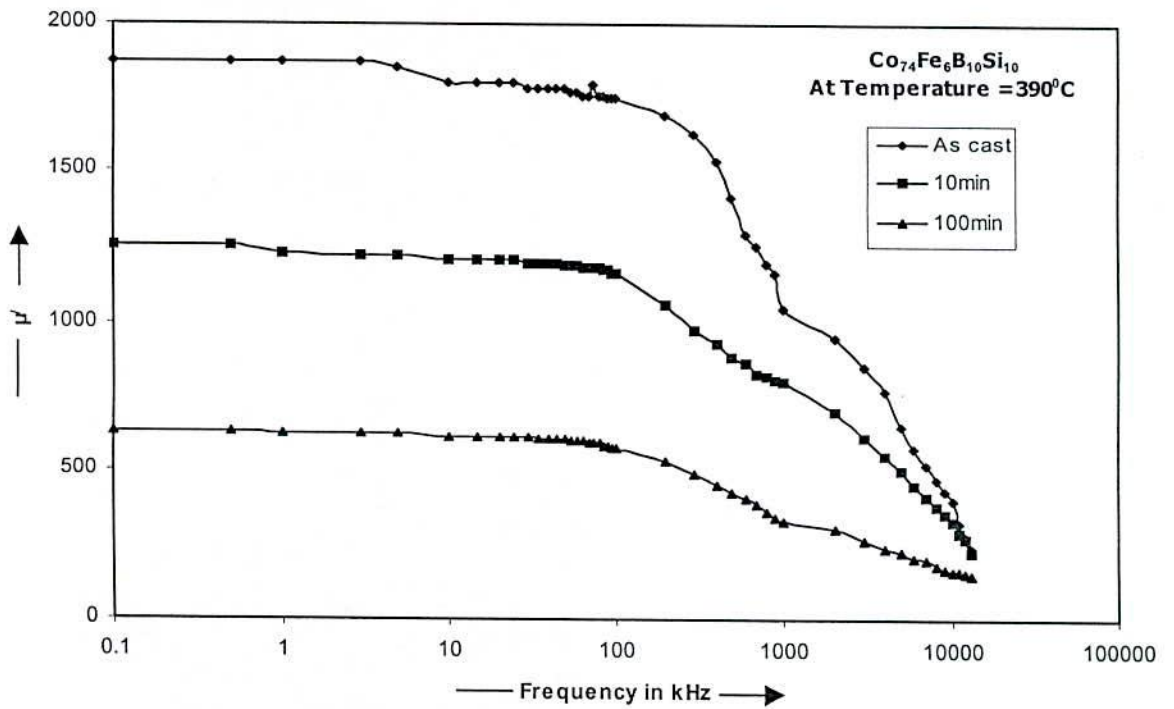


Fig 5.57 Frequency dependence of the real part of initial permeability of amorphous ribbons.

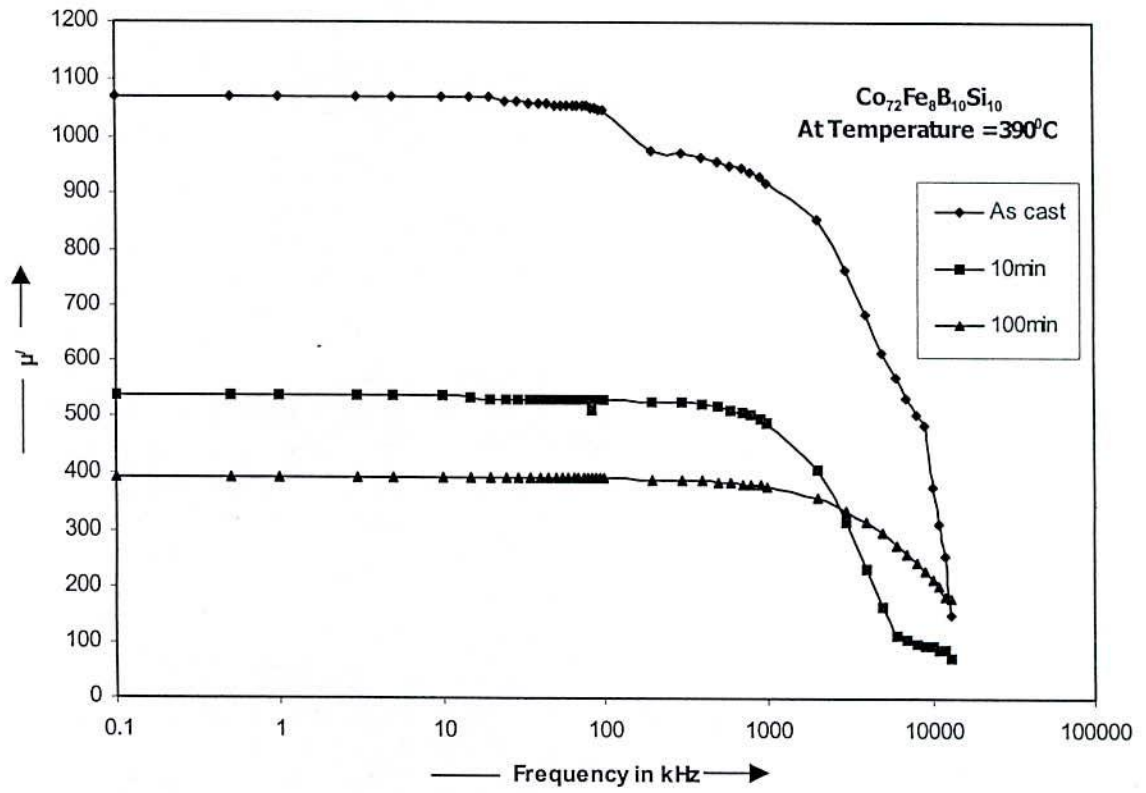


Fig 5.58 Frequency dependence of the real part of initial permeability of amorphous ribbons.

Table- 5.8 : The initial permeability of the amorphous magnetic ribbon  $\text{Co}_{80-x}\text{Fe}_x\text{B}_{10}\text{Si}_{10}$  at different annealing temperature at a constant low field of  $H= 0.11 \text{ A/m}$  and constant 10 minutes time annealing.

Sample	25°C	100°C	200°C	250°C	325°C	350°C	375°C	390°C	425°C	450°C
$\text{Co}_{80}\text{B}_{10}\text{Si}_{10}$	473	469	430	388	346	280	240	197	58	-
$\text{Co}_{78}\text{Fe}_2\text{B}_{10}\text{Si}_{10}$	1510	1453	1216	950	808	664	548	453	60	53
$\text{Co}_{76}\text{Fe}_4\text{B}_{10}\text{Si}_{10}$	1715	1738	1554	1203	808	698	509	457	88	88
$\text{Co}_{74}\text{Fe}_6\text{B}_{10}\text{Si}_{10}$	1875	1962	1492	1315	1314	1296	1276	1229	525	72
$\text{Co}_{72}\text{Fe}_8\text{B}_{10}\text{Si}_{10}$	1071	1111	953	889	767	705	580	535	393	98

Table- 5.9 The initial permeability of the amorphous magnetic ribbons  $\text{Co}_{80-x}\text{Fe}_x\text{B}_{10}\text{Si}_{10}$  at different annealing temperature at a constant low field  $H= 0.11 \text{ A/m}$  and constant 100 minutes time annealing.

Sample	25°C	200°C	250°C	325°C	350°C	375°C	390°C	425°C	450°C
$\text{Co}_{80}\text{B}_{10}\text{Si}_{10}$	473	375	313	295	207	133	66	41	-
$\text{Co}_{78}\text{Fe}_2\text{B}_{10}\text{Si}_{10}$	1510	1040	797	670	477	274	252	36	-
$\text{Co}_{76}\text{Fe}_4\text{B}_{10}\text{Si}_{10}$	1715	1313	919	657	563	424	377	62	90
$\text{Co}_{74}\text{Fe}_6\text{B}_{10}\text{Si}_{10}$	1875	874	866	782	741	672	625	263	53
$\text{Co}_{72}\text{Fe}_8\text{B}_{10}\text{Si}_{10}$	1071	772	723	587	516	464	392	196	76

From table 5.8 and table 5.9 and also from Fig- 5.59 & Fig- 5.60 it is observed that the initial permeability decreases with annealing temperature up to 390°C and then drastically falls to very small value for all the ribbons. This is explained as due to the growth of crystallites whose boundaries create obstacles to the domain wall motion. The effect of annealing on initial permeability ( $\mu_i$ ) is very complex because two factors of apparently opposite effect on  $\mu_i$  takes place. One is the removal of local defects in homogeneity and stresses that hinder the movement of domains by pinning effects and the other is the growth of the nucleation centers of crystallites that also hinders the movement of domain walls. Since effect of annealing is to remove the pinning centers of the first kind and to enhance the growth of the pinning centers of the second kind, the result of annealing depends on the composition of the amorphous ribbons and the conditions of preparation of the as quenched samples. Our results of annealing on cobalt based samples, which show a decrease of  $\mu_i$  with annealing time, are explained as due to the growth of the nucleation centers of the crystallites formed during the preparation. For annealing temperatures, which are above or near the Curie temperature, the absence of domain wall leads to a random distribution of the short-range order configuration and hence, to a significant decrease in domain wall pinning.



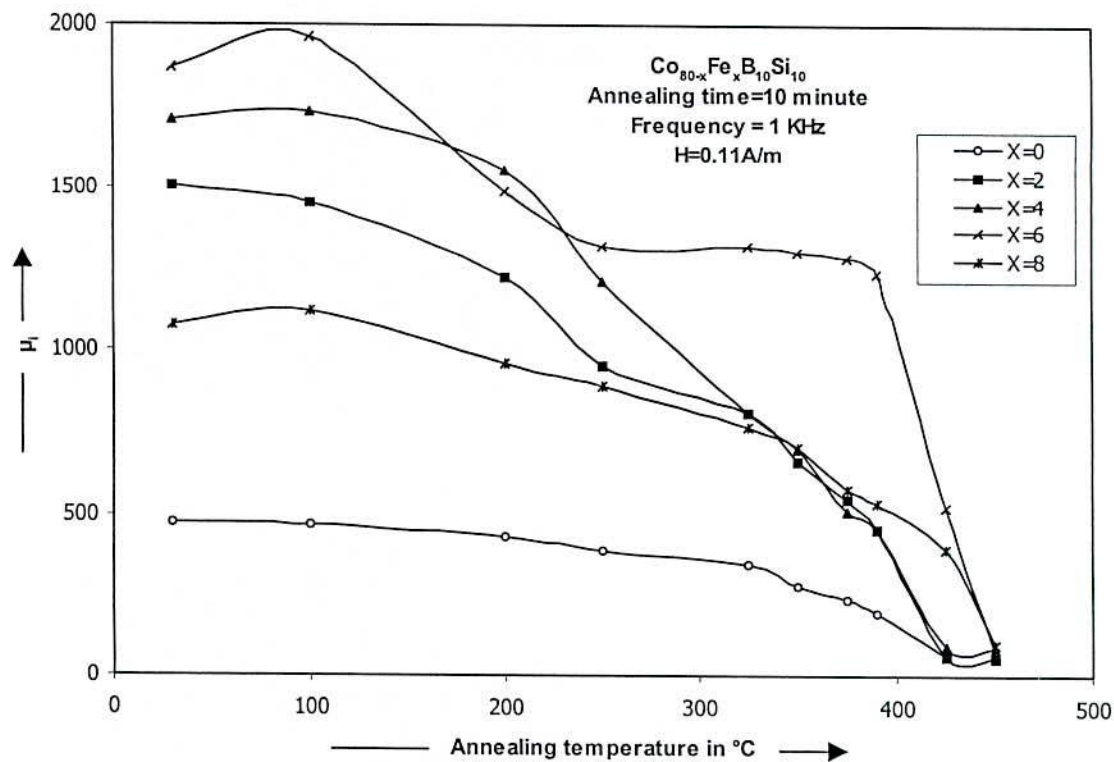


Fig 5.59 Initial permeability versus annealing temperature of amorphous ribbons.

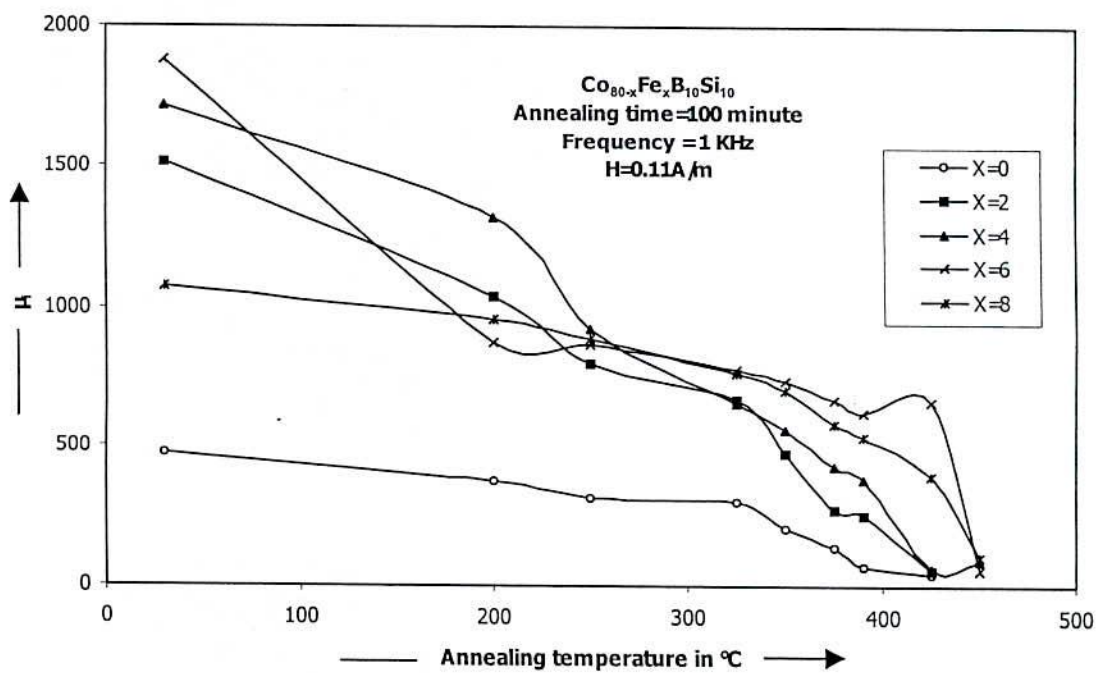


Fig 5.60 Initial permeability versus annealing temperature of amorphous ribbons.

## CHAPTER 6 : CONCLUSIONS

### 6.1 Conclusions



## 6.1 Conclusions

The effects of two-step time annealing on the soft magnetic properties like saturation magnetization and initial permeability of melt-spun  $\text{Co}_{80-x}\text{Fe}_x\text{B}_{10}\text{Si}_{10}$  amorphous alloys has been studied. A prominent thermal stability of these amorphous ribbons are observed in DTA measurement, due to the large difference of composition between the amorphous phase and the competing crystalline phases. For Co-Fe-based amorphous ribbons glass transition temperature ( $T_g$ ) increases sharply with increasing replacement of Co by Fe. The highest value of  $T_g$  which is  $435^\circ\text{C}$  corresponds to the alloy composition  $\text{Co}_{72}\text{Fe}_8\text{B}_{10}\text{Si}_{10}$  at heating rate  $20^\circ\text{C}/\text{min}$ . The  $T_g$  phases depend on the Fe- content substituted for Co in the ribbons but crystallization activation energy slightly increases with increasing of Fe-content. The crystallization temperature ( $T_x$ ) phase does not depend on the substitution of Fe for Co-Fe-based ribbons. The crystallization activation energy close to  $1.54 \pm 0.067\text{eV}$ . Two step annealing time effects on DTA trace at constant annealing temperature  $200^\circ\text{C}$  observed that all the samples are  $T_g$  and  $T_x$  practically unchanged but activation energy products increase with increasing and decreasing annealing time. These kinetics anisotropy reorientation depend on the instantaneous structural state as described in terms of activation energy products.

Magnetization has been measured by VSM as a function of field for the composition  $\text{Co}_{80-x}\text{Fe}_x\text{B}_{10}\text{Si}_{10}$  [ $x = 0, 2, 4, 6 \& 8$ ]. The saturation magnetization for these ribbons have higher values with increasing replacement of Co by Fe. For all the alloy systems saturation specific magnetization depends on the atomic magnetic moments of the constituent 3d transition elements. The effect of the glass forming material is explained as due to transfer of P- electrons to the 3d band. However, a quantitative agreement is not found on the basis of rigid band model. This shows that amorphous systems can not be treated in the same way as crystalline materials in respect of band structure. Amorphous ribbons although have enormous potential, they are in metastable states, and magnetic softness of these materials depend on the annealing process. From the two step annealing time effect on the magnetization curve, it is observed that the saturation behavior responds very sensitively to a small change in increased saturation magnetization ( $\sigma_s$ ) of those samples at constant annealed temperature  $390^\circ\text{C}$ . From the observation of magnetization values after annealing at  $390^\circ\text{C}$  it can be concluded that the



Co-Fe-based ribbon can be used over a long time at elevated temperature without crystallization. Naturally, when used at a lower temperature the metastable state will sustain for much longer time.

The effect of annealing on magnetization has also been measured by VSM and a systematic decrease of saturation magnetic field with increasing annealing time is observed of these samples. These effects of annealing time in the selected annealed temperature is to partially remove the pinning centers of the domain walls and thereby improving the magnetic softness of these ribbons. Since the complex process involves the energy contributions from various aspects such as induced magnetic anisotropy, magnetostriction, demagnetizing factors etc, quantitative analysis of the effect of annealing time and temperature on magnetization process is not possible at the present state of knowledge.

We have performed a comparison between the behavior of the initial permeability and other magnetic properties for a Co-Fe- based amorphous alloy and the corresponding alloy, which depends on two step annealing time and various annealed temperatures. The general composition of  $\text{Co}_{80-x}\text{Fe}_x\text{B}_{10}\text{Si}_{10}$  [ $x= 0, 2, 4, 6 \& 8$ ] is very interesting in respect of the dependence of initial permeability and relative quality factor on the atomic percentage of Fe. The presence of Fe controls the average magnetic moment and the net magnetization of these amorphous samples. This gives an opportunity to tailor the magnetic characteristics of these alloy systems by controlling the composition of the alloy in respect of the fraction of the Fe- atoms present. The maximum permeability is attained at 6 At % of Fe which corresponds to minimum value of net magnetostriction, which arises from the opposite contributions to magnetostriction from Co and Fe atoms. The effects of two step annealing on initial permeability ( $\mu_i$ ) decreases with increasing of the annealing temperature. The effect of annealing on  $\mu_i$  is very complex because two factors of apparently opposite effect on  $\mu_i$  take place. One is the removal of local defects in homogeneity and stress that hinder, the movement of domains by pinning effect. The growth of the nucleation centers of crystallites that also hinders the movement of domain walls. In our results, effects of annealing time and annealing temperature on Co-Fe-based sample which show decrease of  $\mu_i$  are explained as due to the growth of the nucleation centers of the crystallites formed during the preparation. In these samples,



effect of annealing leads to the ordering of magnetic atomic pairs, which increases anisotropy and decreases permeability. In order to obtain decrease in permeability, we have studied these materials for varying annealing temperatures and discovered the considerable permeability spectrum of Co-Fe- based amorphous ribbon by two step annealing time.

Co-Fe-B-Si amorphous magnetic ribbon shows interesting magnetic properties as soft magnetic material. These ribbons can be very useful as a core material in the as quenched condition and at low temperatures. In the low annealing temperature region i.e. up to 250°C for Co- based sample and up to 350°C for Co-Fe- based sample and in as cast ribbon permeability is reasonably higher and remains constant over a large frequency range up to 1 MHz. Magnetic relaxation processes may become important in technical application since they give rise to magnetic losses and magnetic instability with rising annealing time and temperature. There exists a situation for this ribbon where annealing at higher temperature simultaneously decreases the initial ac permeability and increases the dynamic losses. Actually under ac condition the number of domain walls increases and more deeply pinned walls begin to move as the frequency is increased. These effects contribute to an increase of the real part of the permeability but at the same time the imaginary component is also influenced, particularly due to eddy current effects. The magnetic proportion of Co-Fe- based amorphous ribbon are superior to those of Co-based ribbons. The advantages realized are higher saturation induction and better thermal stability with soft magnetic properties at application temperature and annealing time.

Co-Fe-based materials are becoming increasingly important for their potentials as a new magnetic materials both for theoretical understanding and technological application. The possible applications are as inductors, high-density information storage, magnetic head, frequency transformer etc.

Further work with finer variation of composition can be useful in dealing out the effect of glass forming material on magnetic characteristics. Low temperature measurements of magnetization is needed for actual theoretical understanding. Another important study that can be taken up is the measurement of magnetostriction as a function of composition and annealed temperature to confirm the suggestions regarding at the origin of increasing initial permeability. Magnetostriction and coercivity are all

controllable by choosing appropriate composition, altering preparation technique, selecting the annealed temperature and duration of the time annealing. Certain important parameters like induced magnetic anisotropy and magnetostriction need to be studied in detail for their variations with the preparation techniques, composition, annealing temperature and annealing time.

## BIBLIOGRAPHY

## Bibliography

### Chapter- 1

- 1.1. Sadron, Ann, Phys 17, 371, (1932)
- 1.2. Crangle and W.R. Scott, 5, Appl. Phys. 36, 921, (1965).
- 1.3. Fisher G., A Herr, and A. J. P. Meyer, J. Appl. Phys, 39, 2, 454 (1962)
- 1.4. Wojtowicz P. J., and Mrayl, Phys. Rev. Lett, 20 (1968), 1489 Phys. Lett. 28 A, 142 (1968)
- 1.5. Gubanov, A. I. 1960, FIZ. Tver. Tel. 2, 502.
- 1.6. Brenner, A. D. E. Couch and E. K. Williams, 1950, J Res, Nat. Bureau standards. 44, 109.
- 1.7. Duwez, P. R. H. Willens and W. Klem nl, Jr, 1960, J, Appl. Phys. 31, 1136.
- 1.8. Simpson, A. W. and D. R. Brambley, 1971, Phys. Stat. Sol. (b) 43, 291.
- 1.9. Luborsky, F. E., J. J. Becker and R. O. Mc Cary, 1975, IEEE Trans. Magnetics MAG- 11, 1644.
- 1.10. Egami, T., P. J. Flanders and C. D. Graham, Jr., 1975a, AIP Conf. Proc. 24, 697.
- 1.11. Cong B. T., J. Magn. Magn. Mater 117 (1992) 126.
- 1.12. Miyaki T., K. Yamanchi, S. Arakawa, Y. Yoshizawa and S. Nakajima, Bulletin Japan, Inst. Metals. 26 (1987), 299.
- 1.13. Komoto O., H. Hujishima, S, Sumiya, H. Itomasa and T. Ojima, Bulletin Japan Inst, Metals. 27 (1988), 293.
- 1.14. Fujimori H., M. Kikuchi Y. Obi and T. Masumoto, Sci. Rep. RITO, A- 26 (1976), 36.
- 1.15. Warliment H. and R. Bolli, J, Magn, Magn. Mat. 26 (1982), 97.



- 1.16. Sikder S. S., M. A. Asgar, M. A. Hakim and M. A. Mazid "The effect annealing on the magnetization process of Iron-Boron ribbon", Journal of Bangladesh Academy of Science, Vol. 20, N. 2, 237-245 (1996).
- 1.17. Cohen, M. H. and D. Turnbull, 1961, Nature, 189, 131.
- 1.18. Turnbull D., Contemp. Phys. 1969; 10: 473.
- 1.19. Ublmann DR., J. Non- Cryst. Solids, 1972; 7: 1109.
- 1.20. Davics HA, Lewis BG. Scripta Mater, 1975; 9: 1109.
- 1.21. Inouc A, Masumoto T., Mater. Sci. Eng. 1993; 173 A: 1.
- 1.22. Egami T., Mater. Sci. Eng. 1997; A 226- A 228: 261.
- 1.23. Lu ZP, Tan H, Li Y, Ng. SC, Scripta mater. 2000; 42: 667.
- 1.24. Zhu F., N. Wang, R. Busch and P. Haasen, Scr. Metall. Mater. 25 (1991).
- 1.25. Bigot J., N. Lecaude, J. C. Pearson, C. Milan, C. Ramiarijaona and J. F. Rialland, J. Magn. Magn. Mater. 133 (1994) 299-302.
- 1.26. Sikder S.S., M. A. Asgar, M. A. Hakim and M. A. Mazid, Journal of Bangladesh Academy of Science, Vol. 20, No. 2, 237-245, 1996.
- 1.27. Alben, R., J. I. Budnick and G. S. Cargill 111. 1977, in Metallic glasses (eds. H. S. Leamy and J. J. Gilman) (American Society for metals, Metals Park, Ohio) ch. 12.
- 1.28. Felsch, W., 1970, Z. Angew. Phys. 29, 218.
- 1.29. Wright, J. G., 1976, IEEE Trans. Magnetics MAG- 12, 95.
- 1.30. APPINO C. AND F. FIORILLO, Journal of Magnetism and Magnetic Materials, 133, 107., 1994.
- 1.31. KRONMULLER H., N. MOSER AND T. REININGER, Anales de Fisica B 86 (1), 1990.

- 1.32. BARANDIARAN J. M., M. YAZQUEZ, A. HENANADO, J. GONZALEZ AND G. RIVERO IEEE Trans. Magn., 25, 3330, 1989.
- 1.33. Amano E., R. Valenzuela, J. T. S. Irvine and A. R. west, J. Appl. Phys. 67, 5589 (1990).
- 1.34. Irvine J. T. S., E. Amano and R. Valenzuela, Mater. Sci. Eng. A 133, 140 (1991).
- 1.35. Ban G., P. Arato and L. Szentmiklosi, J. Magn. Magn. Mat., 37 (1983) 309.
- 1.36. Polivanov K. M., Izv. Akad. Nauk. SSSR (Ser. Fiz.) 16 (1952) 449.
- 1.37. Buttino G., Aecchetti, M. Poppi and G. Zini, IEEE Trans. Magn. MAG- 18 (1982) 1400.
- 1.38. Hilzinger H. R., IEEE Trans. Magn. MAG- 21 2020 (1985).
- 1.39. Sikder S.S., M. A. Asgar and M. A. Hakim, Indian J. Phys. 73 A 639 (1999).
- 1.40. Irvine J. T. S., E. Amano. A. Huanosta, R. Valenzuela and A. R. West, Solid State Ionics 40/41 220 (1990).
- 1.41. Amano E., R. Valenzuela, J. T. S. Irvine and A. R. West, J. Appl. Phys. 67 5589 (1990).
- 1.42. Irvine J. T. S., E. Amano, and R. Valenzuela, Mater Sci, Eng. A. 133 140 (1991).
- 1.43. Jagielinski, T., Walecki, T.: Phys. Stat. Sol. (a) 60 (1980) K 31.
- 1.44. Sikder S. S., M. A. Asgar, M. A. Hakim and M. A. Mazid; "The effect of annealing in the magnetization process of Iron- Boron- Ribbon"; Journal of Bangladesh Academy of Science; vol.20; No. 2; 237-245; 1996.
- 1.45. Sikder S. S. and M. A. Asgar; "The kinetics of atomic and magnetic ordering of Co-based amorphous ribbons as affected by Iron substitution;" Thermo chimica Acta; 326, 119-126; 1999.
- 1.46. Sikder S. S., M. A. Asgar and F. A. Khan; "Study of the temperature dependence of magnetic anisotropy of amorphous ribbons with composition  $\text{Co}_{80-x}\text{Fe}_x\text{B}_{20}$  [ $x=$

2.5, 5.0, 7.5 & 10]"; Journal of Bangladesh Academe of Science; vol-23; No. 1;43-51;1999.

## Chapter- 2

- 2.1. Klement W. Jr. , R. H. Willens and P. Duwez, Nature , 187, 809, 1960.
- 2.2. Gubanov, A. I. 1960, FIZ. Tver. Tel. 2, 502.
- 2.3. Pond. R. Jr. and R. Maddin, 1969, Trans. Met. SOC. ALME 245, 2475.
- 2.4. Mizoguchi T., IBM Research Report RC 6054, 1976.
- 2.5. Alben R., J. I. Budnick, G. S. Cargill, III, Metallic glasses (American SOC. for Metals. 1978) P- 304.
- 2.6. Gyorgy E. M., ibid P-275.
- 2.7. Cargill G. S. III, Solid State Physics, Vol- 30 Ed. Ehrenreich *et. al.*, Academic Press, New York (1975) P- 257 .
- 2.8. Masumoto T., S. Ohnuma, K. Shirakawa, M. Nose and K. Kobayshi, Int. Conf. on liquid and Amorphous Metals, Grenoble France, 1980.
- 2.9. Cargill III, G. S., 1976, in Rapidly quenched metals section I (eds. N. J., Grant and B. C. Giessen) (MIT Press., Cambridge, Mass) P. 293.
- 2.10. Asgar M. A., Vol (1984) Mechanical Engineering Research Bulletin (BUET) P.I.
- 2.11. Alben R., J. I. Budnick and G. S. Cargill III, 1977. in Metallic glasses (eds. H. S. Leamy and J. J. Gilman) (American Society for Metals, Metals Park, ohio) ch. 12.
- 2.12. Turnbull, D., 1969, Contemp. Phys. 10, 473.
- 2.13. Duwez, P., R. H. Willens and W. Klement, Jr., 1960, J. Appl. Phys. 31, 1136.
- 2.14. Chen H. S., Rep, Prog. Phys. 43, 23 (1980).

### Chapter- 3

- 3.1. Turnbull, D., 1974, J. de Physique 35, C 4-1.
- 3.2. Takayama, S., 1976, J. Materials Sci. 11, 164.
- 3.3. Cohen, M. H. and D. Turnbull, 1961, Nature 189, 131.
- 3.4. Avrami, M., 1939. J. Chem. Phys. 7, 1103.
- 3.5. Avrami, M., 1940. J. Chem. Phys. 8. 212.
- 3.6. Avrami, M., 1941. J. Chem. Phys. 9. 177.
- 3.7. Luborsky, F. E., 1978, J. Magn. & Magn. Mater. 7,143.
- 3.8. Kissinger, H. E., 1957, Anal. Chem. 29,1702.
- 3.9. Boswell, F. G., 1980, J. Thermal Anal. 18,353.
- 3.10. Egami, T., 1978b. Mater. Res. Bull. 13,2589.
- 3.11. Egami, T., 1984, Magnetic amorphous alloys, in: Rep. Progr. Phys, 47, 1601.
- 3.12. Egami, T., 1978 a, J. Mater. Sci 13,2587.
- 3.13. Woldt, E., and H. Neuhauser. 1980. J. Non- Cryst. Solids 37. 241.
- 3.14. Gibbs, M. R. J. J. E. Evetts and J. A. Leake. 1983. J. Mater. Sci. 18. 278.
- 3.15. Fish, G. E., 1985, IEEE Trans. Magn. MAG- 21. 1986
- 3.16. Primak, W., 1955, Phys, Rev. 100, 1677.
- 3.17. Chen. H. S., 1978 a, in : Metallic Glasses, eds J. J. Gilman and H. J. Leamy (Metal Park, Ohio) P. 75.
- 3.18. Anderson, P. M., and A. E. Lord , 1980, Mater. Sci. & Eng. 44, 279.
- 3.19. Yamaguchi K. and T. Mizaguchi, J. Phys. Soc. Japan, 39, 541, 1975.
- 3.20. Harris, R. , M. Phischke and M. J. Zuckerman, 1973, Phys. Rev. Lett. 31, 160.
- 3.21. Hamdrich, K., 1972, Phys. Stat. Sol. (b) 53, K17.
- 3.22. Egami T., 1984, J. Magn. Magn. Mat. , 7,143.
- 3.23. Waseda Y., K. T. Aust, 1981, J. Mater, Sci 16. 2337.



- 3.24. Lubonsky F. E., 1978, J. Magn. Magn. Mat., 7,143.
- 3.25. Hilzinger H. R., IEEE Trans. Magn, MAG- 21 2020 (1985)
- 3.26. Sikder S. S., M, A. Asgar and M. A. Hakim, Indian J. Phys. 73A 639 (1999)
- 3.27. Irvine J. T. S., E. Amano, A. Huanosta, R. Valenzuela. and A. R. West, Solid State Ionics 40/41, 220, (1990).
- 3.28. Amano E., R. Valenzuela, J. T. S. Irvine and A. R. West, J. Appl. Phys. 67, 5589 (1990).
- 3.29. Jones R. M., IEEE Trans. Mag. MAG- 18, 1559 (1982).
- 3.30. Gibbs M. R. J., Proc. Conf. Metallic Glasses Science and Technology, Budapest 1980, Vol. 2C. Hargitai, J. Bakonyi and T. Kemeny (Kultura, Budapest) P. 37.
- 3.31. Snoek J. L., Physica, 14, 207 (1948).
- 3.32. Nill L., J. Phys. Radi., 13, 249 (1952)
- 3.33. Luborsky, F. E. 1977 a, Materials Sci, Eng, 28, 139.

#### **Chapter- 4**

- 4.1. Chatelier, H. Le., Bull SOC. franc. mineral, 1887, 10, 204.
- 4.2. Mazid M. A. and M. A. Chowdhury, "Design and Construction of a Forner type vibrating sample magnetometer." , AECD/ MMD/ 1, June, 1986 (Bangladesh).
- 4.3. Forner S., Rev. Sci. Instr. 27, 548 (1956).

#### **Chapter- 5**

- 5.1. Clements W.G. and B. Cantor, 1976, in Rapidly quenched metals, Section-1, (eds. N.J. Grant and B.C. Giessen) (MIT Press Cambridge, Mass) P.267.
- 5.2. Luborsky, F.E., Materials Sci. Engg-28(1977), P.139.

- 5.3. Minch Le, Bach Thanh Cong, Nguyen Chau M. Huq, M. A. Mazid, M. A. Asgar, Proceedings of the Vietnamese National Conference on Physics and Engineering, Hanoi 1975, 412-417.
- 5.4. Turnbull D., Contemp. Phys. 1969; 10:473
- 5.5. Lu Z P, Tan H, LiY, Ng SC, Scripta mater . 2000; 42:667.
- 5.6. Inouc A , Masumoto T., Mater . Sci . Eng. 1993; 173 A : 1.
- 5.7. APPINO C. AND F.FIORILLO, Journal of Magnetism and Magnetic Materials, 133, 107., 1994.
- 5.8. KRONMULLER H., N. MOSER ANDT. REININGER, Anales de Fisica B 86(1), 1990.
- 5.9. BARANDIARAN J.M., M. VAZQUEZ, A. HENANADO, J. GONZALEZ AND G. RIVERO IEEE Trans. Magn., 25, 3350, 1989.
- 5.10. ANDERSON P.W., B.I. HALPERIN AND C.M. VARMA, Phil. Mag., 25(1),1972.
- 5.11. PHILLIPS W.A., J. Low. Temp. Phys., 7, 351,1972.
- 5.12. Overshott K.J., IEEE Trans. Magn. **MAG-17** 2698 (1931).

**PUBLICATIONS**

## List of Publications

1. Z. H. Khan, S. S. Sikder, M. A. Asgar & A. K. M. Zakaria, “ The Effect of annealing temperature on the complex permeability of  $\text{Co}_{74}\text{Fe}_6\text{B}_{10}\text{Si}_{10}$  amorphous ribbons” Biennial Symposium on Physics and Modern Development, A30, 30-31, March 2002, AEC Dhaka, Bangladesh.
2. Z. H. Khan, S. S. Sikder, M. A. Asgar & A. H. Bhuiyan, “The effect of annealing temperature on ac initial permeability of amorphous ribbon with composition  $\text{Co}_{80-x}\text{Fe}_x\text{B}_{10}\text{Si}_{10}$  [ $x= 0, 2, 4, 6 \text{ \& } 8$ ]” International conference on Physics for understanding and Applications, 22-24 February 2004, BUET Dhaka, Bangladesh.
3. Z. H. Khan, S. S. Sikder, M. A. Hakim & A. H. Bhuiyan, “Effect of partial substitution of Fe by Co on the crystallization behavior and activation energy of Co-Fe-based amorphous ribbons” accepted for presentation in the Regional Physics Conference- 2004 to be held in 2005.